ULTRAVIOLET INTERFERENCE FILTERS

by

Verne Robert Costich

Submitted in Partial Fulfillment

of the

Requirements for the Degree

DOCTOR OF PHILOSOPHY

Supervised by Dr. P. W. Baumeister

Institute of Optics

The University of Rochester

Rochester, New York

1965

VITA

The author was born [redacted] In September 1956 he entered Rensselaer Polytechnic Institute, Troy, New York, and obtained from this institute the Bachelor of Science degree in Physics in June, 1960. While at Rensselaer, he received a New York State Regents Engineering Scholarship and several Rensselaer tuition scholarships.

From September 1960 to date the author has been enrolled as a graduate student in the Institute of Optics at the University of Rochester. He has held three research and two teaching assistantships with tuition scholarships. During this time he has worked primarily with Dr. P. W. Baumeister of the Institute of Optics.

ACKNOWLEDGEMENTS

The author wishes to express his appreciation to Professor Philip W. Baumeister for the suggestion of this problem as well as his advice and encouragement during the course of the work.

The computer program used in the computation of the transmittance of multilayers was written by Dr. Baumeister and Mr. Stephen Pieper. Parts of this program were used in computer programs, written by the author to generate data for Figures 5-25, and are gratefully acknowledged.

Some electronic parts of the monitoring system were designed and constructed by Mr. Daniel J. Healey.

Instrument makers Rudolf Hamberger and Patrick Borelli have been extremely helpful in the construction of innumerable parts for the vacuum and monitoring systems.

The financial support of the National Aeronautics and Space Administration is gratefully acknowledged.

ABSTRACT

Ultraviolet bandpass interference filters are designed and produced which have low transmission in the visible spectral region and a narrower transmission peak than conventional ultraviolet filters. These filters contain many thin films deposited by vacuum evaporation on a transparent fused quartz substrate. The basic filter design is a single metal layer sandwiched between two many-layered stacks which are designed so that, for light of the desired wavelength, multiple reflections between the layer interfaces destructively interfere with the reflections from the metal surfaces. In a limited spectral region near the wavelength of interest, the reflectance is greatly reduced. This antireflection of the metal film enhances its transmission in that spectral region.

The maximum attainable transmittance is derived from basic principles. In addition, it is proved that the maximum transmittance occurs only when the reflectance from either side is zero.

Systematic techniques for designing this type of filter are developed and illustrated in an example, which

has a peak transmittance of 0.64 at 0.2537 microns, a full bandwidth at half-maximum of 0.0065 microns, and 0.025 background transmittance. The contrast and peak transmittance are computed and illustrated as functions of the thickness, refractive index and absorption constant of the metal film. Since aluminum is the best metal to use in this type of ultraviolet filter, the peak transmittance, contrast, and bandpass are indicated for aluminum versus film thickness and wavelength.

Several experimental bandpass filters of this type were produced using aluminum as the metal. The measured transmittance properties of these filters parallel closely their computed curves. Among the experimental parameters varied are the phase dispersion and absorption in the antireflection stacks, the aluminum film thickness, and the film thickness monitoring procedure.

TABLE OF CONTENTS

LIST OF FIGURES

Page

I. Introduction

Prior to this investigation, the possibility of designing and constructing ultraviolet bandpass interference filters containing a single metal film had not been explored. Since such filters would have very desirable long-wave rejection characteristics and a narrower passband than the conventional Fabry-Perot filter, it was decided to investigate whether the "single metal layer bandpass filter" could be designed for the ultraviolet. Techniques for designing such filters were developed which would predict the band width, maximum transmittance, contrast and other attributes of the filter. Finally, filters of this type were constructed, which exhibited transmittance properties close to those predicted.

Interest in Ultraviolet Filters

The ultraviolet region from 2000 to 3000 Å was opened to astronomical observation when rocket- and satellite-borne instruments were first raised above the atmosphere. A great deal of interest was then generated in bandpass filters for the ultraviolet. Some of these instruments

have utilised the absorption in chemical solutions, glass filters and doped or irradiated crystals.[1,2] The ultraviolet transmittances of materials commonly used in absorption filters were recently reviewed by Pellicori.[3]

In addition to astronomical applications, filters have been used to reduce the scattered light in ultraviolet spectrometers.[4] Photochemical studies often use filters to provide the required high luminous flux in the ultraviolet and low flux in the visible.[5,6]

Properties of Interference Filters

To construct an absorption filter with specified wavelength, bandpass, and transmittance requires materials which transmit the desired wavelength and absorb nearby wavelengths. An interference filter can be designed to pass a wavelength which is not near the optical absorption edge for any of the materials used in the filter. Since the wavelength of the passband of an interference filter is determined by its layer thicknesses, the passband of a particular design may be continuously shifted in wavelength. This property is used in the wedge filter with spectral characteristics which vary with the position on the filter surface.

Interference filters are lightweight, small, and compatible with optical equipment. While chemical absorption solutions should not be overheated or overcooled and are often enclosed in bulky, breakable liquid cells, interference filters are relatively insensitive to temperature and are easier to mount in an optical system.

Two Problems in Designing an All-Dielectric Bandpass Interference Filter for the Ultraviolet

Below 3000 Å there are few thin film materials which are optically transparent and are not degraded by exposure to humidity. Cryolite, chiolite, and magnesium fluoride satisfy these requirements and provide a selection of materials having low refractive index. However, all-dielectric interference filters require the use of some high refractive index layers. For such high index layers, one must resort to less commonly used materials, which usually have a slight amount of optical absorption and are sensitive to humidity. Honcia and Krebs[7,8] have studied the properties of several high index materials for use in the ultraviolet. In particular they measured the optical properties of PbF_2, Sb_2O_3, Bi_2O_3, and TeO_2.

Blocking the longer wavelength transmission bands

of an all-dielectric interference filter is often accomplished by using an absorbing substrate. However, there are few suitable substrate materials which absorb in the region above 3000 Å while transmitting in the region below 3000 Å.

Filters Which Contain Metal Films

Most of the commercially available interference filters for the ultraviolet contain two or more metal layers. This produces a filter which is self-blocking, i.e., it does not require another interference filter or an absorbing substrate to reject unwanted sidebands. High index dielectric materials are not needed in the construction of these filters. The major disadvantage of such a filter is the low transmittance in the passband.

Most common is the evaporated Fabry-Perot filter, which consists of two metal layers separated by an evaporated dielectric spacer. Stacking two of these filters on one substrate, gives a filter having three metal layers as first described by Geffcken.[9] This design was investigated as a bandpass filter for the ultraviolet by Schroeder.[10]

In 1957, Berning and Turner discussed a bandpass

filter design which contains a single metal film.[11] Although their filter used silver and was tuned to 5500 Å, it was indicated that the concept was applicable to other spectral regions and metals. This type of filter yields higher transmittance and a narrower passband than does the conventional first-order Fabry-Perot filter using the same total metal thickness.

Berning and Turner called this type of filter an induced transmission filter. Since we shall later be considering filters having more than one metal film, a general notation is needed. A filter is designated by the number of metal layers it contains and the letter "M." Thus the induced transmission filter which contains one metal layer is a 1M filter. Similarly, the Fabry-Perot filter is a 2M filter and the Geffcken filter is a 3M filter.

II. Theory

The theory is developed in this section by which we can compute the reflectance, transmittance, and other properties of a filter which consists of a single metal layer sandwiched between two dielectric stacks. It is seen that the transmittance of such a filter depends markedly on the properties of the dielectric stack. For example, a film of aluminum with a physical thickness of 300 Å deposited on a fused quartz substrate has a reflectance of 0.90, a transmittance of 0.02 and an absorbance of 0.08 for light of wavelength 2500 Å. The low transmittance is due to high reflectance more than it is due to absorption in the film. In fact, the transmittance of this aluminum film may be increased to 0.64, if it is antireflected by dielectric stacks.

Some insight is gained into the antireflection of a metal film by first considering the antireflection of a bulk metal. Then the equations for the transmittance and energy flow of a stack of absorbing films are computed from electromagnetic theory. These properties are then computed as functions of the film thickness and optical

constants.

A systematic technique for designing a bandpass filter which consists of a metal layer between two multilayer stacks is illustrated in an example.

The effect of altering the phase dispersion of the antireflection stacks is determined. Examples are given with stack designs having both very high and very low phase dispersion.

Antireflection of Bulk Substrates

The antireflection of bulk substrates of aluminum and chromium was reported by Lupashko and Sklyarevskii.[12] Their antireflection multilayers were tuned to 5600 Å and were of the same type as used by Turner and Berning. In Figure 1 a. is shown a typical multilayer antireflection coating on a metallic substrate. The quarter-wave stack has been replaced in Figure 1 b. by an effective interface as described by S. D. Smith.[13]

The result is an asymmetric Fabry-Perot filter. One of the mirrors is a multilayer and has no absorption, while the other is the metallic substrate, which has no transmission. The minima in reflectance will occur when the spacer thickness is

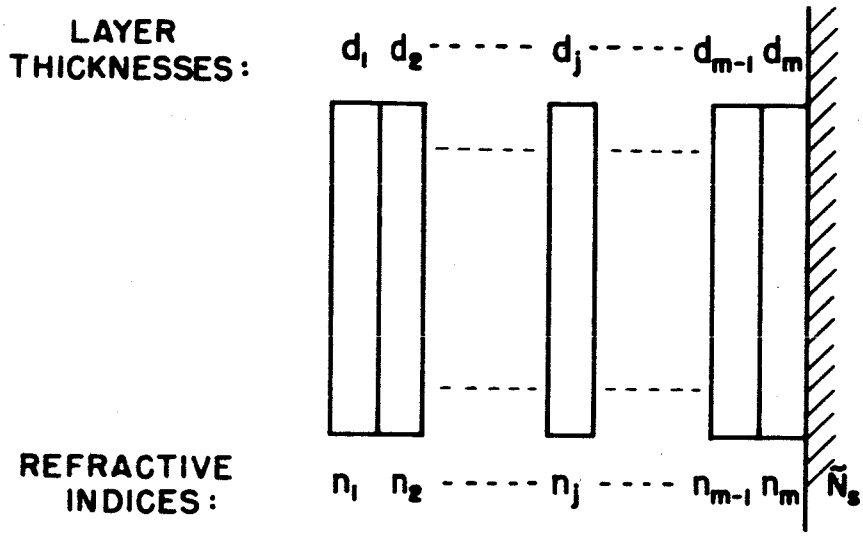

Figure I a. Antireflection of a Metallic Substrate

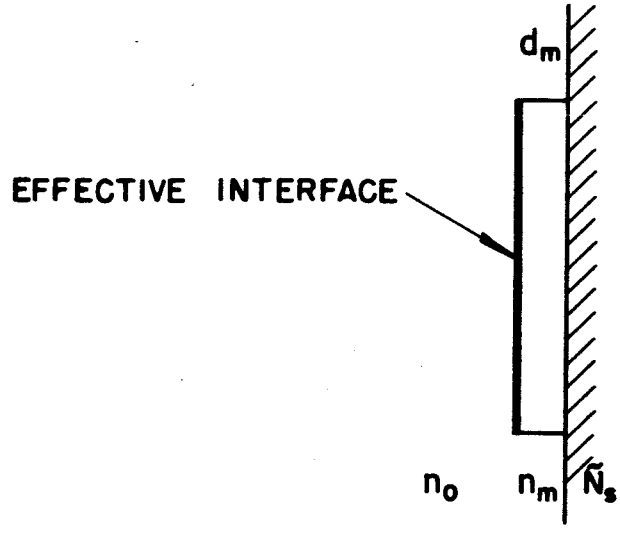

Figure I b. Replacement of the Quarter-wave Stack with an Effective interface

$$d_m = \frac{\lambda_o \left((M-1)\pi + \frac{\delta}{2} + \frac{\delta'}{2} \right)}{2\pi n_m} \qquad (1)$$

where δ is the phase change upon reflection at the quarter wave stack, δ' is the same at the metallic substrate, M is an integral order number, λ_o is the wavelength being considered, and n_m is the index of refraction of the dielectric spacer.

The Fresnel coefficient for a metallic-dielectric interface is

$$r = |r| e^{+i\delta} = \frac{n_m - \tilde{N}_s}{n_m + \tilde{N}_s} = \frac{n_m - n_s + i k_s}{n_m + n_s - i k_s} \qquad (2)$$

From this the phase change upon reflection at the substrate interface is

$$\delta = \tan^{-1} \left[\frac{+2 k_s n_m}{n_m^2 - n_s^2 - k_s^2} \right] \qquad (3)$$

and the reflectance at the same interface is

$$R = |r|^2 = \frac{(n_m - n_s)^2 + k_s^2}{(n_m + n_s)^2 + k_s^2} \qquad (4)$$

Assuming that n_m is 1.38 and $\tilde{N}_s$ is 0.20-i2.50, we find that δ is ~~50.0~~ 122 degrees or ~~0.86~~ 2.1 radians and R is 0.90. The phase change upon reflection at the quarter wave stack is either zero or π radians for light of the design wavelength, depending on whether the quarter-wave stack is terminated with a high or a low index layer next to the spacer. Assuming the film next to the spacer is of high index and assuming that M is unity, the spacer thickness for antireflection is

$$d_m = \frac{\lambda_o\left(\cancel{} + \frac{\pi}{2} + \cancel{0.43}\ 1.06\right)}{2\pi n_m} = \frac{\cancel{0.18}\ 0.42}{1.38}\lambda_o \qquad (5)$$

The optical thickness is thus $\cancel{0.18}\ 0.42\ \lambda_o = \cancel{0.73}\ 1.68\left(\frac{\lambda_o}{4}\right)$ or about one and three-quarters of a quarter-wave optical thickness. If the reflectance is to be close to zero in either of the two above cases, the reflectance of the two Fabry-Perot

mirrors must be nearly equal as seen from the spacer layer. Thus the reflectance of the quarter-wave stack should be about 0.90. A quarter-wave stack having a reflectance of 0.90 must have many layers. If we can use PbF_2, which has an index of refraction of 2.1 at 2537 Å, as the high index material, the stack would contain seven layers; if we use ThF_4 with an idex of 1.55, it would have twelve layers. The phase change upon reflection of a quarter-wave stack varies more rapidly than the phase change upon reflection of a metal film. For this reason the minimum of reflectance is much narrower than it would be in a first-order Fabry-Perot filter having metal films for the mirrors.

Antireflection of Metal Films

The pioneering work in the antireflection of metal films was done in 1951 by F. Dow Smith[14] for interferometer plate coatings. By decreasing the outer surface reflectance of the metal films on the interferometer plates, he was able to obtain high contrast reflection fringes as was more recently reported by Shkliarevskii.[15] Two recent papers by Kard[16,17] contain extensive theory pertaining to increasing or decreasing the transparency of metallic films, which were found too general to be

useful in this work.

The design procedure developed in this thesis differs from that of the "spacerless filter" approach developed by Turner,[11] which requires recomputation whenever the design of the antireflection stack is changed. In addition to obviating this recomputation, my design technique affords insight into the variation of the filter's characteristics when the antireflection stacks are altered.

Fundamental Considerations

The computation of the transmittance and reflectance of a multilayer involves the solution of the wave equation with the appropriate boundary conditions at the interfaces. The matching of the E and H fields at the interface between two media is facilitated by the concept of admittance, which was first applied to thin film optics by Leurgans.[18] In this subsection the admittance concept is developed from Maxwell's equations.

Maxwell's equations in the Gaussian system of units are[19]

$$\nabla \times \vec{E} = -\frac{1}{c}\frac{\partial \vec{B}}{\partial t} \tag{6}$$

$$\nabla \times \vec{H} = \frac{1}{c} \frac{\partial \vec{D}}{\partial t} + \frac{4\pi}{c} \vec{J} \tag{7}$$

$$\nabla \cdot \vec{D} = 4\pi\rho \tag{8}$$

$$\nabla \cdot \vec{B} = 0 \tag{9}$$

where E, D, H, B, J, and ρ have the usual meanings. The medium in which the electromagnetic wave propagates is isotropic and homogeneous.

We assume a righthanded Cartesian coordinate system and consider that the electromagnetic wave is polarised with the electric vector in the x direction and is propagating in the z direction. As is shown in many texts,[20] the wave equation follows:

$$\nabla^2 \vec{E} = \frac{\epsilon\mu}{c^2} \frac{\partial^2 \vec{E}}{\partial t^2} \tag{10}$$

The two linearly independent solutions to this equation are

$$E_\rho^+ = \hat{x}\, E_{o\rho}^+ \exp\left[i(\omega t - 2\pi\sigma\tilde{N}_\rho z)\right] \tag{11}$$

$$E_\rho^- = \hat{x}\, E_{o\rho}^- \exp\left[i(\omega t + \alpha + 2\pi\sigma\tilde{N}_\rho z)\right] \tag{12}$$

where $\tilde{N}_\rho$ is the complex index of refraction and σ is $\frac{1}{\lambda}$. The first is a wave traveling toward positive z while the second is traveling in the opposite direction. The quantity α in the second equation represents the relative phase of the two waves at the origin of the coordinate system.

If we assume that the positive traveling wave is the incident wave and the negatively directed wave is the reflected wave, then the amplitude coefficient of reflection of the electric field is a function of z,

$$r = \frac{E_p^-}{E_p^+} = \frac{E_{op}^-}{E_{op}^+} \exp\left[i(\alpha + 4\pi\sigma\tilde{N}_p z)\right] \tag{13}$$

Note that within a nonabsorbing medium both E_{op}^- and E_{op}^+ are constant, thus $|r|$ is constant while $\exp\left[i(\alpha+4\pi\sigma\tilde{N}_p z)\right]$ varies such that increasing z by $\frac{1}{4\tilde{N}_p\sigma}$ causes a phase change of π .

The boundary conditions for the electric and magnetic fields are

$$(E_p)_p = (E_{p+1})_p \quad \text{and} \quad (H_p)_p = (H_{p+1})_p \tag{14}$$

where the subscripts inside the parentheses indicate the layers and the outer subscript indicates the interface being considered. If we were not considering normal incidence, only the tangential component of the electric and magnetic waves would be matched.

We define the admittance, Y, as the ratio of the magnetic to the electric field strength. Then Y is the same on either side of an interface as long as the waves

are incident normal to the interface. The generalization to nonnormal incidence is straightforward and is given elsewhere.[21] For normal incidence the total electric field is

$$E_\rho = E_\rho^+ + E_\rho^- \tag{15}$$

and the total magnetic field is

$$H_\rho = H_\rho^+ + H_\rho^- \tag{16}$$

But from Maxwell's equations the magnetic and electric fields of each of the traveling waves are related by the optical constant of the medium:

$$H_\rho^+ = \tilde{N}_\rho E_\rho^+ \tag{17}$$

$$H_\rho^- = -\tilde{N}_\rho E_\rho^- \tag{18}$$

Thus

$$Y = \frac{H_\rho^+ + H_\rho^-}{E_\rho^+ + E_\rho^-}$$

$$= \frac{\tilde{N}_\rho E_{o\rho}^+ \exp\left[i(\omega t - 2\pi\sigma\tilde{N}_\rho z)\right] - \tilde{N}_\rho E_{o\rho}^- \exp\left[i(\omega t + \alpha + 2\pi\sigma\tilde{N}_\rho z)\right]}{E_{o\rho}^+ \exp\left[i(\omega t - 2\pi\sigma\tilde{N}_\rho z)\right] + E_{o\rho}^- \exp\left[i(\omega t + \alpha + 2\pi\sigma\tilde{N}_\rho z)\right]} \tag{19}$$

Dividing this equation by $E_{o\rho}^+ \exp\left[i(\omega t - 2\pi\sigma\tilde{N}_\rho z)\right]$ yields

$$Y = \frac{\tilde{N}_\rho - \tilde{N}_\rho r}{1 + r} \tag{20}$$

If we now define the reduced admittance, y, by

$$y = \frac{Y}{\tilde{N}_\rho} \tag{21}$$

then,

$$y = \frac{1 - r}{1 + r} \tag{22}$$

from which we can solve for r as a function of y

$$r = \frac{1 - y}{1 + y} \tag{23}$$

It is seen that the r and y coordinates are connected by a bilinear transformation. Thus the straight lines of constant real or imaginary value in the reduced admittance plane are transformed into circles in the amplitude reflection coefficient plane, as illustrated below.

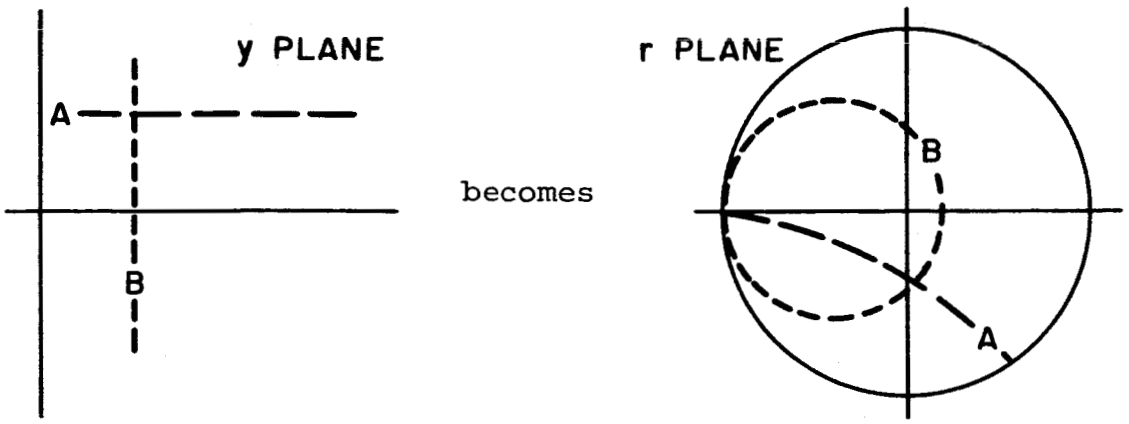

We use the convention that the phase of r is measured counterclockwise from the positive real axis.

Since the Y on opposite sides of an interface is the same,

$$\left(\tilde{N}_p\, y_p\right)_p = \left(\tilde{N}_{p+1}\, y_{p+1}\right)_p \tag{24}$$

This allows us to determine the reduced admittance on one side of an interface given the admittance on the other side of the interface and given the ratio of the two indices.

Nonabsorbing Films

Consider a wave entering at normal incidence a multilayer stack consisting of m homogeneous films of physical thicknesses d_γ and optical indices $\tilde{N}_\gamma = n_\gamma - i k_\gamma$ where γ is the number of the film. The subscript, γ, ranges from 1 for the first film the wave encounters to m for the last film before the substrate. The lefthand medium is of optical constant N_0, while the righthand medium is of optical constant N_s. Both of these terminal media are assumed boundless in the z coordinate. All the layers and the terminal media are considered independent of the x and y coordinates, that is, their interfaces are parallel planes of infinite extent. It will be convenient if we label the interface between the γ th and the $(\gamma+1)$th film as the γ th interface. The interfaces thus range from 0 to m.

Since the righthand medium is infinite in extent there can be no returning wave, thus the single right-traveling wave provides a reduced admittance of unity in this medium. From equation 24 we then see that

$$(y_m)_m = \frac{\tilde{N}_s (y_s)_m}{\tilde{N}_m} = \frac{\hat{N}_s}{\tilde{N}_m} \qquad (25)$$

where the subscript inside the parentheses indicates the layer and the outer subscript indicates the interface at which the reduced admittance is being evaluated.

After determining the reduced admittance in the mth film at the mth interface, the amplitude reflection coefficient may be determined by simply plotting the reduced admittance value on the r plane using the transformed coordinate system. The reflection coefficient at the other interface of the mth layer may then be determined.

$$(r_m)_{m-1} = (r_m)_m \exp\left[i 4\pi\sigma \tilde{N}_m d_m\right] \qquad (26)$$

The case of the absorbing film will be considered below. For the nonabsorbing film this represents a reduction of the phase of the reflection coefficient without changing its amplitude. The reduced admittance in the mth film at the (m-1)th interface may then be read in the r plane from the transformed y axes.

The general boundary matching equation may now be written as

$$(\gamma_\gamma)_\gamma = \frac{\tilde{N}_{\gamma+1}}{\tilde{N}_\gamma}(\gamma_{\gamma+1})_\gamma \tag{27}$$

while the general equation for determining the amplitude reflection coefficient at the left interface of the γ th film as a function of that at the right interface of the same film is

$$(r_\gamma)_{\gamma-1} = (r_\gamma)_\gamma \exp[i4\pi\sigma\tilde{N}_\gamma d_\gamma] \tag{28}$$

Absorbing Films

If r_j is the amplitude reflection coefficient of the electric field (as determined in the jth medium) due to the jth interface and the film structure to the right of that interface, then the electric field amplitude of the wave traveling to the left at the jth interface is

$$(E_j^-)_j = r_j \, (E_j^+)_j$$

(29)

The total electric field amplitude in the jth film at a distance d from the jth interface is thus

$$E(d) = E_j^+ + E_j^-$$

$$= E_j^+ \left[\exp(i 2\pi\sigma \tilde{N}_j d) + r_j \exp(-i 2\pi\sigma \tilde{N}_j d) \right]$$

(30)

If the jth film thickness is d_j, then the total electric field amplitude at the (j-1)th interface is

$$E_{j-1} = E_j^+ \left[\exp(i\phi_j) + r_j \exp(-i\phi_j) \right]$$

(31)

where $\phi_j = 2\pi\sigma \tilde{N}_j d_j$ is the complex phase thickness of the jth layer.

In a medium of index $\tilde{N}_j$ the magnetic field amplitude of the traveling waves are

$$H_j^+ = \tilde{N}_j E_j^+ \tag{32}$$

and

$$H_j^- = -\tilde{N}_j E_j^- \tag{33}$$

Thus,

$$H_{j-1} = E_j^+ \left[\tilde{N}_j \exp(i\phi_j) - \tilde{N}_j r_j \exp(-i\phi_j) \right] \tag{34}$$

In order to determine the admittance at one interface of an absorbing film in terms of that at the other interface, we revert to the definition of admittance.

$$Y_{j-1} = \frac{H_{j-1}}{E_{j-1}} \tag{35}$$

and substitute for the electric and magnetic field strengths, the expressions given in equations 31 and 34. Thus,

$$Y_{j-1} = \frac{E_j^+ \left[\tilde{N}_j \exp(i\phi_j) - \tilde{N}_j r_j \exp(-i\phi_j) \right]}{E_j^+ \left[\exp(i\phi_j) + r_j \exp(-i\phi_j) \right]} \tag{36}$$

$$Y_{j-1} = \tilde{N}_j \left[\frac{\exp(i\phi_j) - r_j \exp(-i\phi_j)}{\exp(i\phi_j) + r_j \exp(-i\phi_j)} \right] \tag{37}$$

But from equation 20

$$r_j = \frac{\tilde{N}_j - Y_j}{\tilde{N}_j + Y_j} \tag{38}$$

$$Y_{j-1} = \tilde{N}_j \left[\frac{(\tilde{N}_j + Y_j)\exp(i\phi_j) - (\tilde{N}_j - Y_j)\exp(-i\phi_j)}{(\tilde{N}_j + Y_j)\exp(i\phi_j) + (\tilde{N}_j - Y_j)\exp(-i\phi_j)} \right] \tag{39}$$

$$Y_{j-1} = \tilde{N}_j \left[\frac{2i\tilde{N}_j \sin(\phi_j) + 2Y_j \cos(\phi_j)}{2\tilde{N}_j \cos(\phi_j) + 2iY_j \sin(\phi_j)} \right] \tag{40}$$

Dividing both numerator and denominator by $2\cos(\phi_j)$ yields

$$Y_{j-1} = \tilde{N}_j \left[\frac{i\tilde{N}_j \tan(\phi_j) + Y_j}{\tilde{N}_j + iY_j \tan(\phi_j)} \right] \tag{41}$$

or

$$Y_{j-1} = \frac{Y_j + i\tilde{N}_j \tan(\phi_j)}{1 + i(Y_j/\tilde{N}_j)\tan\phi_j} \tag{42}$$

This relation in combination with equations 27 and 28 can be used to determine the reflectance of a multilayer containing metallic films.

The Single Metal Layer Filter

In this section filters containing only one metal film sandwiched between two multilayered dielectric stacks are analysed. Using the relations derived above to evaluate the energy into and out of the metal layer, the potential transmittance of the single metal layer is derived. From this, the maximum possible transmittance is determined. These two relations (equations 51 and 68) were cited without derivation by Turner and Berning.[11]

The relationship between the admittance of the matching stacks and the transmittance of the filter is derived in order to obtain a convenient design technique. This systematic design technique is illustrated in an example.

The maximum transmittance and contrast of single

metal layer filters are dependent on the thickness and optical constants of the metal layer. This dependence is illustrated graphically below.

Potential Transmittance of a Metal Layer

Our objective is to determine the value of the Poynting vector at the two interfaces of the jth film. These values correspond to the power flowing into and out of the metal film. The Poynting vector averaged over one period of oscillation is[19]

$$P = \frac{c}{8\pi} \mathcal{R}_e (E H^*) \tag{43}$$

where E and H are the complex amplitudes of the magnetic and electric field strengths and where $\mathcal{R}_e$ denotes "the real part of." At the (j-1)th interface, from equation 34 we have

$$H_{j-1}^* = (E_j^+)^* \left[\tilde{N}_j^* \exp(-i\phi_j^*) - \tilde{N}_j^* r_j^* \exp(i\phi_j^*) \right] \tag{44}$$

Combining this equation with equation 31 gives

$$E_{j-1}\, H_{j-1}^{*} =$$

$$|E_j^{+}|^2\left[\tilde{N}_j^{*} \exp(4\pi\sigma k_j d_j) - \tilde{N}_j^{*}|r_j|^2 \exp(-4\pi\sigma k_j d_j)\right.$$

$$\left. + \tilde{N}_j^{*} r_j \exp(-i4\pi\sigma n_j d_j) - \tilde{N}_j^{*} r_j^{*} \exp(i4\pi\sigma n_j d_j)\right]$$

(45)

Substituting $|r_j| \exp(i\rho_j)$ for r_j, we get

$$E_{j-1}\, H_{j-1}^{*} =$$

$$|E_j^{+}|^2\left[\tilde{N}_j^{*} \exp(4\pi\sigma k_j d_j) - \tilde{N}_j^{*}|r_j|^2 \exp(-4\pi\sigma k_j d_j)\right.$$

$$\left. + 2i\,\tilde{N}_j^{*}|r_j| \sin(\rho_j - 4\pi\sigma n_j d_j)\right]$$

(46)

Then

$$P_{j-1} = \frac{c}{8\pi} |E_j^+|^2 \left[n_j \exp(4\pi\sigma k_j d_j) - n_j |r_j|^2 \exp(-4\pi\sigma k_j d_j) - 2k_j |r_j| \sin(\rho_j - 4\pi\sigma n_j d_j) \right]$$

(47)

To determine the Poynting vector at the other interface of the jth film we might set d_j equal to zero in the above expression or we may compute it directly:

$$P_j = \frac{c}{8\pi} \mathrm{Re} \left[(E_j^+ + r_j E_j^+)(\tilde{N}_j E_j^+ - \tilde{N}_j r_j E_j^+)^* \right]$$

(48)

$$P_j = \frac{c}{8\pi} \mathrm{Re} \left[\tilde{N}_j^* |E_j^+|^2 - \tilde{N}_j^* |r_j|^2 |E_j^+|^2 + N_j^* r_j |E_j^+|^2 - N_j^* r_j^* |E_j^+|^2 \right]$$

(49)

$$P_j = \frac{c}{8\pi} |E_j^+|^2 \left[n_j - n_j |r_j|^2 - 2k_j |r_j| \sin(\rho_j) \right]$$

(50)

The ratio of the Poynting vector evaluated at the jth interface to that evaluated at the (j-1)th interface is called the potential transmittance.

$$\psi_j = \frac{P_j}{P_{j-1}} =$$

$$\left\{\left[n_j - n_j|r_j|^2 - 2k_j|r_j|\sin(\rho_j)\right] \Big/ \left[n_j \exp(4\pi\sigma k_j d_j)\right.\right.$$

$$\left.\left. - n_j|r_j|^2 \exp(-4\pi\sigma k_j d_j) - 2k_j|r_j|\sin(\rho_j - 4\pi\sigma n_j d_j)\right]\right\}$$

(51)

Maximum Transmittance Attainable

We now wish to show that the contours of constant potential transmittance are circles in the r plane. If we use the trigonometric identity

$$\sin(A-B) = \sin A \cos B - \cos A \sin B$$

(52)

then,

$$\psi_j = \left\{\left[1 - |r_j|^2 - 2\left(\frac{k_j}{n_j}\right)|r_j|\sin(\rho_j)\right] \Big/ \left[\exp(4\pi\sigma k_j d_j)\right.\right.$$

$$-|r_j|^2 \exp(-4\pi\sigma k_j d_j) - 2\left(\frac{k_j}{n_j}\right)|r_j|\left(\sin(\rho_j)\cos(4\pi\sigma n_j d_j)\right.$$

$$\left.\left.\left. - \cos(\rho_j)\sin(4\pi\sigma n_j d_j)\right)\right]\right\} \tag{53}$$

Substituting

$$r_j = U_j + i V_j \tag{54}$$

$$\psi_j = \left\{\left[1 - U_j^2 - V_j^2 - 2\left(\frac{k_j}{n_j}\right)V_j\right] \Big/ \left[\exp(4\pi\sigma k_j d_j)\right.\right.$$

$$-(U_j^2 + V_j^2)\exp(-4\pi\sigma k_j d_j) - 2\left(\frac{k_j}{n_j}\right)\left(V_j \cos(4\pi\sigma n_j d_j)\right.$$

$$\left.\left.\left. - U_j \sin(4\pi\sigma n_j d_j)\right)\right]\right\} \tag{55}$$

Setting the right side of the above equation equal to a

constant, C,

$$1 - U_j^2 - V_j^2 - 2\left(\frac{k_j}{n_j}\right) V_j = C\left\{\exp(4\pi\sigma k_j d_j)\right.$$

$$-(U_j^2 + V_j^2)\exp(-4\pi\sigma k_j d_j)$$

$$\left. -2\left(\frac{k_j}{n_j}\right)\left[V_j \cos(4\pi\sigma n_j d_j) - U_j \sin(4\pi\sigma n_j d_j)\right]\right\}$$

(56)

Separating this equation into terms involving powers of U_j and V_j ,

$$U_j^2\left[C\exp(-4\pi\sigma k_j d_j) - 1\right] + U_j\left[-2\left(\frac{k_j}{n_j}\right) C \sin(4\pi\sigma n_j d_j)\right]$$

$$+ V_j^2\left[C\exp(-4\pi\sigma k_j d_j) - 1\right] + V_j\left[2\left(\frac{k_j}{n_j}\right) C \sin(4\pi\sigma n_j d_j) - 2\left(\frac{k_j}{n_j}\right)\right]$$

$$+\left[1 - C\exp(4\pi\sigma k_j d_j)\right] = 0$$

(57)

Dividing by $\left[C\exp(-4\pi\sigma k_j d_j)-1\right]$ yields

$$U_j^2 + V_j^2 + U_j\left[\frac{-2\left(\frac{k_j}{n_j}\right)C\sin(4\pi\sigma n_j d_j)}{C\exp(-4\pi\sigma k_j d_j)-1}\right]$$

$$+V_j\left[\frac{2\left(\frac{k_j}{n_j}\right)C\cos(4\pi\sigma n_j d_j)-2\left(\frac{k_j}{n_j}\right)}{C\exp(-4\pi\sigma k_j d_j)-1}\right]$$

$$-\left[\frac{C\exp(4\pi\sigma k_j d_j)-1}{C\exp(-4\pi\sigma k_j d_j)-1}\right] = 0$$

(58)

This can be written in the form

$$\left[U_j-\frac{\left(\frac{k_j}{n_j}\right)C\sin(4\pi\sigma n_j d_j)}{C\exp(-4\pi\sigma k_j d_j)-1}\right]^2+\left[V_j-\frac{\left(\frac{k_j}{n_j}\right)\left(1-C\cos(4\pi\sigma k_j d_j)\right.}{C\exp(4\pi\sigma k_j d_j)-1}\right]^2 =$$

$$\frac{C^2-2C\cosh(4\pi\sigma k_j d_j)+1+\left(\frac{k_j}{n_j}\right)^2\left[C^2-2C\cos(4\pi\sigma n_j d_j)+1\right]}{\left[C\exp(-4\pi\sigma k_j d_j)-1\right]^2}$$

(59)

which represents a circle centered at

$$r_j = \frac{\left(\frac{k_j}{n_j}\right)C\sin(4\pi\sigma n_j d_j)}{C\exp(-4\pi\sigma k_j d_j)-1} + i\,\frac{\left(\frac{k_j}{n_j}\right)\left[1-C\cos(4\pi\sigma n_j d_j)\right]}{C\exp(-4\pi\sigma k_j d_j)-1}$$

(60)

and of radius

$$R = \left\{ \frac{C^2 - 2C\cosh(4\pi\sigma k_j d_j) + 1 + \left(\frac{k_j}{n_j}\right)^2 \left[C^2 - 2C\cos(4\pi\sigma n_j d_j) + 1\right]}{\left[C\exp(4\pi\sigma k_j d_j) - 1\right]^2} \right\}^{1/2} \tag{61}$$

For C equal to zero this circle is centered at

$$r_j = -i\left(\frac{k_j}{n_j}\right) \tag{62}$$

and its radius is

$$R = \sqrt{1 + \left(\frac{k_j}{n_j}\right)^2} \tag{63}$$

In order to determine the maximum potential transmittance we examine the degenerate circle for which the radius is zero. The denominator of the expression for the radius is always greater than zero, since both C and $\exp(-4\pi\sigma k_j d_j)$ are less than unity. Therefore setting the numerator equal to zero represents the condition of zero radius. Gathering terms in powers of C:

$$C^2\left[1+\left(\frac{k_j}{n_j}\right)^2\right]+C\left[-2\cosh\left(4\pi\sigma k_j d_j\right)-2\left(\frac{k_j}{n_j}\right)^2\cos\left(4\pi\sigma n_j d_j\right)\right]$$

$$+\left[1+\left(\frac{k_j}{n_j}\right)^2\right]=0$$

(64)

Dividing by $\left[1+\left(\frac{k_j}{n_j}\right)^2\right]$ gives

$$C^2+C\left[\frac{-2\cosh\left(4\pi\sigma k_j d_j\right)-2\left(\frac{k_j}{n_j}\right)^2\cos\left(4\pi\sigma n_j d_j\right)}{1+\left(\frac{k_j}{n_j}\right)^2}\right]+1=0$$

(65)

If we define

$$\mu=\frac{\cosh\left(4\pi\sigma k_j d_j\right)+\left(\frac{k_j}{n_j}\right)^2\cos\left(4\pi\sigma n_j d_j\right)}{1+\left(\frac{k_j}{n_j}\right)^2}$$

(66)

then the solution to equation 65 is

$$C = \mu \pm \sqrt{\mu^2 - 1} \tag{67}$$

This is the maximum potential transmittance for the jth layer and will be referred to below as ψ_{max} .

$$\psi_{max} \equiv \mu \pm \sqrt{\mu^2 - 1} \tag{68}$$

We define Φ by

$$\cosh \Phi \equiv \mu \tag{69}$$

$$\psi_{max} = \cosh \Phi \pm \sinh \Phi \tag{70}$$

$$\psi_{max} = e^{-\Phi} \tag{71}$$

where the negative sign is taken since conservation of energy requires that

$$\psi_{max} \leq 1.0 \tag{72}$$

Note that for either d_j or k_j equal to zero we have, from equations 66 and 68

$$\mu = 1.0 \tag{73}$$

$$\psi_{max} = 1.0 \tag{74}$$

From equations 66 and 68 we conclude that ψ_{max} depends only on the optical constants of the metal film and the ratio of its physical thickness to the wavelength of the light.

$$\psi_{max} = F\left(\tilde{N}_i, \frac{d_j}{\lambda}\right) \tag{75}$$

The value of r_j for maximum potential transmittance is obtained by substituting ψ_{max} into equation 60.

$$(r_j)_{\psi=\psi_{max}} = \frac{\left(\frac{k_j}{n_j}\right)\psi_{max}\sin(4\pi\sigma n_j d_j)}{\psi_{max}\exp(-4\pi\sigma k_j d_j) - 1}$$

$$+ i\,\frac{\left(\frac{k_j}{n_j}\right)\left(1-\cos(4\pi\sigma n_j d_j)\right)}{\psi_{max}\exp(-4\pi\sigma k_j d_j) - 1}$$

(76)

From equations 75 and 76 we conclude that this value of r_j depends on the optical constants of the metal film and the ratio of its physical thickness to the wavelength of the light.

$$(r_j)_{\psi=\psi_{max}} = F\left(\tilde{N}_j, \frac{d_j}{\lambda}\right)$$

(77)

Admittance at the Peak

It is shown in this subsection that in order to maximize the transmittance through a given metallic film, it is necessary that the admittances of the antireflection stacks be equal when measured as shown in Figure 2.

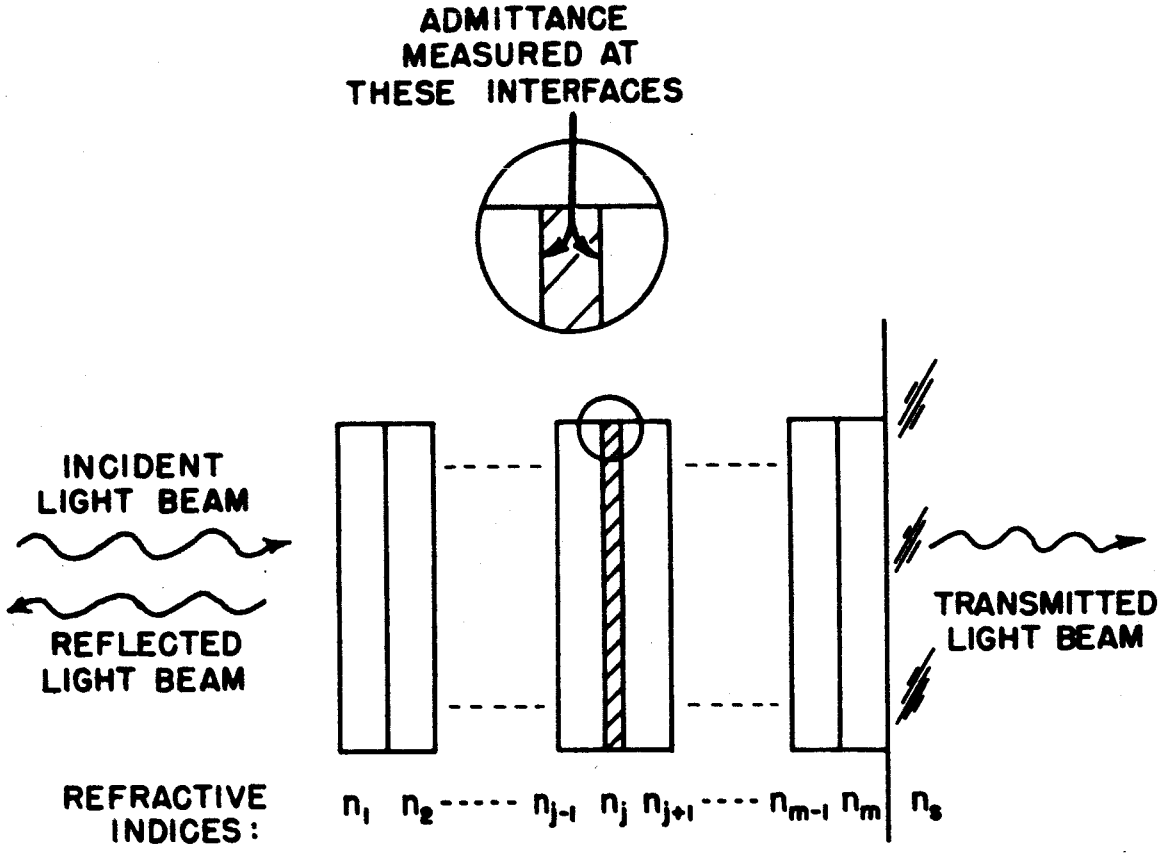

Figure 2. Geometry of the Single Metal Layer Filter

Equations are derived for the admittance of the stacks which yield maximum transmittance.

Assume the admittance of the right-hand stack corresponds to the maximum potential transmittance and call it Y_{pk}.

$$Y_j = Y_{pk} \tag{78}$$

Then from equation 20

$$Y_j = \frac{\tilde{N}_j (1 - r_j)}{(1 + r_j)} \tag{79}$$

From the definition of the potential transmittance in equation 51

$$\psi_j = \left(\frac{T}{1-R}\right)_j \tag{80}$$

and is independent of the stack to the left of the jth layer. Berning proved[11] that the stack to the left of the metal layer can be adjusted to reduce the reflectance to zero. In this case

$$T = \psi_{max} \tag{81}$$

We now assume a beam incident normally from the right side. The transmittance is still ψ_{max}. Since there is only one value of r_j which corresponds to the maximum potential transmittance, the value of r_j for the reversed beam is equal to that for the beam from the right. Therefore, the admittances of the two stacks are equal.

Again taking the beam normally incident from the left, equation 42 may be used to find the admittance at the left interface of the jth film.

$$Y_{j-1} = \left[\frac{Y_j + i \tilde{N}_j \tan \phi_j}{1 + i \left(\frac{Y_j}{\tilde{N}_j} \right) \tan \phi_j} \right] \tag{82}$$

The complete filter can be analysed using the concept of effective interfaces.[13] The left-hand stack is taken as one of the interfaces, while the metal layer and the stack on the right are taken as the other interface. The reflectance of this combination is zero if the admittances seen from the spacer are complex conjugate to one another. Therefore,

$$Y_{j-1} = Y_{pk}^{*} \tag{83}$$

where * denotes the "complex conjugate of." Therefore from equations 78, 82 and 83:

$$Y_{pk}^{*} = \left[\frac{Y_{pk} + i \tilde{N}_j \tan \phi_j}{1 + i \left(\frac{Y_{pk}}{\tilde{N}_j} \right) \tan \phi_j} \right] \tag{84}$$

Solving this equation for the real and imaginary parts of Y_j fixes the position of the transmittance peak on the admittance plane. In order to accomplish this, define

$$Y_{pk} = U + i V \tag{85}$$

$$\tan \phi_j = \alpha + i \beta \tag{86}$$

$$\tilde{N}_j = n - i k \tag{87}$$

Rewriting equation 84:

$$U - iV + i\frac{(U^2+V^2)(\alpha+i\beta)}{(\eta-ik)} =$$

$$U + iV + i(\eta - ik)(\alpha+i\beta)$$

(88)

Canceling the U's and multiplying by $\frac{(\eta-ik)}{i}$ yields

$$-2V(\eta-ik) + (U^2+V^2)(\alpha+i\beta)$$

$$-(\eta-ik)^2(\alpha+i\beta) = 0$$

(89)

Separating this into real and imaginary parts which are each set equal to zero:

$$-2V\eta + \alpha(-\eta^2+k^2+U^2+V^2) - \beta(2\eta k) = 0$$

(90)

$$+2Vk + \beta(-\eta^2+k^2+U^2+V^2) + \alpha(2\eta k) = 0$$

(91)

Dividing the first equation by α and the second one by β and separating them into powers of U and V,

$$V^2 + U^2 - \left(\frac{2n}{\alpha}\right)V - \frac{2\beta nk}{\alpha} + k^2 - n^2 = 0 \tag{92}$$

$$V^2 + U^2 + \left(\frac{2k}{\beta}\right)V + \frac{2\alpha nk}{\beta} + \left(k^2 - n^2\right) = 0 \tag{93}$$

The difference between these equations is

$$2V\left(\frac{n}{\alpha} + \frac{k}{\beta}\right) + 2nk\left(\frac{\beta}{\alpha} + \frac{\alpha}{\beta}\right) = 0 \tag{94}$$

Solving for V,

$$V = -\frac{nk\left(\frac{\beta}{\alpha} + \frac{\alpha}{\beta}\right)}{\left(\frac{n}{\alpha} + \frac{k}{\beta}\right)} = -\frac{nk\left(\beta^2 + \alpha^2\right)}{\beta n + k\alpha} \tag{95}$$

Thus the imaginary part of the admittance at the peak is

$$V = -\frac{nk\left|\tan\phi_j\right|^2}{\mathrm{Im}\left(\hat{N}_j^{*}\tan\phi_j\right)} \tag{96}$$

Rearranging equation 92 yields an expression for the real part of the admittance at the peak.

$$U = \left\{ -V^2 + \left(\frac{2n}{\alpha}\right)V + \frac{2\beta n k}{\alpha} - k^2 + n^2 \right\}^{1/2} \tag{97}$$

If α is nearly zero and smaller than β, a more accurate value of U, obtained from equation 93 is given by

$$U = \left\{ -V^2 - \left(\frac{2k}{\beta}\right)V - \frac{2\alpha n k}{\beta} - k^2 + n^2 \right\}^{1/2} \tag{98}$$

Both α and β are identically zero only when the film is nonabsorbing or its thickness is zero. In either case the value of Y_{RL} is not unique.

Transmittance versus Admittance

In the foregoing subsection it was shown that if we wish to maximize the passband transmittance of the 1M filter, the admittance of the matching stacks must be equal. In this subsection the transmittance of the symmetrically

matched 1M filter is determined versus the admittance of the matching stacks. This is the basis of the computations for the design technique illustrated later in this thesis.

If the metallic film is split in half and the filter analysed as a "spacerless Fabry-Perot," the transmittance of the whole filter is[22]

$$T = \frac{T_o^2}{(1-R_o)^2 + 4R_o \sin^2(\rho_o)}$$

$$= \frac{(T_o/1-R_o)^2}{1 + \frac{4R_o \sin^2(\rho_o)}{(1-R_o)^2}} \qquad (99)$$

where T_o and R_o are respectively the transmittance and reflectance of the half filters as seen from a reference medium of arbitrary refractive index. The phase change upon reflection has been represented by ρ_o. If the admittance of the film combinations on either side of the metal film are assumed to be equal and designated as Y_i, then the admittance of the half filters as seen from the reference medium is given by

$$Y_o = \left[\frac{Y_j + i \tilde{N}_j \tan(\phi_j/2)}{1 + i\left(\frac{Y_j}{\tilde{N}_j}\right) \tan(\phi_j/2)} \right] \tag{100}$$

where

$$\phi_j = 2\pi\sigma \tilde{N}_j d_j \tag{101}$$

is the complex phase thickness of the metal layer before it was split in half for analysis. The amplitude coefficient of reflection seen from the reference medium of unit refractive index is thus

$$r_o = \frac{1 - Y_o}{1 + Y_o} \tag{102}$$

from which

$$R_o = \frac{|1 - Y_o|^2}{|1 + Y_o|^2} \tag{103}$$

and

$$R_o \sin^2 \rho_o = \left[\mathrm{Im}\left(\frac{1 - Y_o}{1 + Y_o} \right) \right]^2 \tag{104}$$

where $\mathfrak{Im}$ means "imaginary part of." Using the ratio of the Poynting vector evaluations at the two interfaces of the metal film, we get

$$\left(\frac{T_o}{1-R_o}\right) = \frac{P_j}{P_o} =$$

$$\frac{1-|r_j|^2+2\left(\frac{k_j}{n_j}\right) r_j \sin(\rho_j)}{e^{\mathfrak{Im}}(2\pi\sigma k_j d_j) - |r_j|^2 e^{\mathfrak{Im}}(-2\pi\sigma k_j d_j) - 2\left(\frac{k_j}{n_j}\right)|r_j| \sin(\rho_j - 2\pi\sigma n_j d_j)}$$

(105)

where r_j is the amplitude coefficient of reflection for the electric field at the boundary of the metal film, evaluated in the metalic medium. The argument of r_j is ρ_j. Rewriting equation 20, the amplitude coefficient of reflection is given by

$$r_j = \frac{\tilde{N}_j - Y_j}{\tilde{N}_j + Y_j}$$

(106)

Substituting these expressions into equation 99 determines the transmittance of the complete filter as a function of Y_j, $\tilde{N}_j$, and d_j/λ. T_{max}, the maximum transmittance of the symmetrically matched 1M filter, occurs at the

matching stack admittance of Y_{pk} and is equal to ψ_{max}. As is shown in the next subsection, the transmittance at $Y_j = 1.0$ is a measure of the transmittance at wavelengths outside the passband and its neighboring high rejection zones. The ratio of the T_{max} to the transmittance at $Y_j = 1.0$ is called the contrast.

Graphical Presentation of T_{max}, Contrast and Y_{pk}

In order to display the dependence on the optical constants of the metallic film of T_{max} and the contrast as well as the admittance at the peak, Y_{pk}, these three quantities were computed for an array of optical constants. The computation was carried out for four different values of the scaled film thickness of the metal film, d_j/λ. The contours depicted in Figure 3 a. are contours of constant T_{max} for a scaled film thickness of 0.05 plotted on the complex index of refraction plane. The range of optical constants includes those of most metals in the ultraviolet spectral region. In Figure 3 b. are shown the contours of constant contrast for the same thickness. Note that although T_{max} is in some regions very high, the contrast is low throughout the complex N plane.

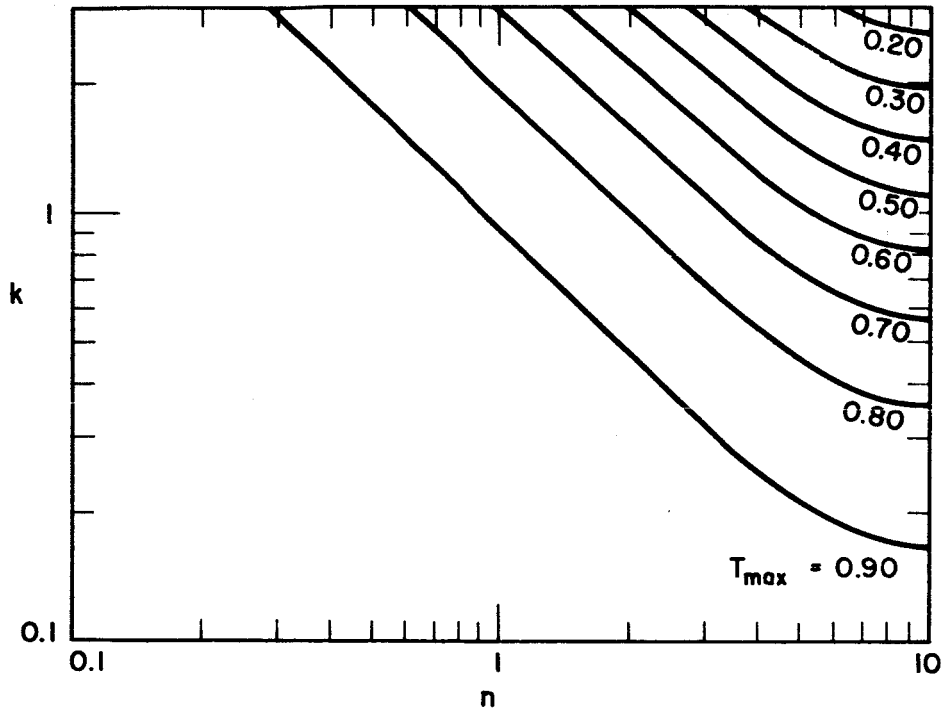

Figure 3 a. T_{max} Contours on the Complex N Plane for d = 0.05λ

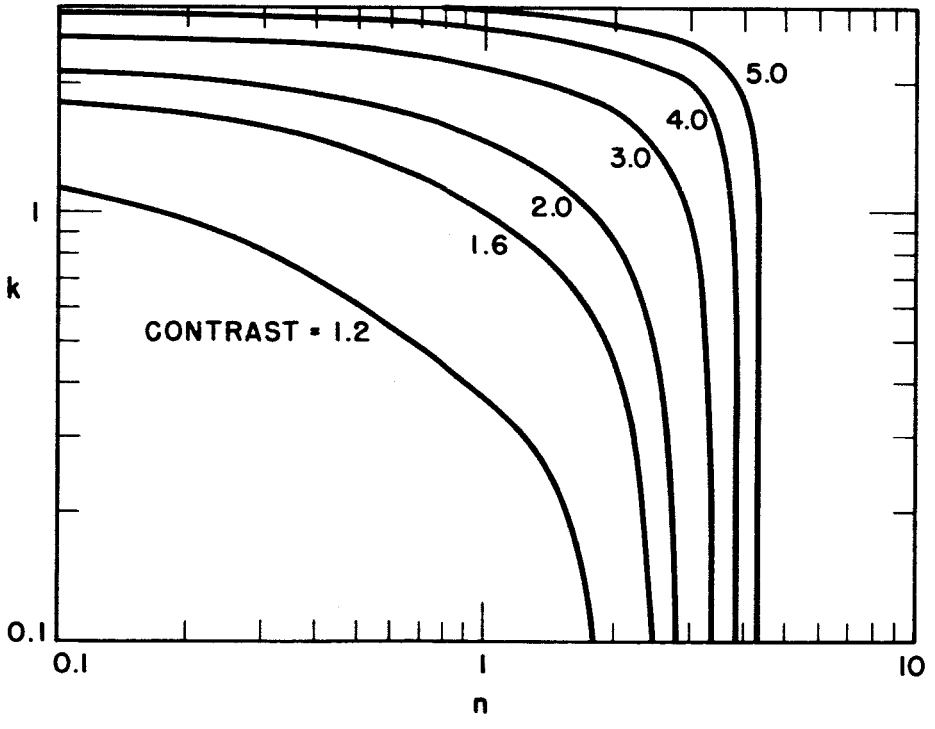

Figure 3 b. Contrast Contours on the Complex N Plane for d = 0.05λ

Curves of constant T_{max} and contrast plotted in the same manner for scaled film thicknesses of 0.10, 0.15, and 0.20 are shown in Figures 4, 5, and 6 respectively.

The information contained in Figures 3 through 6 is more conveniently displayed in Figures 7 through 10, where an optical constants grid is plotted on T_{max} versus contrast coordinates. Assuming a normalized physical thickness for the metallic film, these figures determine the optical constants required to give a filter with desired T_{max} and contrast. On the other hand, if the metal to be used has been determined and the optical constants known, these figures as well as Figures 3 through 6 can be used to determine the thickness to be used.

With the above set of normalized film thicknesses, the complex value of the admittance at the peak of the transmittance function, Y_{pk}, was computed for an array of optical constants. The array of values of Y_{pk} so generated are shown in Figures 11 to 14. For the normalized film thickness of 0.05 the mesh is so condensed that only the outline may be drawn. Thicker films expand the mesh until at a normalized thickness of 0.20 a large portion of the third quadrant of the r plane is covered.

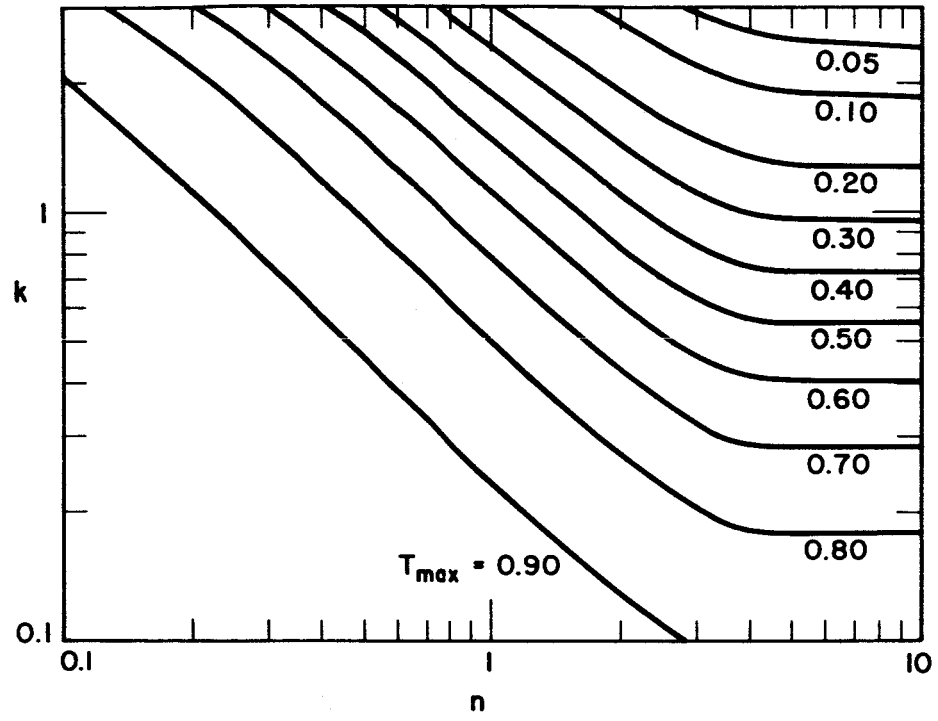

Figure 4a. T_{max} Contours on the Complex N Plane for d = 0.10λ

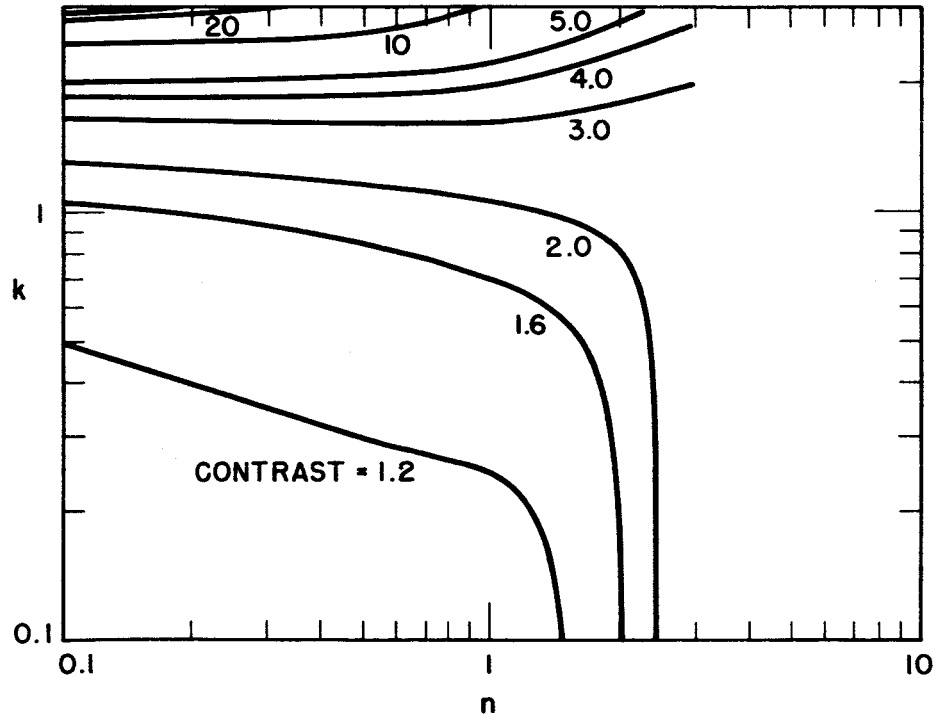

Figure 4b. Contrast Contours on the Complex N Plane for d = 0.10λ

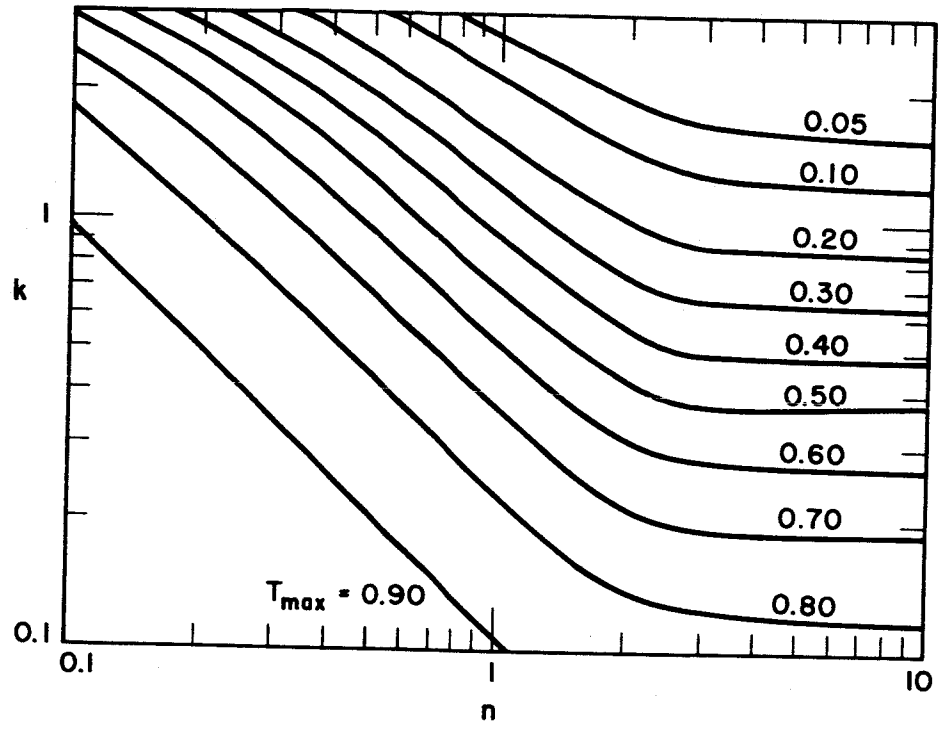

Figure 5a. T_{max} Contours on the Complex N Plane for $d = 0.15\lambda$

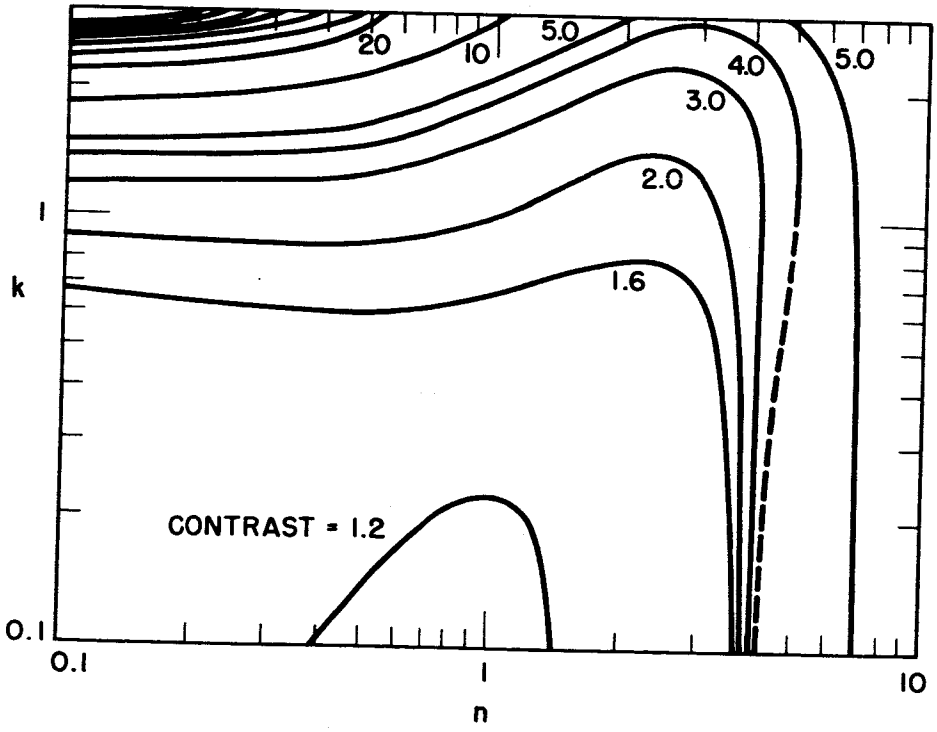

Figure 5b. Contrast Contours on the Complex N Plane for $d = 0.15\lambda$

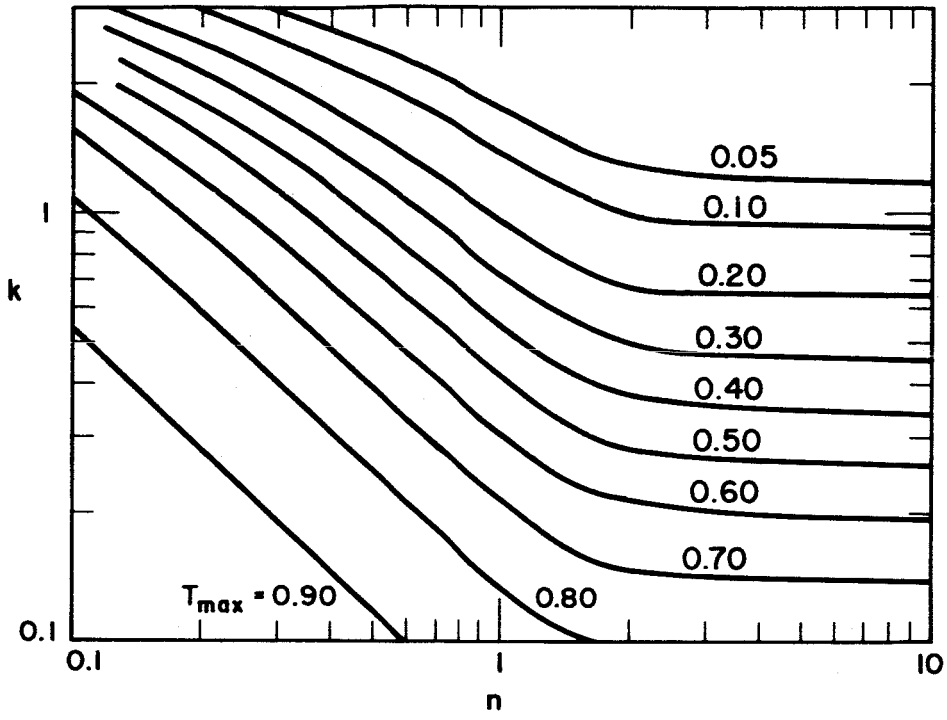

Figure 6 a. T_{max} Contours on the Complex N Plane for d = 0.20λ

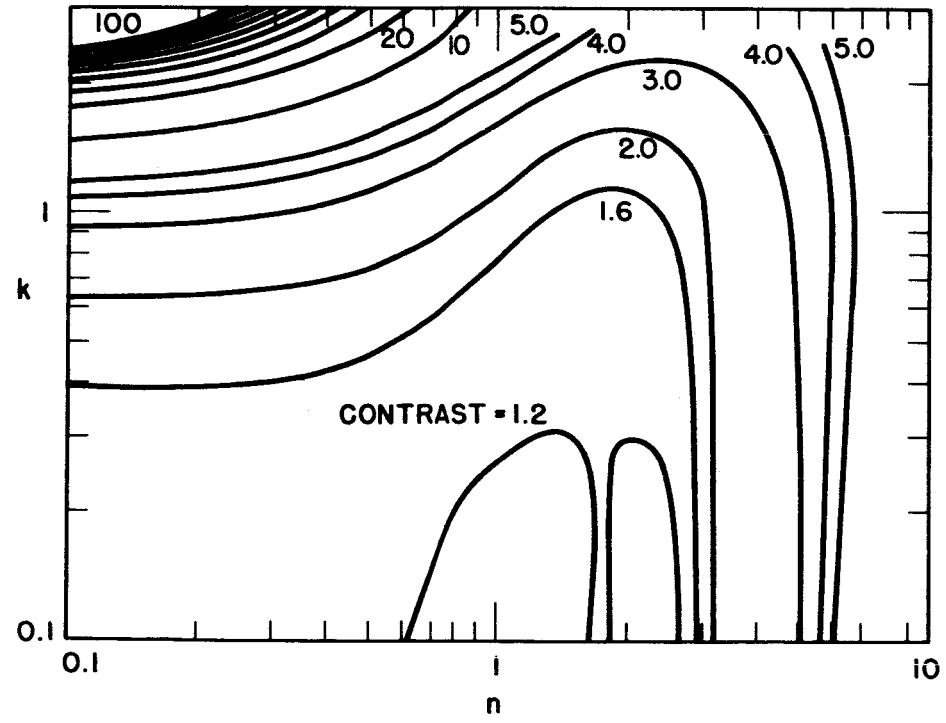

Figure 6 b. Contrast Contours on the Complex N Plane for d = 0.20λ

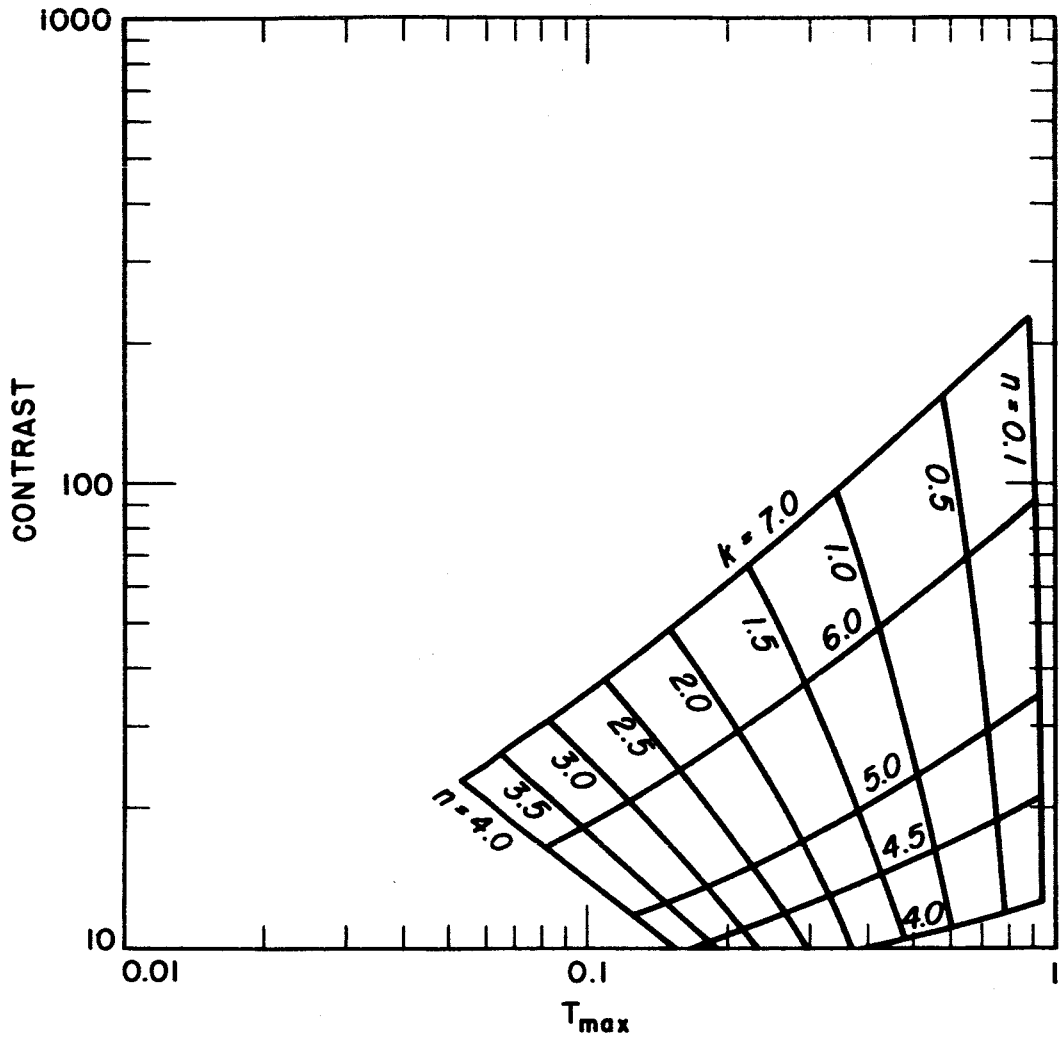

Figure 7. Complex N Mesh on Contrast versus T_{max} Coordinates for $d = 0.05\lambda$

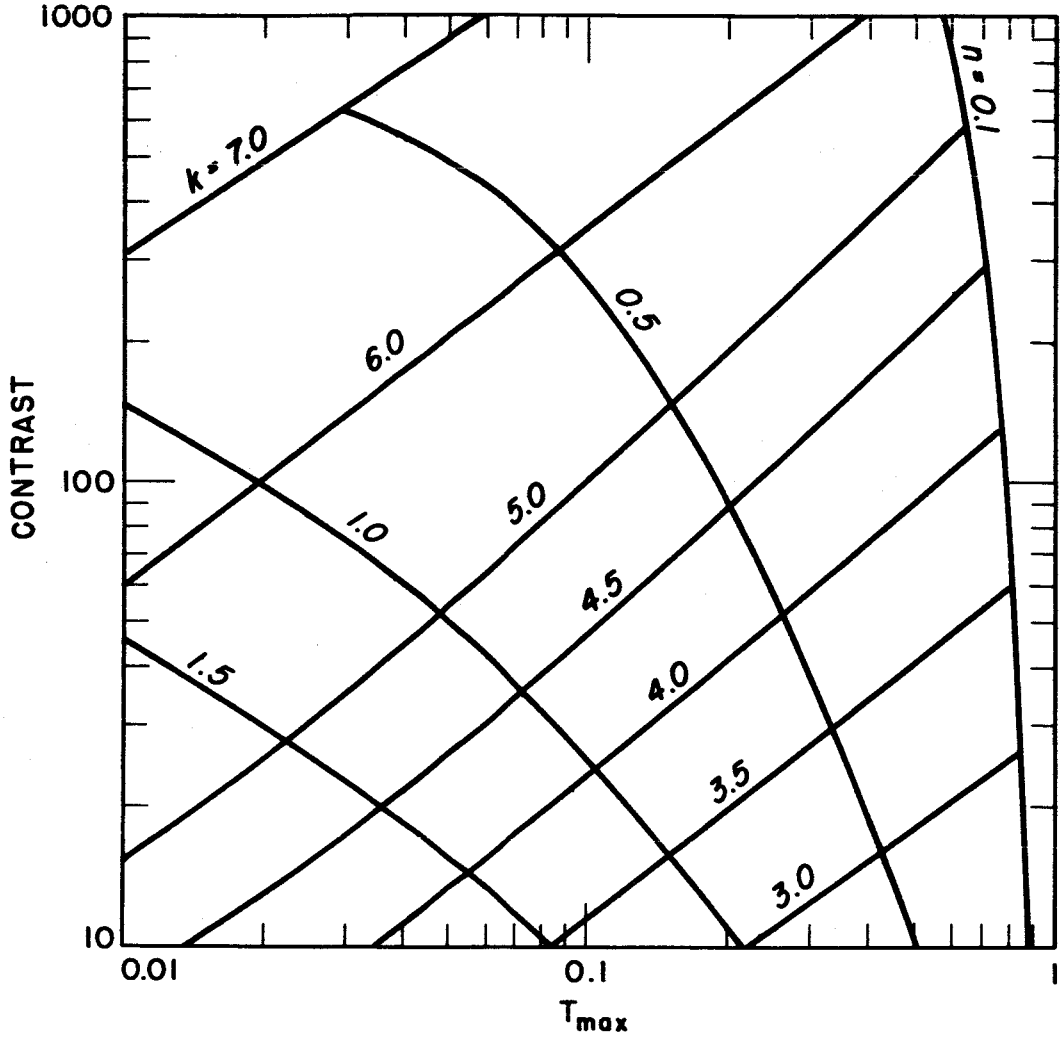

Figure 8. Complex N Mesh on Contrast versus T_{max} Coordinates for $d = 0.10\lambda$

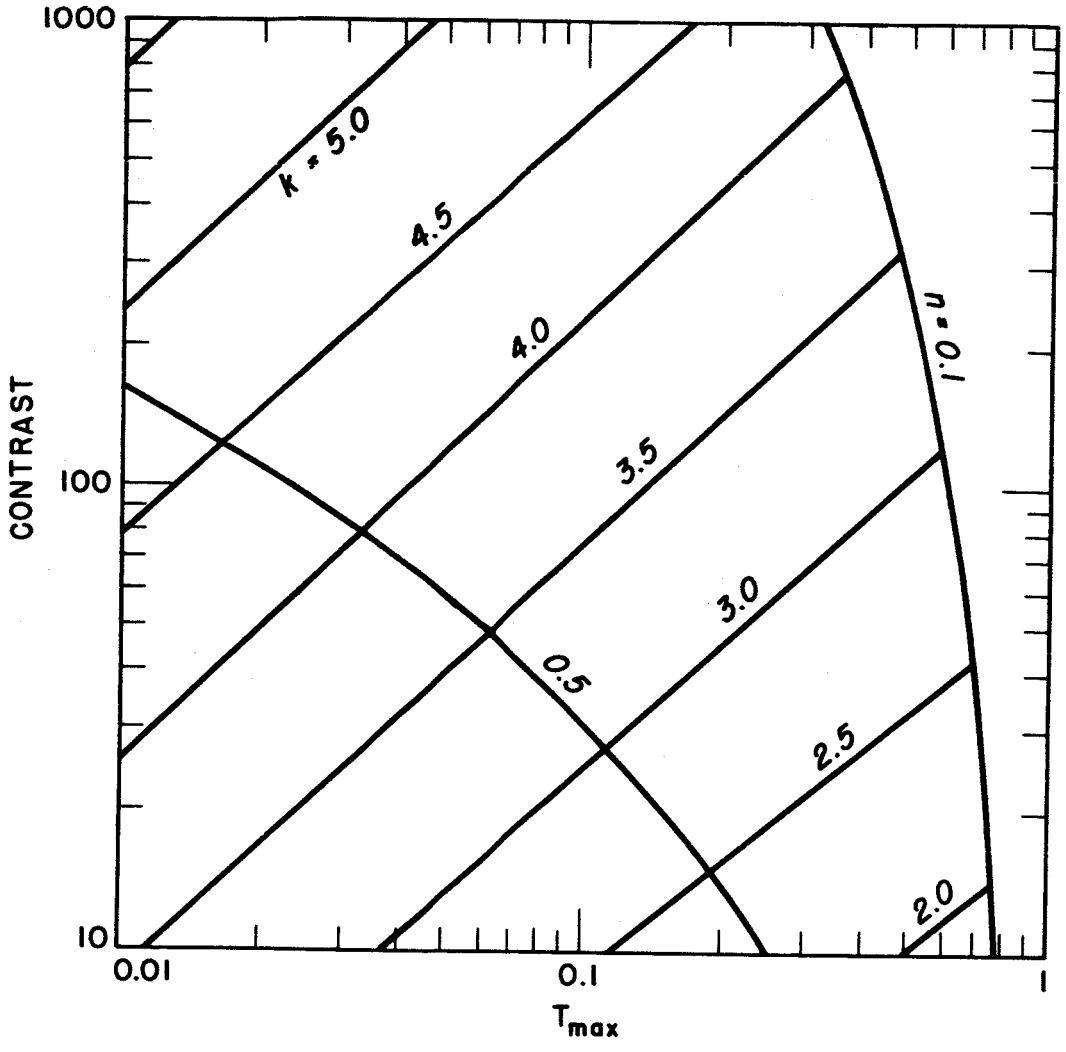

Figure 9. Complex N Mesh on Contrast versus T_{max} Coordinates for $d = 0.15\lambda$

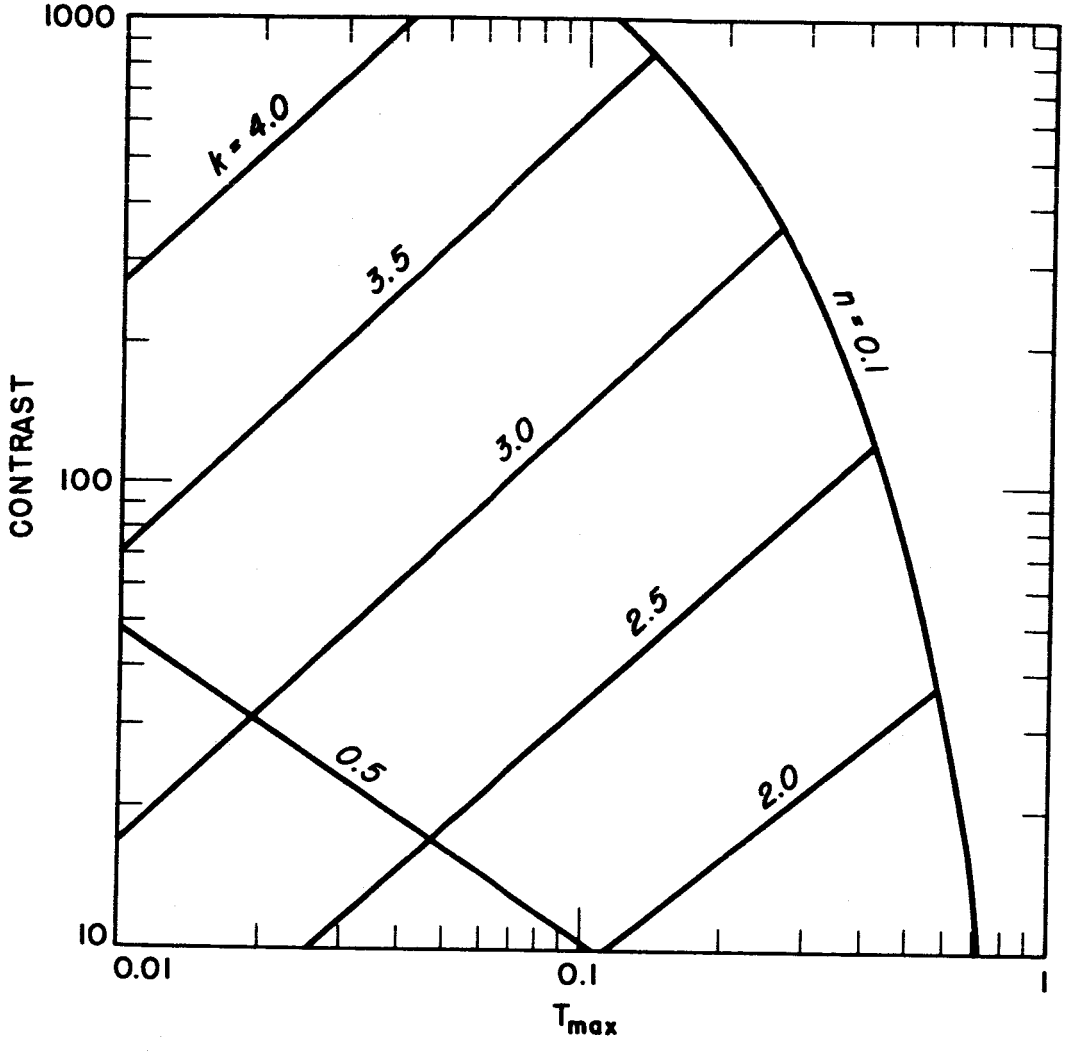

Figure 10. Complex N Mesh on Contrast versus T_{max} Coordinates for $d = 0.20\lambda$

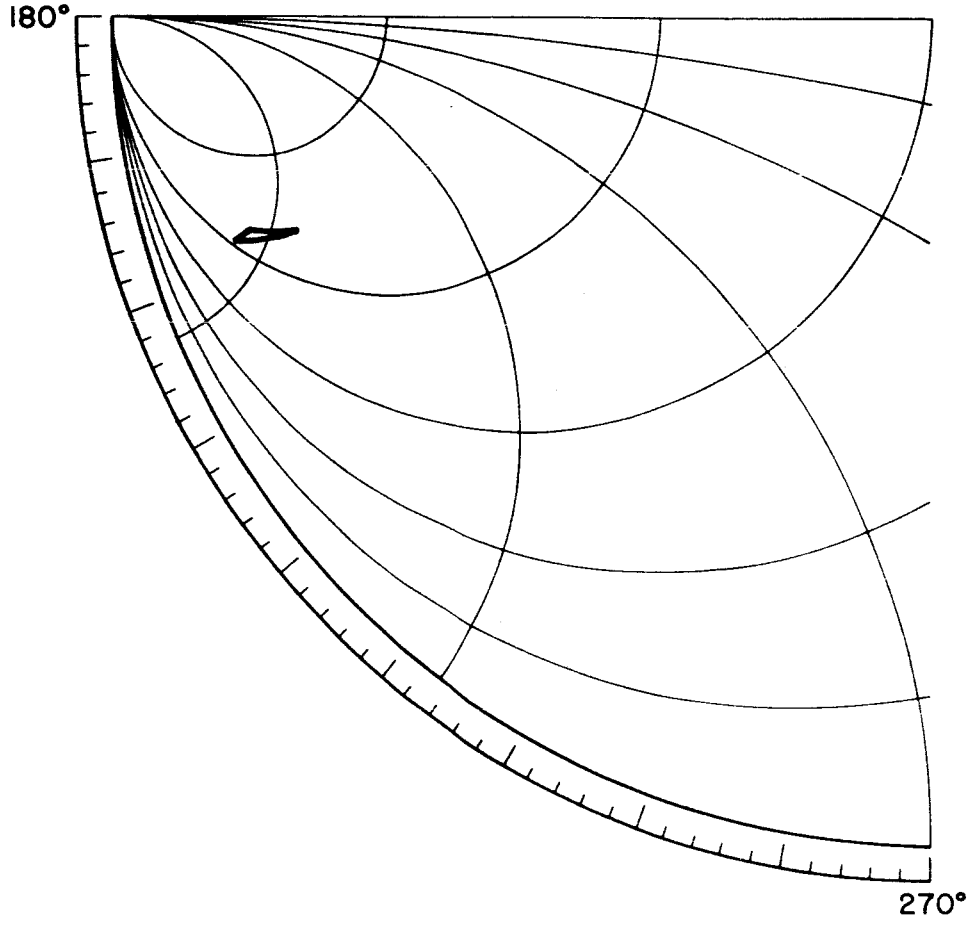

Figure 11. Complex N Mesh on the Complex r Plane for d = 0.05λ

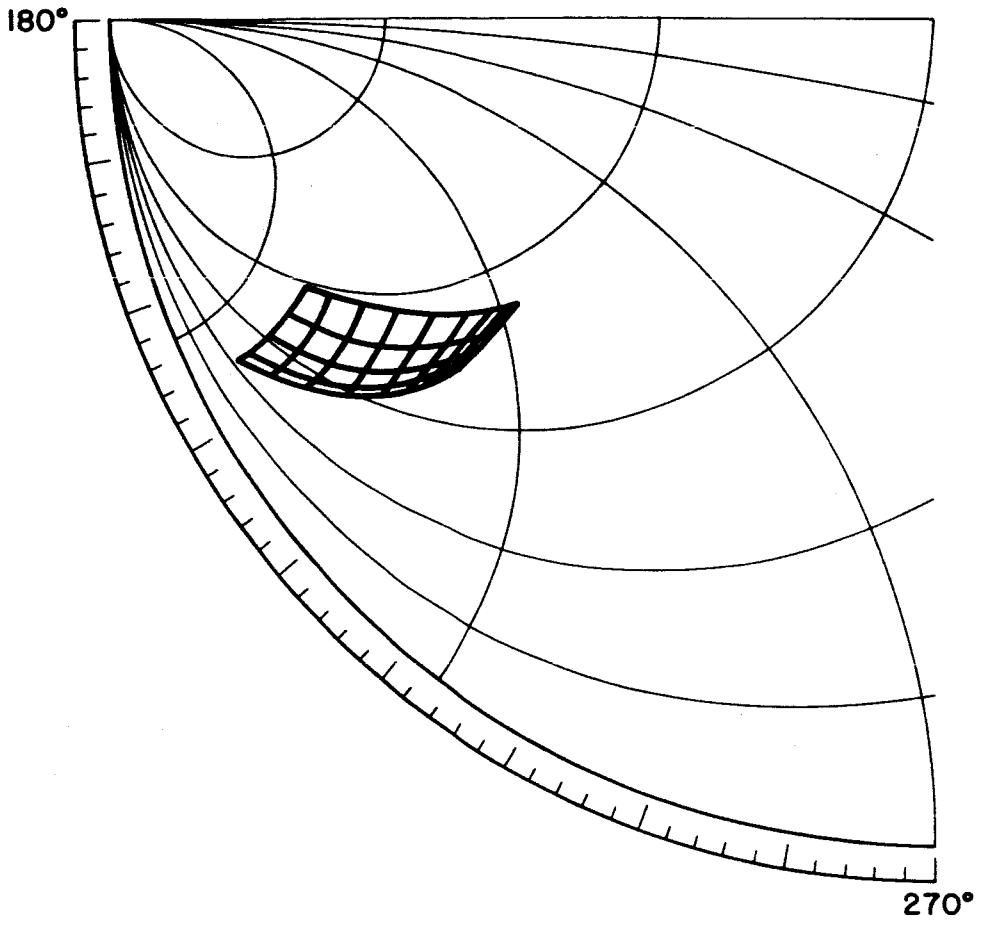

Figure 12. Complex N Mesh on the Complex r Plane for d = 0.10λ

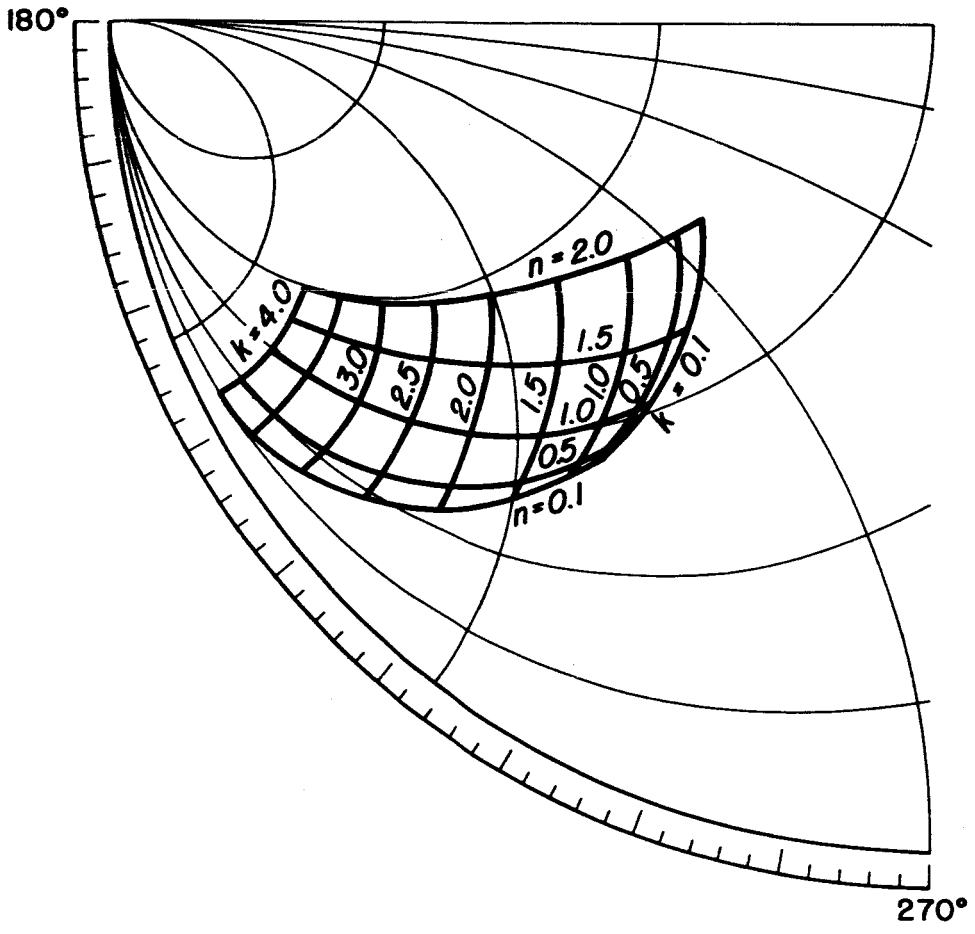

Figure 13. Complex N Mesh on the Complex r Plane for d = 0.15λ

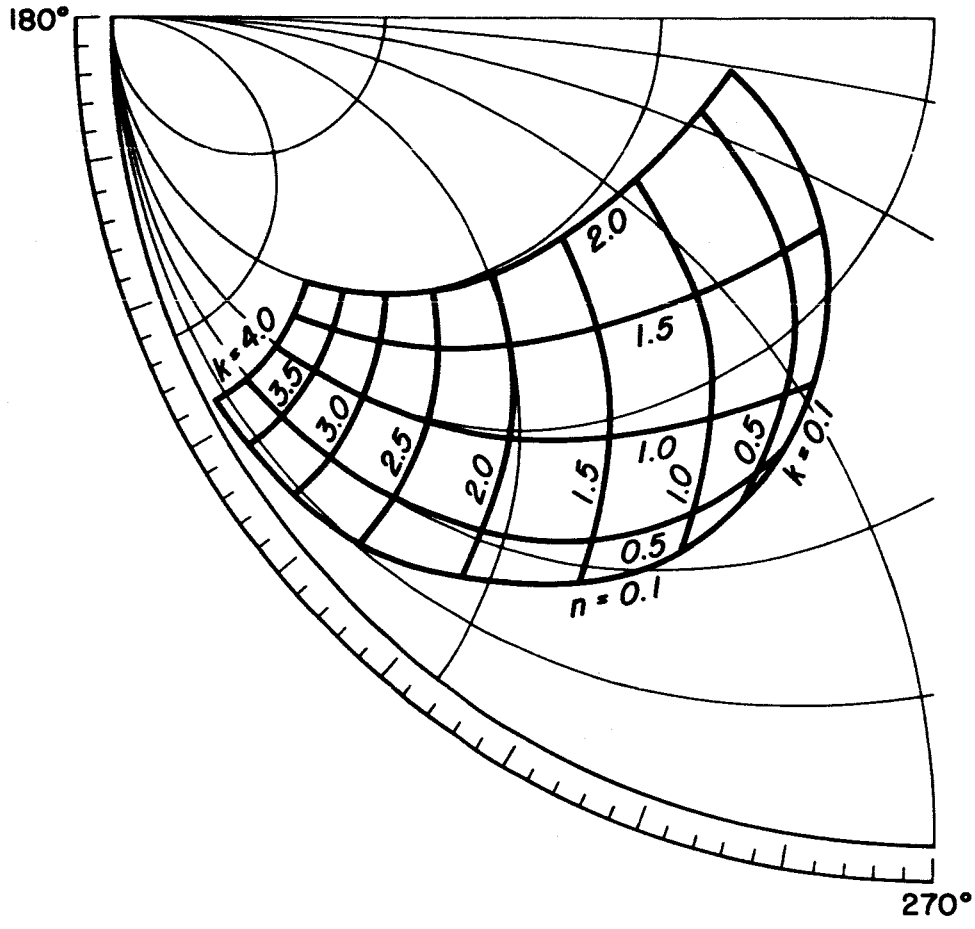

Figure 14. Complex N Mesh on the Complex r Plane for d = 0.20λ

A more convenient set of figures is obtained if these same meshes are plotted on axes of reflectance and phase change upon reflection as shown in Figures 15 through 18.

A Systematic Design Technique Illustrated

In order to illustrate the use of a systematic design technique for a 1M filter we choose as an example a 300 Å film of aluminum with $\tilde{N}_j = 0.195\text{-}i2.75$ at a wavelength of 2537 Å. A contour map of the transmittance function versus Y_j is given on a Smith chart in Figure 19. Note that the maximum transmittance in Figure 19 is 0.64 and occurs at $Y_j = 0.89 + i3.0$.

The most straightforward design for an antireflection stack is a quarter-wave stack plus a phase-matching layer. The parametric plot of the admittance versus wavelength of such a stack is shown in Figure 20. It passes through the region of the peak of the transmittance function at a wavelength of 2537 Å. At wavelengths above 3000 Å the admittance of this stack is in the region of $Y_j = 1.0$, which corresponds to low matching stack reflectance.

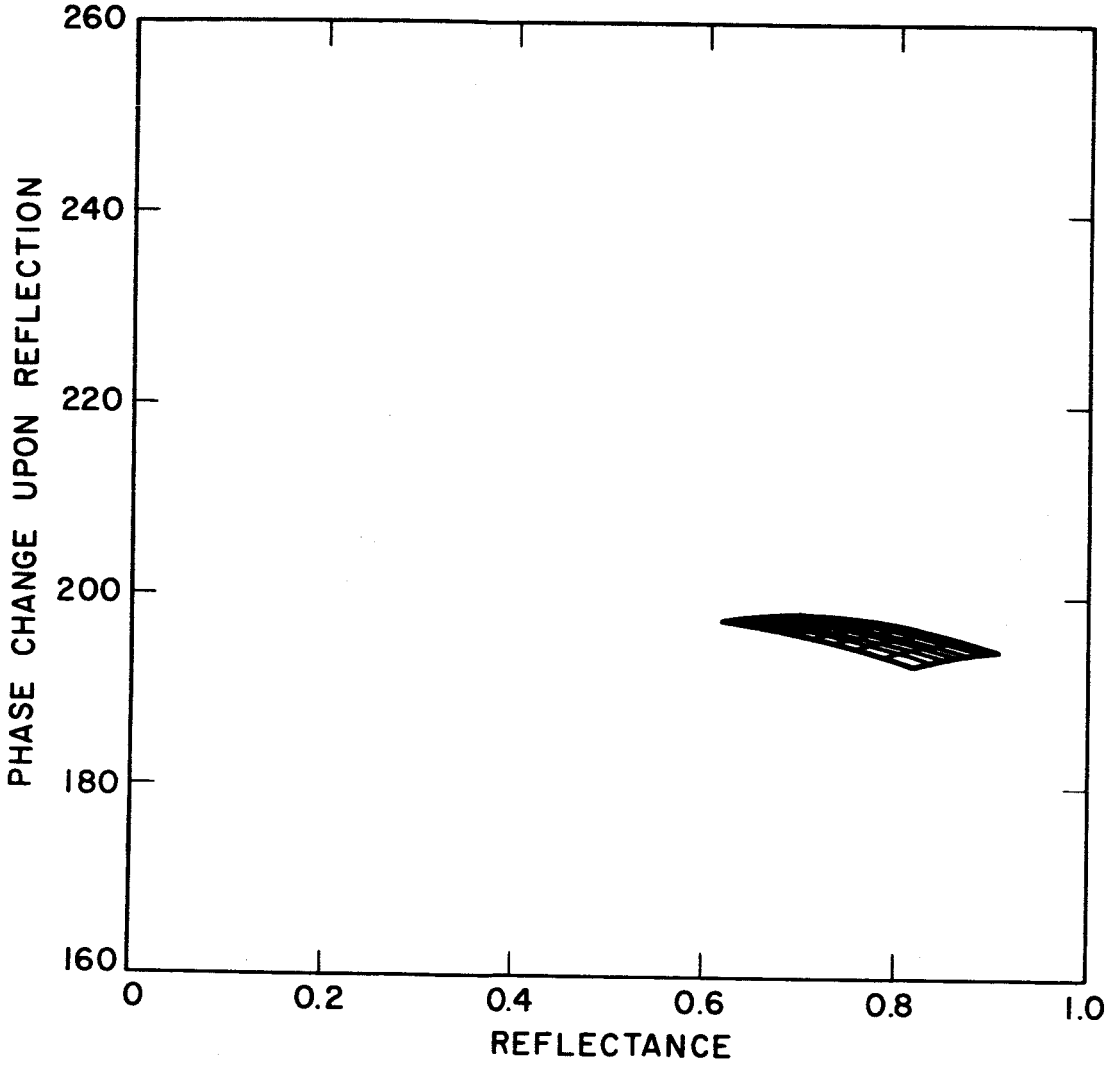

Figure 15. Complex N Mesh on Phase Change versus Reflectance Coordinates for d = 0.05λ

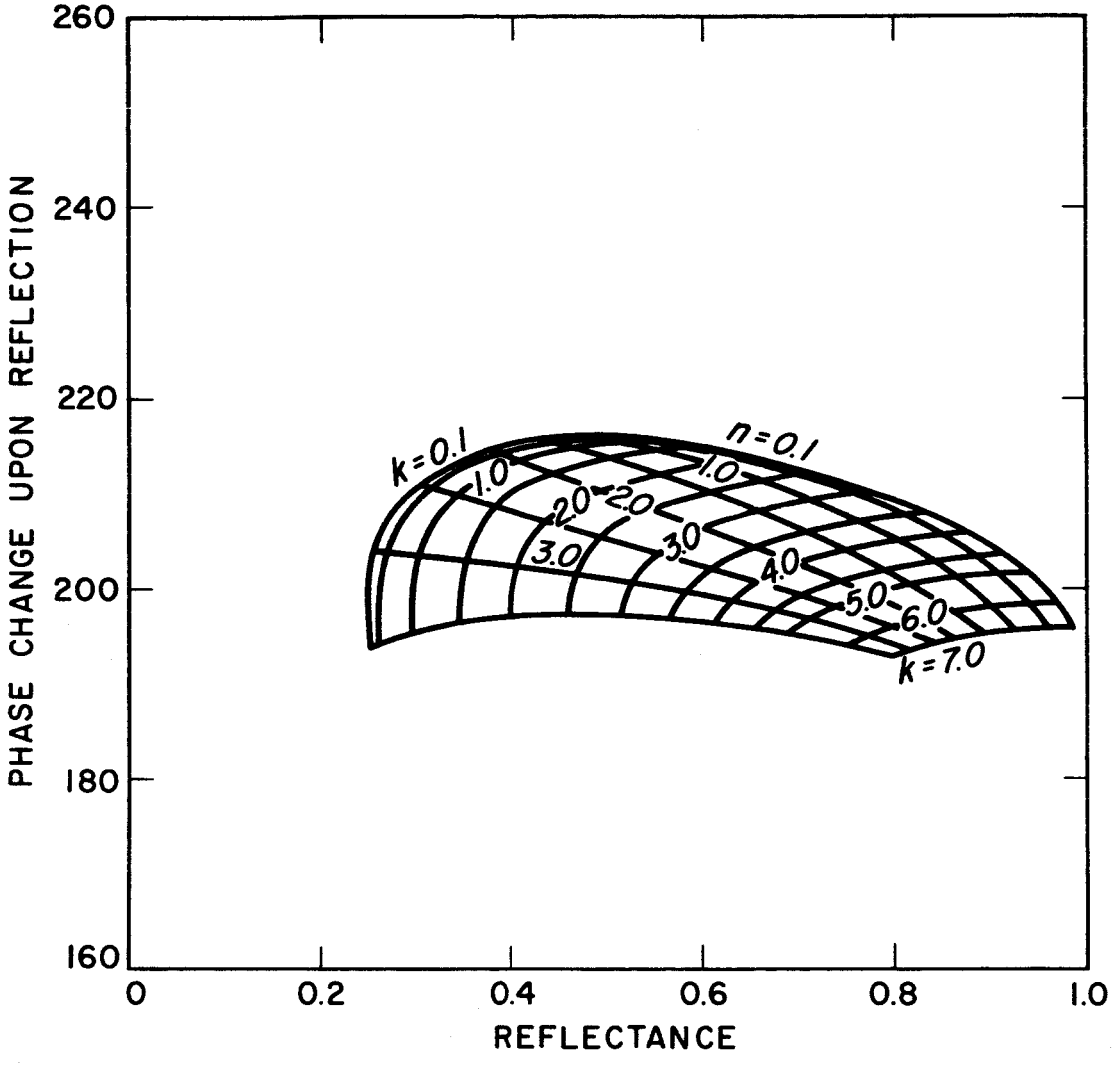

Figure 16. Complex N Mesh on Phase Change versus Reflectance Coordinates for d = 0.10λ

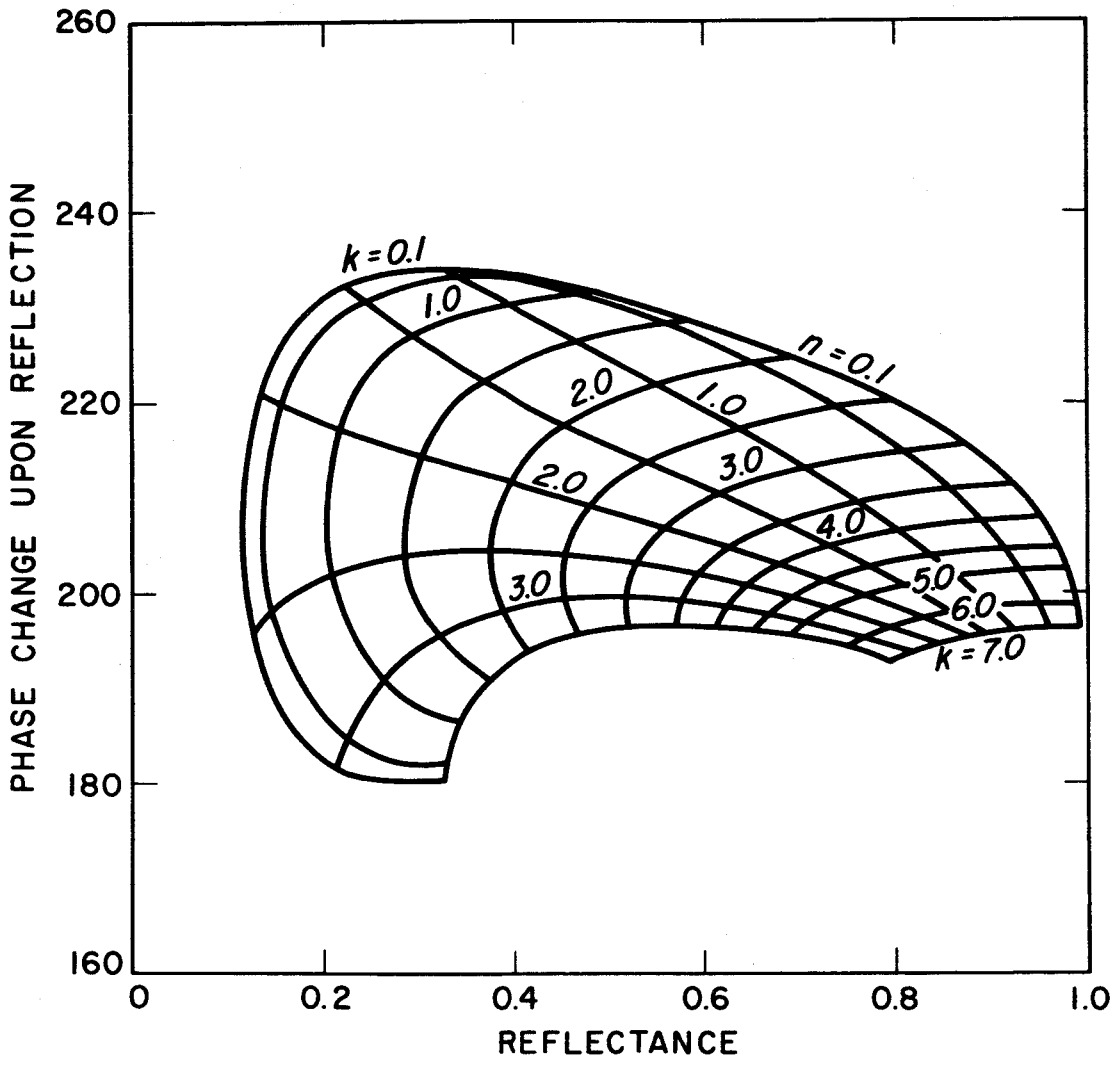

Figure 17. Complex N Mesh on Phase Change versus Reflectance Coordinates for d = 0.15λ

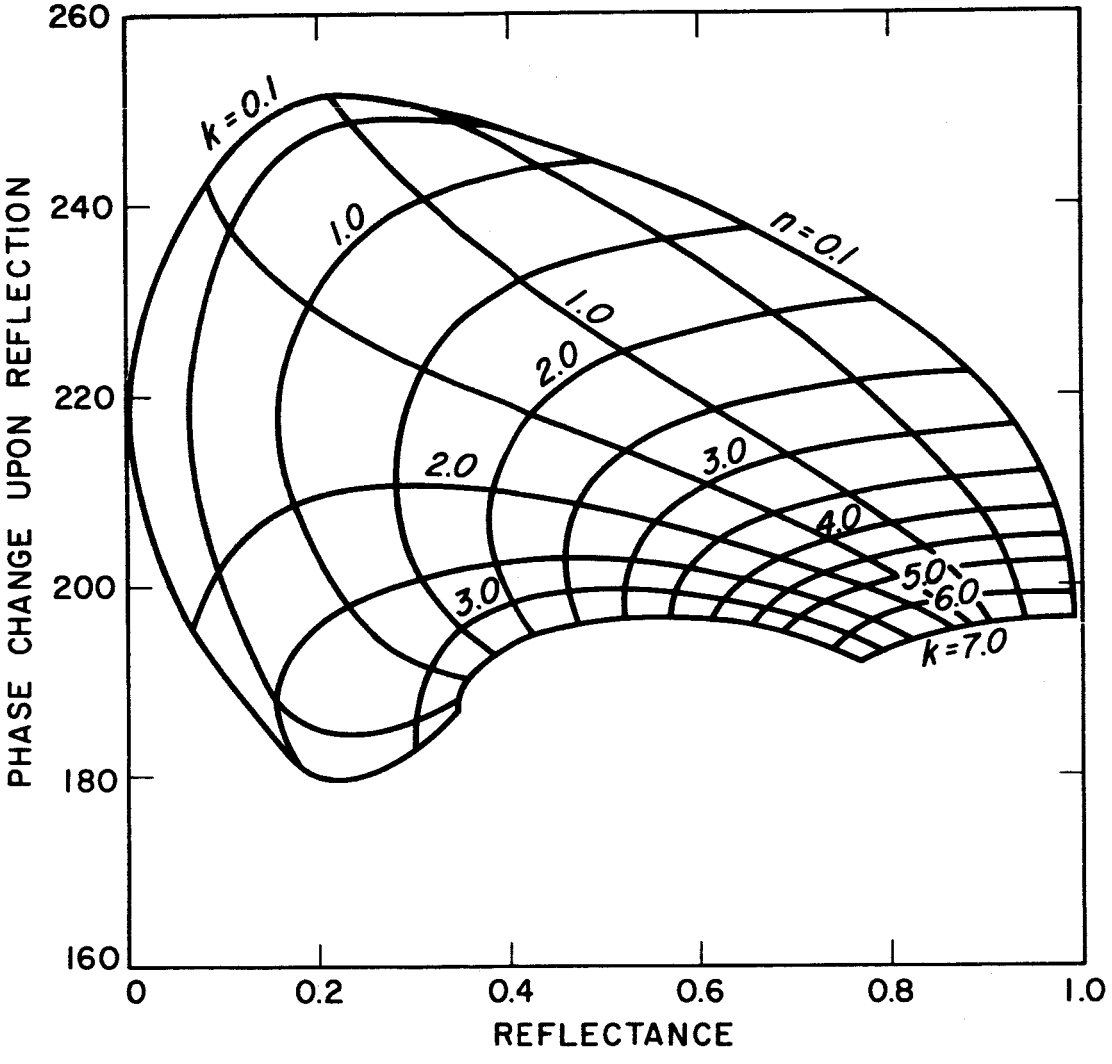

Figure 18. Complex N Mesh on Phase Change versus Reflectance Coordinates for d = 0.20λ

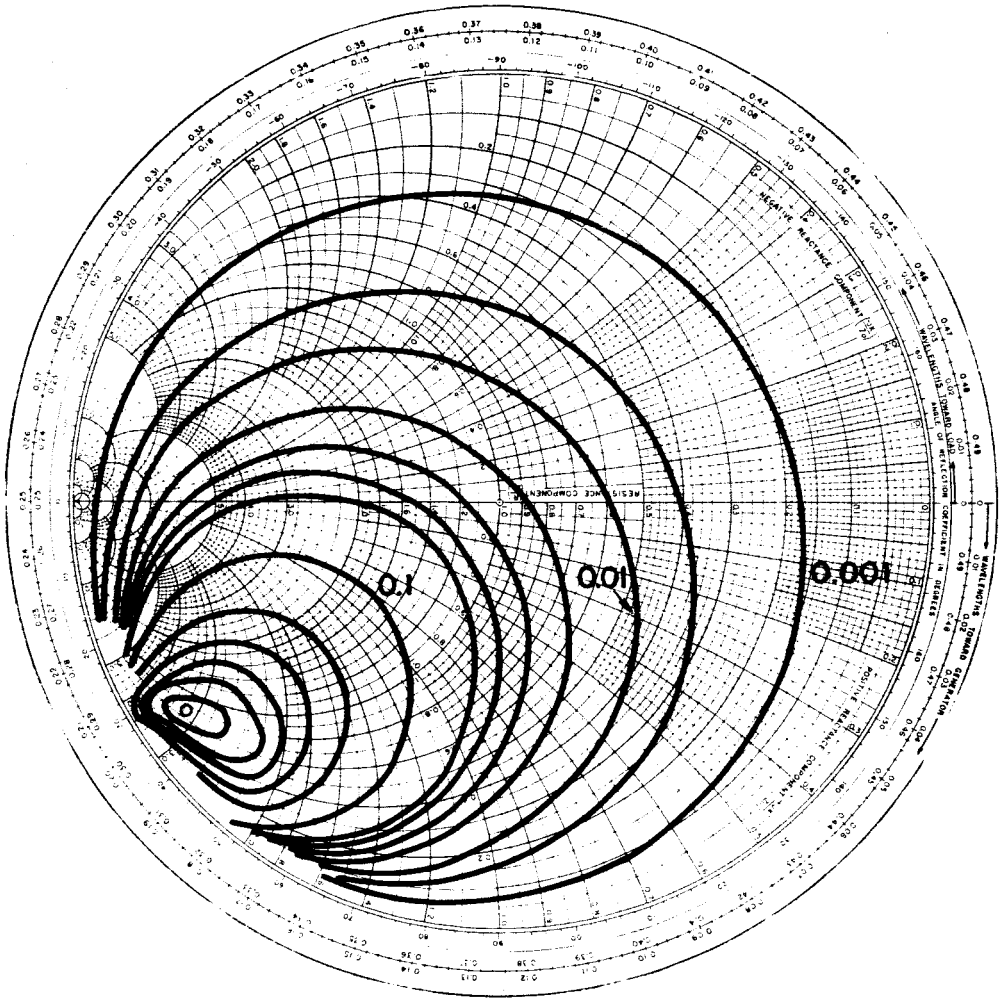

CONTOUR VALUES	
0.001	0.1
0.005	0.2
0.01	0.3
0.02	0.4
0.03	0.5
0.04	0.6
0.05	

Figure 19. Computed 2537 Å isotransmittance Contours for a 300Å Film of Aluminum

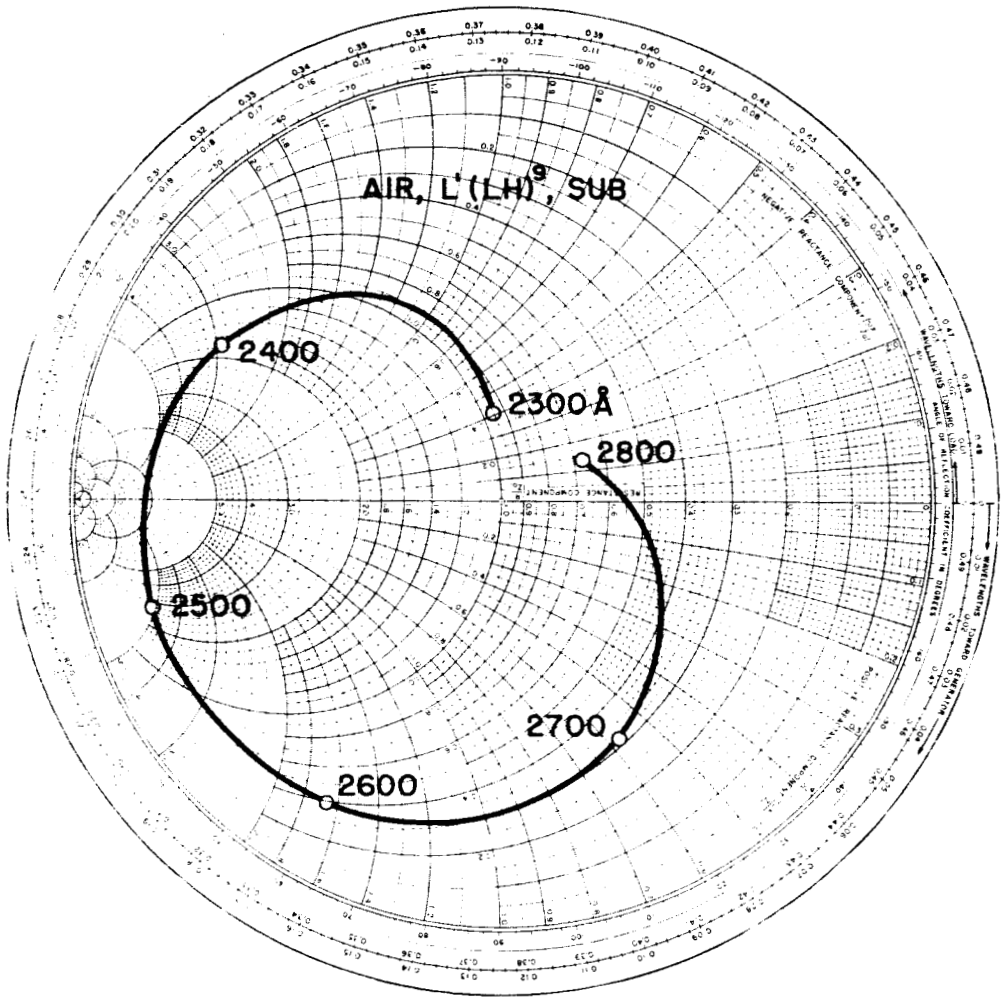

Figure 20. Parametric Admittance Plot for a Possible Matching Stack

With the antireflection stack of Figure 20 on one side of the 300 Å aluminum film and another of similar design admittance matching the aluminum to air interface, the transmittance curve shown in Figure 21 is computed. Notice that the transmittance reaches 0.64 at 2537 Å and is approximately 0.02 at wavelengths above 3000 Å. As would be expected, this corresponds to the transmittance for $Y_j = 1.0$ which from Figure 19 is 0.025. The ratio between T_{max} and the transmittance at $Y_j = 1.0$ is a measure of the contrast attainable. In this example, the computed contrast is 26.

Filters Which Contain One Aluminum Layer

Our specific interest is directed toward filters for the ultraviolet. In this region, aluminum is the only thin film material with k high enough to provide both good contrast and reasonable transmittance, as can be seen from Figures 3 through 6. To show the characteristics of ultraviolet filters with a single aluminum film, computations are made at seven evenly spaced wavelengths from 1600 to 4000 Å and for each of five film thicknesses from 100 to 500 Å. The quantities computed are T_{max},

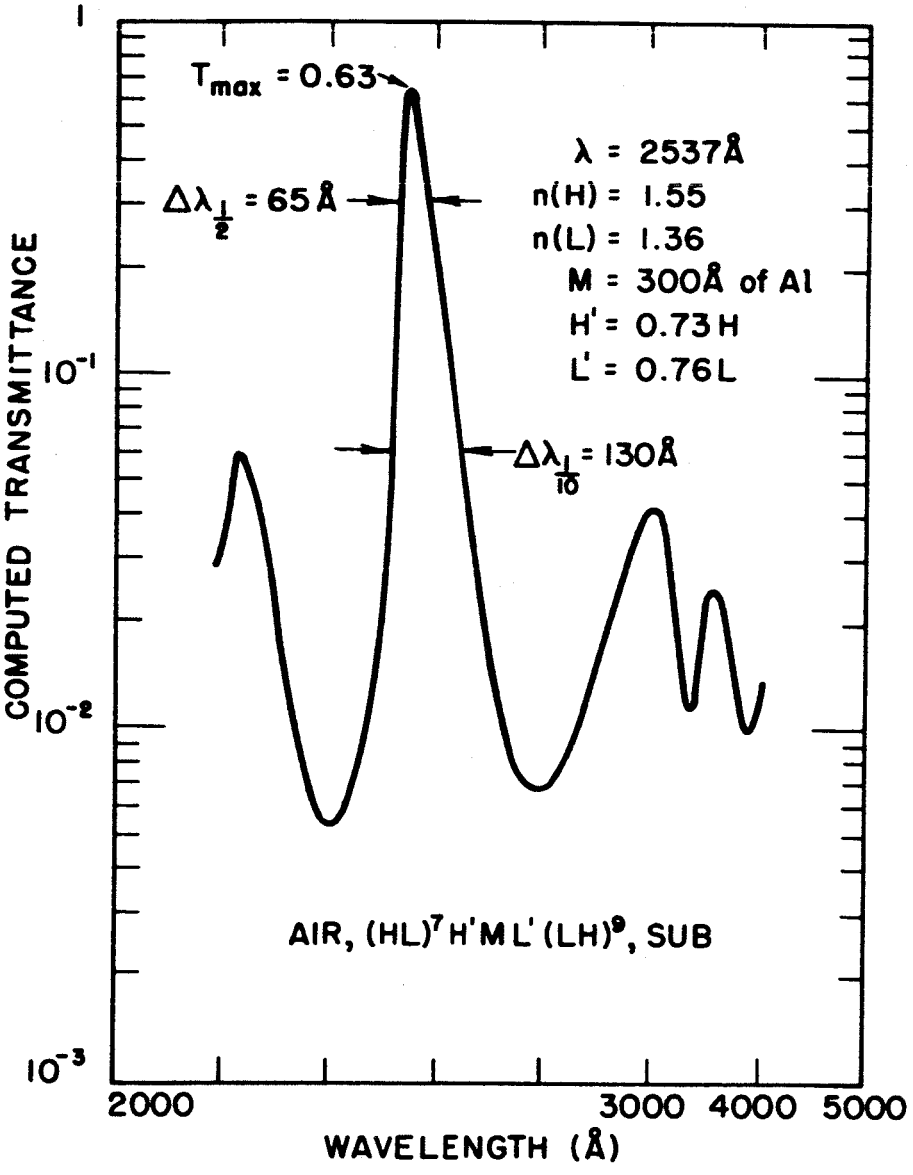

Figure 21. Computed Transmittance of a 1M Filter

contrast, and finesse angle, which is a measure of the bandpass of the filter.

The optical constants assumed for the computations of Figures 22 through 25 were obtained from Hunter[23] and are presented in Table 1 for the wavelengths being considered.

Table 1.

Optical Constants of Aluminum

Wavelength (Å)	Wavenumber (cm^{-1})	n	k
1600	62500	.0863	1.6248
2000	50000	.1263	2.1617
2400	41667	.1758	2.6728
2800	35736	.2342	3.1694
3200	31250	.3015	3.6561
3600	27778	.3772	4.1352
4000	25000	.4612	4.6077

The value of T_{max} versus wavelength is shown in Figure 22 in the ultraviolet region from 1600 to 4000 Å for filters containing a single aluminum film. The numbers on the curves correspond to the thickness of the aluminum

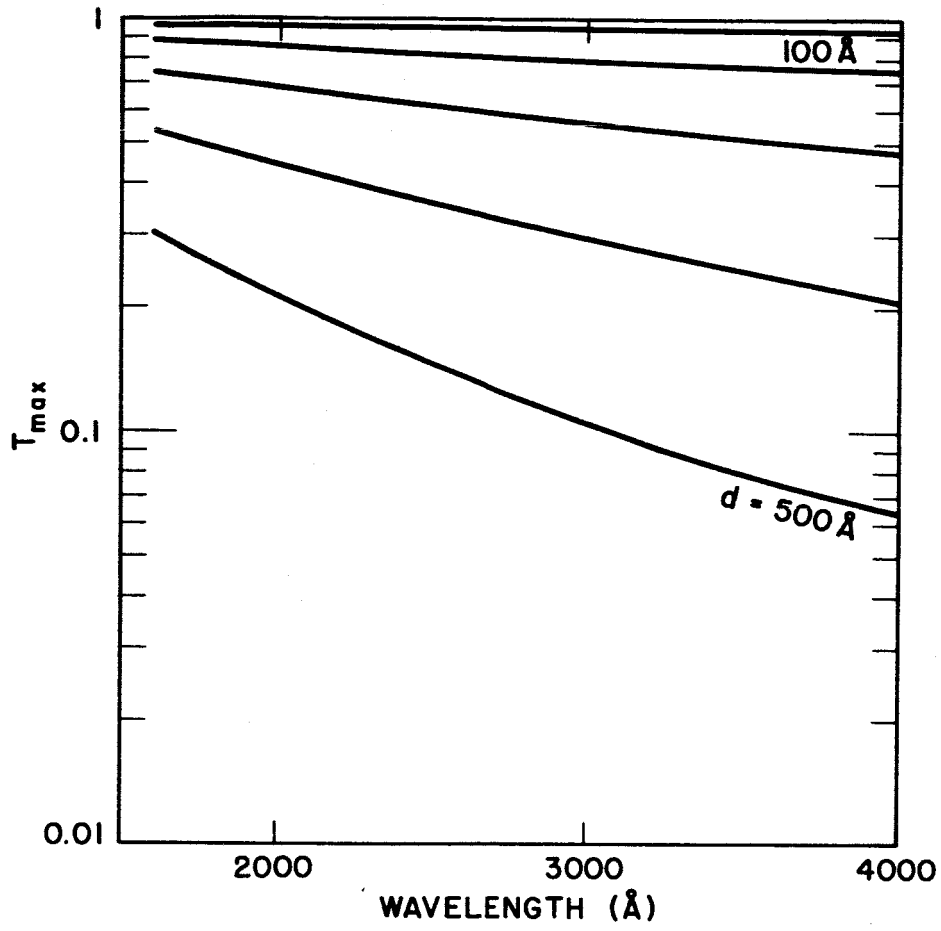

Figure 22. T_{max} versus Wavelength and d for Aluminum

film. Similarly, Figure 23 presents the contrast versus wavelength and aluminum film thickness in the 1M filter.

As can be seen by referring to Figures 19 and 20, the bandpass of the 1M filter depends on the phase dispersion of the antireflection stacks as well as the shape of the transmittance peak in the r plane. Therefore, we cannot determine the bandpass versus wavelength and aluminum film thickness for an aluminum 1M filter. However, a measure of the bandpass is the angle subtended at the origin of the r plane by the arc segment which passes at constant amplitude through Y_{pk} and is inside the $1/2(T_{max})$ transmittance contour. Figure 24 a. illustrates how this finesse angle is defined.

Assume that the amplitude reflection coefficient of the antireflection stacks may be represented by

$$r = |r| \exp\left[i\left(\delta_0 + \delta_1 \frac{\Delta\lambda}{\lambda_0}\right)\right] \tag{107}$$

where

$$\Delta\lambda = \lambda - \lambda_0 \tag{108}$$

If we set

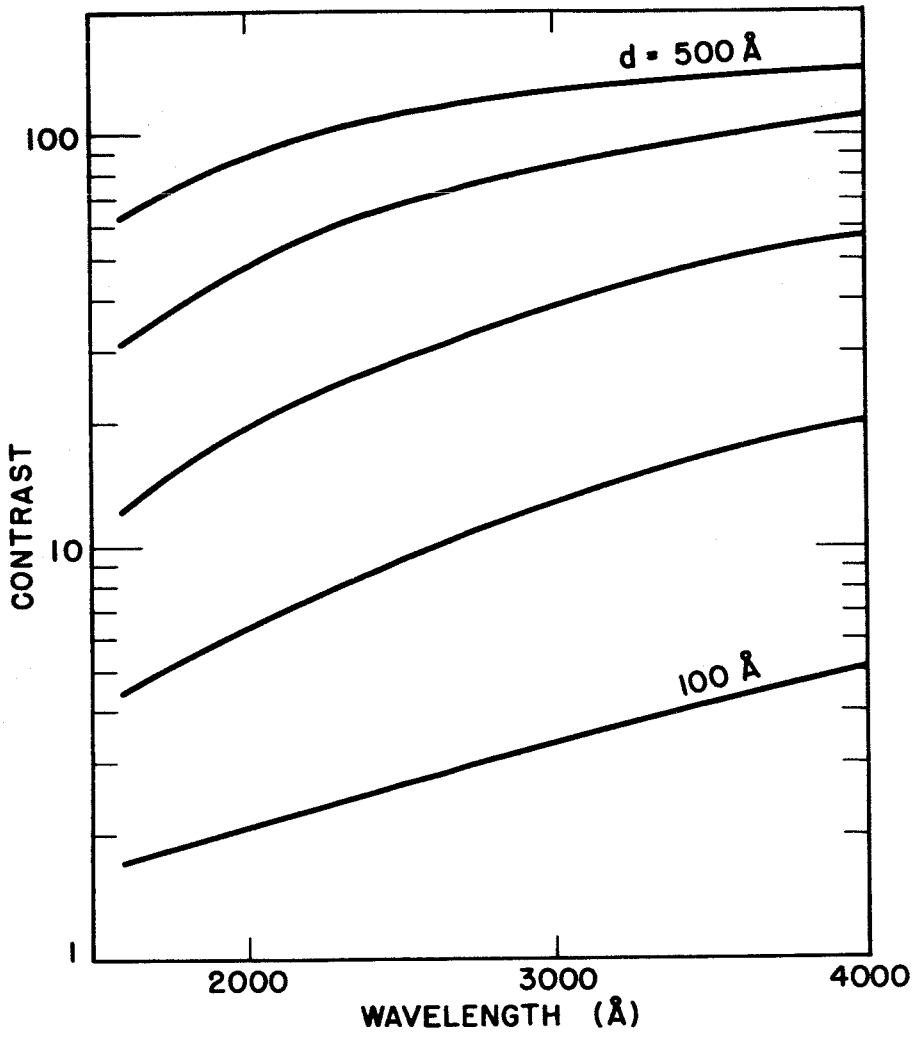

Figure 23. Contrast versus Wavelength and d for Aluminum

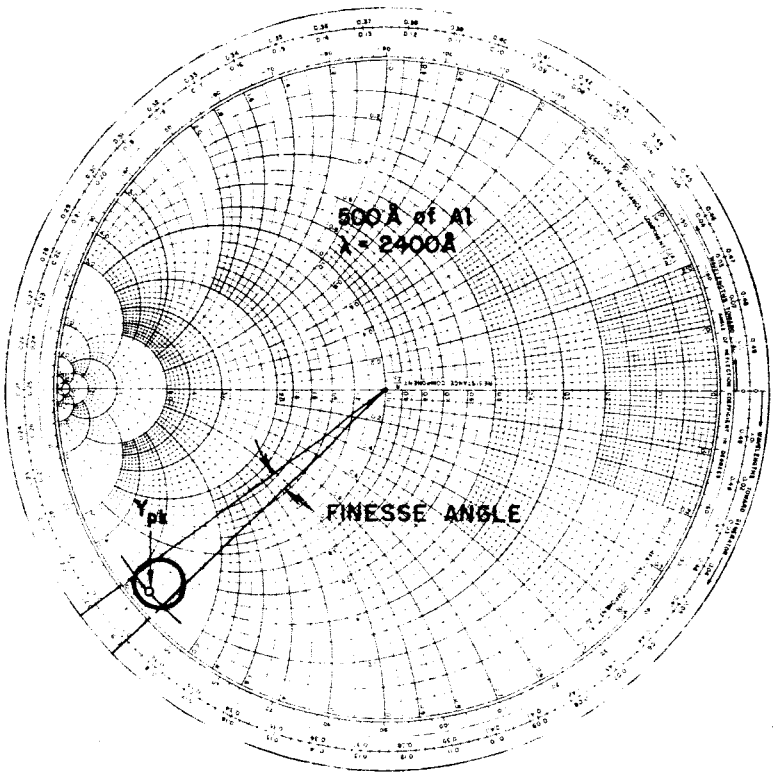

Figure 24 a. Illustration of the Determination of the Finesse Angle

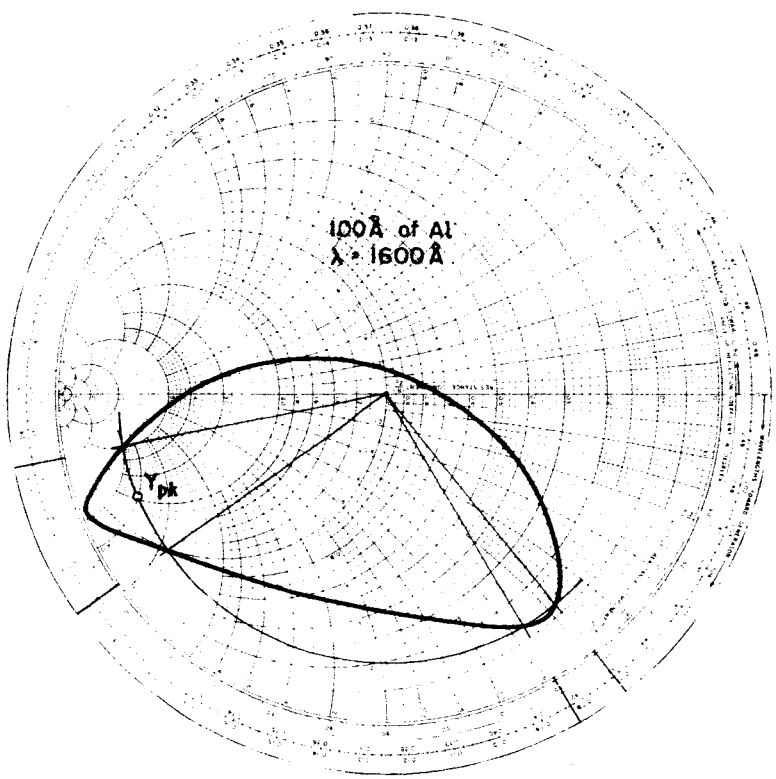

Figure 24 b. Example in Which the Finesse Angle Is Meaningless

$$\frac{\delta_1 \Delta\lambda}{\lambda_0} = \frac{1}{2}\,(\text{Finesse Angle}) \tag{109}$$

then the passband, i.e., the full width at $1/2(T_{max})$ is

$$\Delta\lambda_{\frac{1}{2}} = \frac{\lambda_0}{\delta_1}\,(\text{Finesse Angle}) \tag{110}$$

and the resolution obtainable is given by

$$\frac{\lambda_0}{\Delta\lambda_{\frac{1}{2}}} = \frac{\delta_1}{(\text{Finesse Angle})} \tag{111}$$

The assumption of equation 103 is good for anti-reflection stacks of the type illustrated in Figure 20 but is quite poor for some stack designs (cf. Figure 31). As shown in Figure 24 b., the arc representing equation 103 may cut the $1/2(T_{max})$ contour twice. This corresponds to a situation in which there are two maxima, the second more than half as high as the first, in which case the finesse angle is not a very useful concept.

The values of the finesse angle, determined graphically for the wavelengths and aluminum film thicknesses

being considered, are shown in Figure 25. The data corresponding to an aluminum 100 Å thick are not included because they result from a situation of the type shown in Figure 24 b. and are so erratic that they would confuse Figure 25. It should be noted that for the antireflection stack illustrated in Figure 4 the magnitude of δ_1, is 18.1 radians or 1040. degrees.

Use of the Computed Characteristics

To show how Figures 22, 23 and 25 are used in determining the design, assume that there is need for a 30 Å bandpass filter at 2000 Å with a contrast greater than thirty and a peak transmittance above 0.10. From Figure 22 we note that the thickness of the aluminum film must be less than 550 Å to get a peak transmittance above 0.10, while from Figure 23 a contrast greater than 30. corresponds to a thickness above 350 Å. This gives us a range of film thickness to investigate with respect to bandpass.

Solving equation 107 for the finesse angle as a function of the phase dispersion and the desired resolution:

$$\text{Finesse Angle} = \frac{\delta_1}{\left(\frac{\lambda_0}{\Delta\lambda_{\frac{1}{2}}}\right)} \qquad (112)$$

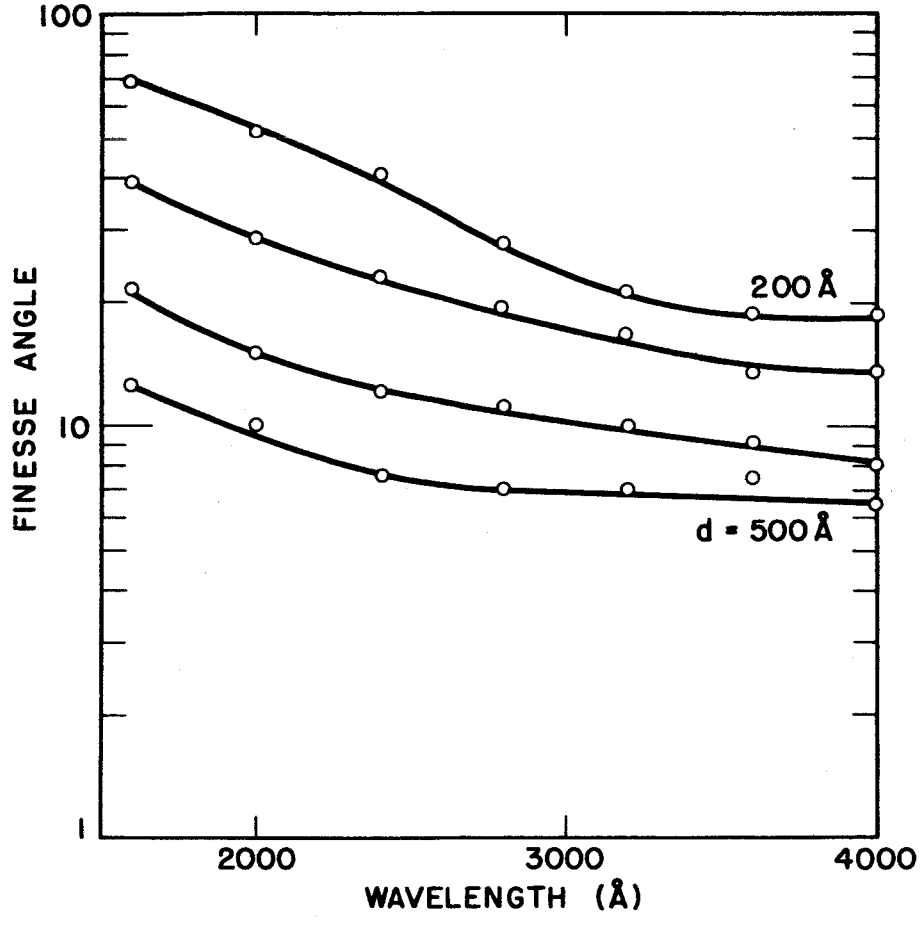

Figure 25. Finesse Angle versus Wavelength and d for Aluminum

Using the above value of 18. radians for the phase dispersion of the matching stacks and the specified resolution, (2000/30) = 67., the maximum finesse angle is

$$\text{Finesse angle} \leq \frac{18.}{67.} = 0.27 \text{ radians} = 15.5^{\circ} .$$

The corresponding minimum film thickness in Figure 25 is 400 Å. A reasonable compromise between this thickness and the 550 Å mentioned above is 450 Å, which provides the following computed features:

$T_{max} = 0.32$

Contrast = 66.

Finesse angle = $12.^{\circ}$ = .21 radians

Resolution = 86.

Bandpass = 23. Å

These quantities are well within the specifications and should be obtainable in practice. A relatively thin film is chosen from the range 400-500 Å because the tolerances on the antireflection stacks are less stringent for thinner films.

Dependence on the Optical Constants of the Aluminum

In order to determine the dependence of the filter on the optical constants of the aluminum, refer to Figure 4. In the neighborhood of $N = .195-2.75$, which is the index of refraction of aluminum at 2537 Å, a change in n will not greatly affect the value of the contrast and only slightly change T_{max}. In the same region, a change in k will greatly alter the contrast while still only slightly affecting T_{max}. In Figure 26 a. the 2537 Å isotransmittance contours are shown for a 300 Å film of aluminum which has its value of n increased by ten per cent of its original value. The shape and size of the peak are essentially unchanged. The second part of Figure 26 shows the result of decreasing k by ten per cent of its original value. In this case the peak retains its shape and nearly the same peak transmittance but expands in such a manner that the contrast is decreased to half its previous value.

Overmatching to Obtain Narrower Bandpass

The transmittance contours of Figures 19 and 26 indicate that a narrower transmittance peak would result if the parametric admittance of the matching stacks were to

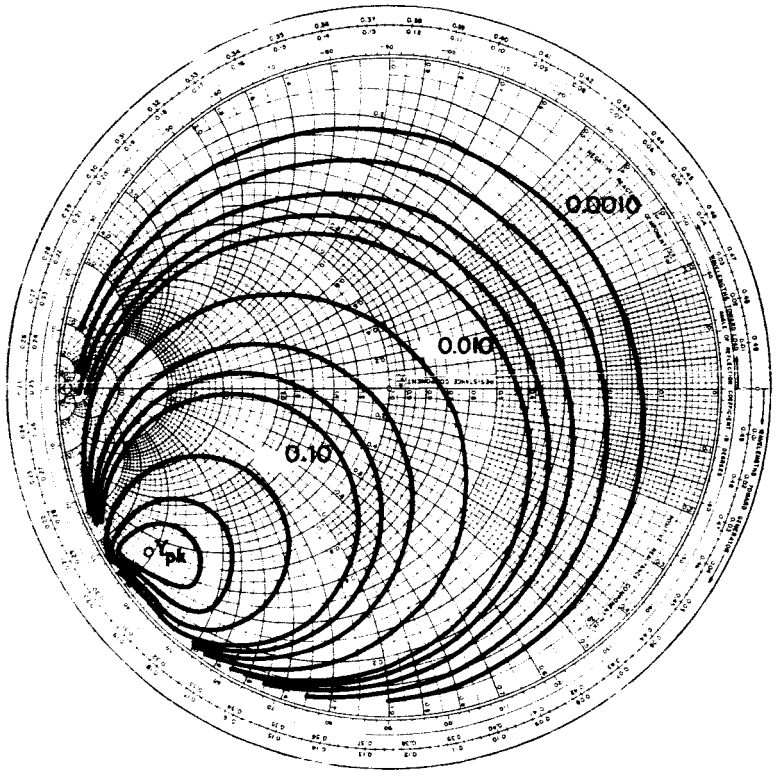

CONTOUR VALUES

0.75 x T_{max}
0.50
0.25
0.10
0.075
0.050
0.025
0.010
0.0075
0.0050
0.0025
0.0010

(T_{max} = 0.61)

Figure 26a. 2537Å Isotransmittance Contours for a 300Å Film of Aluminum When n Is Increased Ten Percent

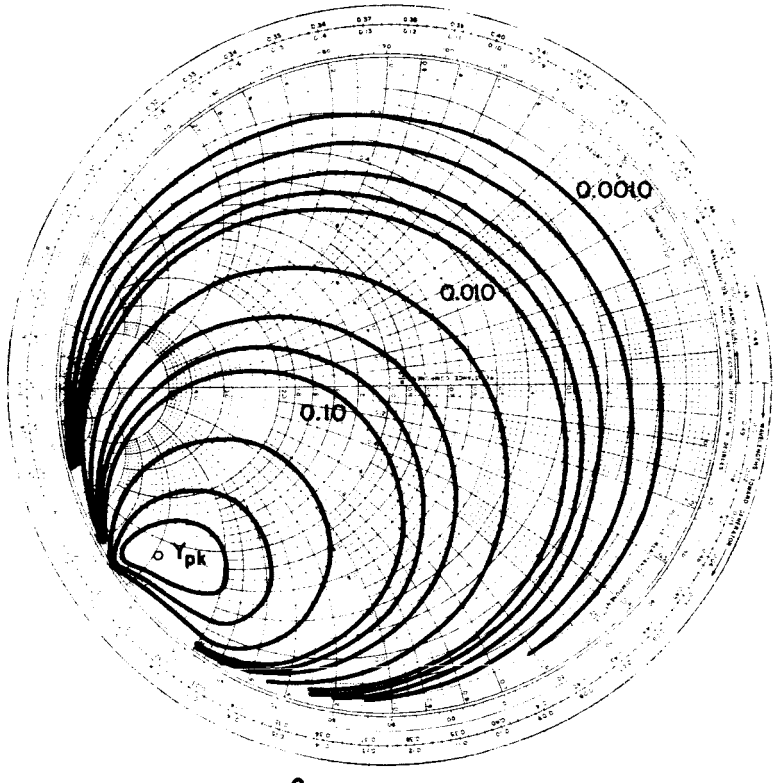

CONTOUR VALUES

0.75 x T_{max}
0.50
0.25
0.10
0.075
0.050
0.025
0.010
0.0075
0.0050
0.0025
0.0010

(T_{max} = 0.68)

Figure 26b. 2537Å Isotransmittance Contours for a 300Å Film of Aluminum When k Is Decreased Ten Percent

bypass Y_{pk} at a greater distance from the origin of the r plane. Such a filter is called an overmatched 1M filter and might be designed by increasing the number of periods in the quarter-wave stacks used as the basis of anti-reflection multilayers. The results of varying the number of periods in this manner to produce both overmatched and undermatched 1M filters is shown in Figure 27. Over-matching yields a narrower transmittance peak with little loss of peak transmittance.

Results of Using Different Matching Stacks

It may be that the large number of layers in the design shown in Figure 21 is undesirable. Fewer layers would suffice to reach Y_{pk} if the mismatch between the high and low index materials were increased. At wave-lengths longer than 2300 $\mathring{A}$ we can use PbF_2. The paper by Honcia and Krebs[8] is the source of the optical constants of PbF_2 which are given in Table 2.

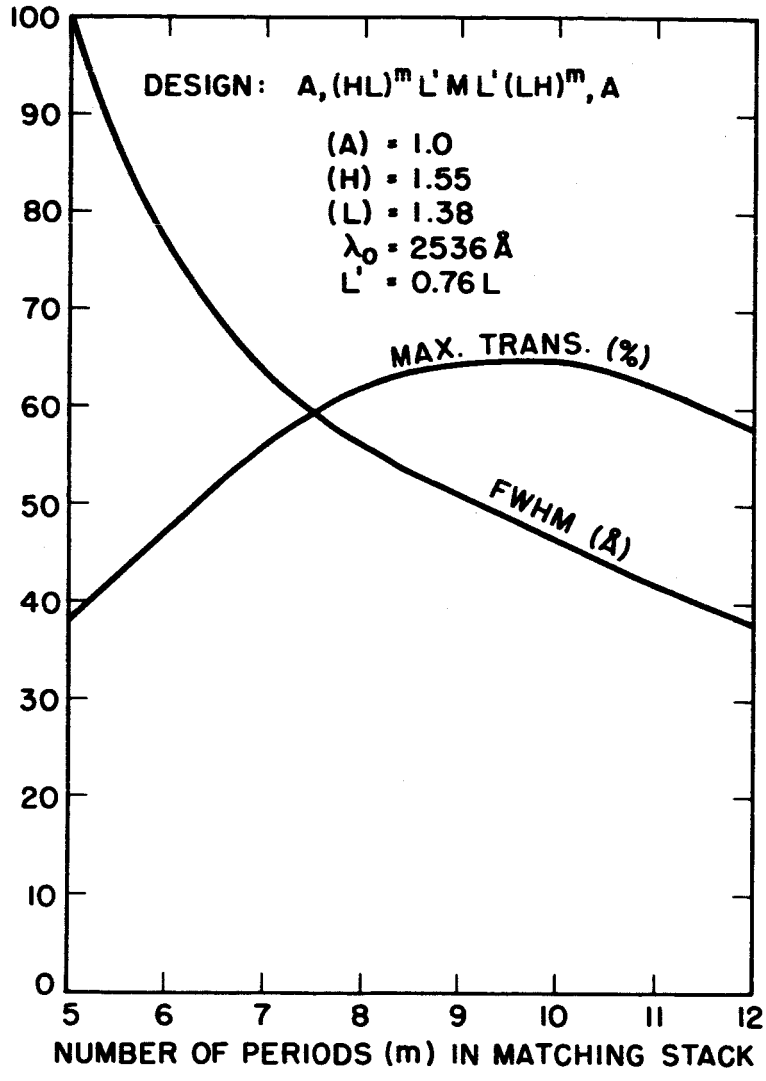

Figure 27. T_{max} and Bandpass for Overmatched and Undermatched 1M Filters

Table 2.

Optical Constants of PbF_2

Wavelength (Å)	Wavenumber (cm^{-1})	n	k
2285	43750	2.50	0.040
2352	42500	2.30	0.030
2500	40000	2.08	0.015
2666	37500	1.99	0.009
2857	35000	1.93	0.004
3333	30000	1.89	0.002
4000	25000	1.78	0.000

These optical constants were used in the computations for Figure 28 of the transmittance of an aluminum film 400 Å thick with matching stacks composed of cryolite and lead fluoride. Although a broader transmittance peak is expected when fewer layers are used in the matching stacks, the peak in Figure 28 is narrower than that in Figure 21 due to the increased aluminum thickness as well as the dispersion of the optical constants of PbF_2. Note also that the onset of absorption in the PbF_2 rids the filter of the shorter wavelength sidepeaks.

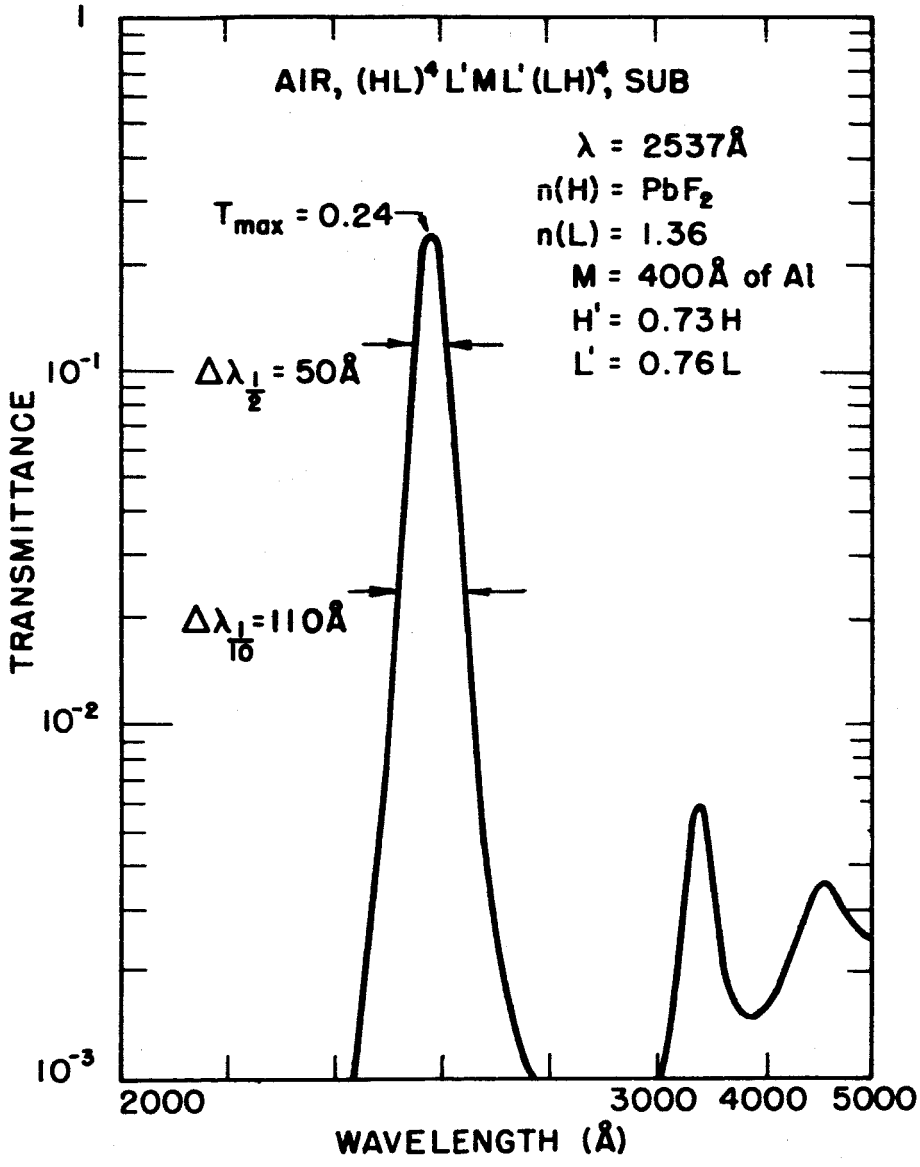

Figure 28. Transmittance of a 1M Filter Using PbF_2 as the High Index Material

I noticed that the sidepeaks of Figure 21 do not occur at the same wavelengths as those of Figure 28. This suggested a hybrid filter design using one of each of the two types of antireflection stack. Such a filter, shown in Figure 29, has less pronounced longer wavelength peaks than does the filter of Figure 28.

The matching stacks need not be of the conventional design used in the preceding examples. A different type of stack, similar to a design due to Bigelmaier[23] has the parametric admittance plot of Figure 30 a. It passes through the region of the peak very rapidly at three different wavelengths. The transmittance of a 300 Å aluminum film with such a stack on either side is shown in Figure 30 b.

It is generally true that a nonabsorbing film combination which has high phase dispersion from one side will have relatively low phase dispersion when viewed from the other side. This is illustrated by Figure 31 a, in which the above stack is reversed. In this case the admittance lingers in the region of the peak for almost 1000 Å. This causes the filter using the reversed stacks to exhibit one broad transmittance peak rather than the three narrow peaks exhibited in Figure 30 b.

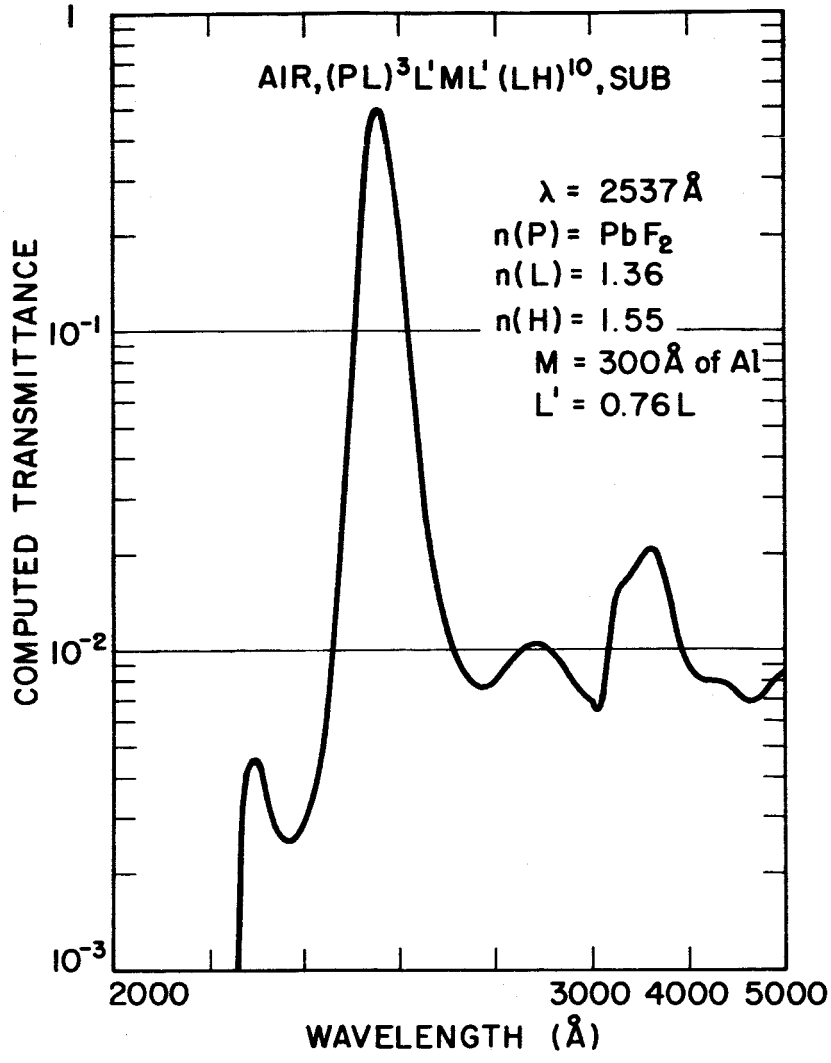

Figure 29. Hybrid 1M Filter's Computed Transmittance

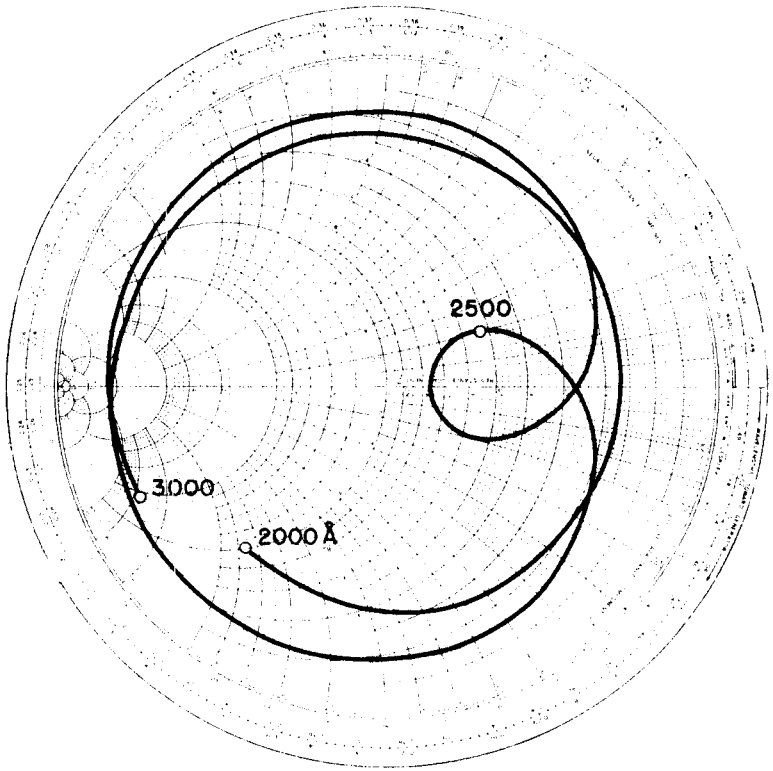

Figure 30 a. Parametric Admittance of a Stack Having High Phase Dispersion

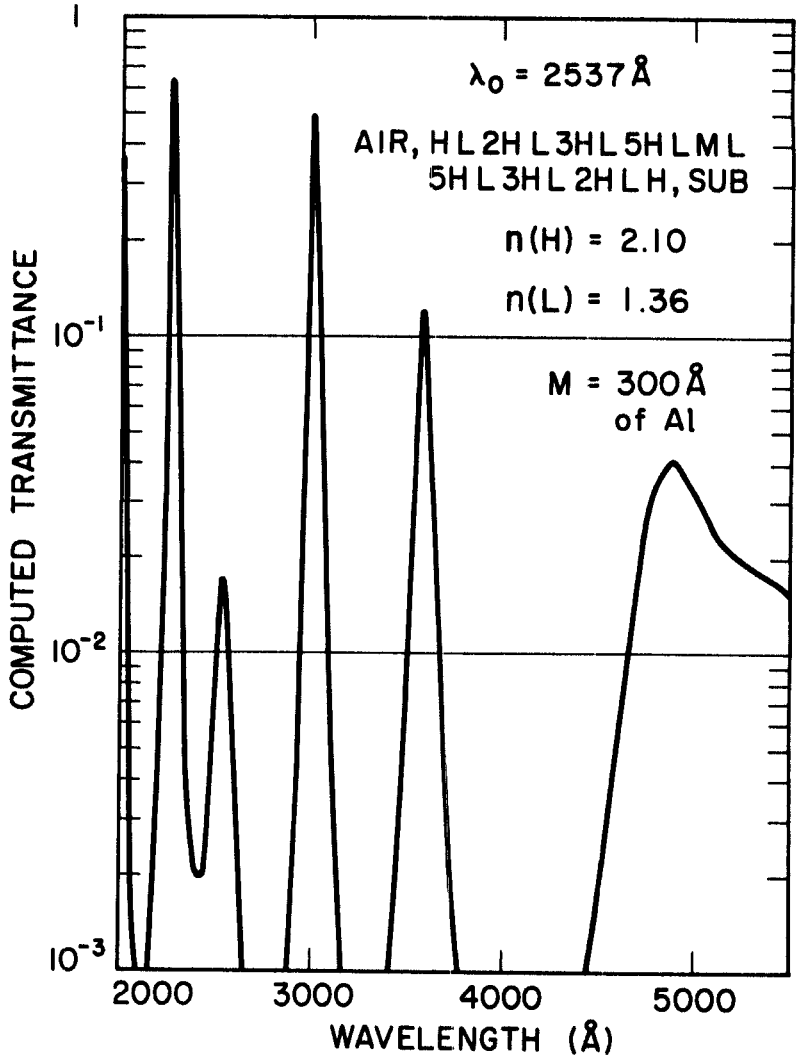

Figure 30 b. Computed Transmittance of a 1M Filter Using This Stack

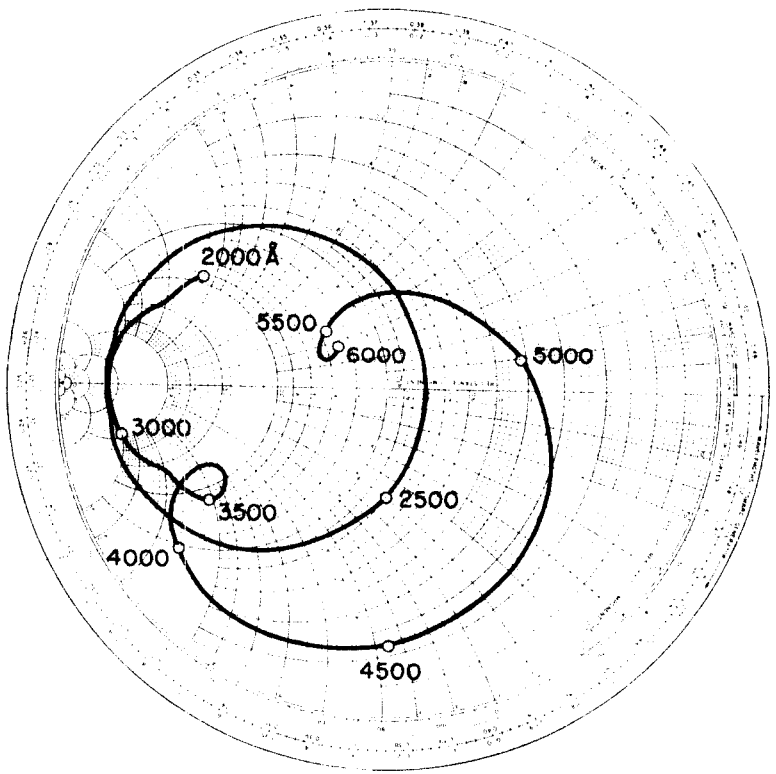

Figure 31 a. Parametric Admittance of a Stack Having Low Phase Dispersion

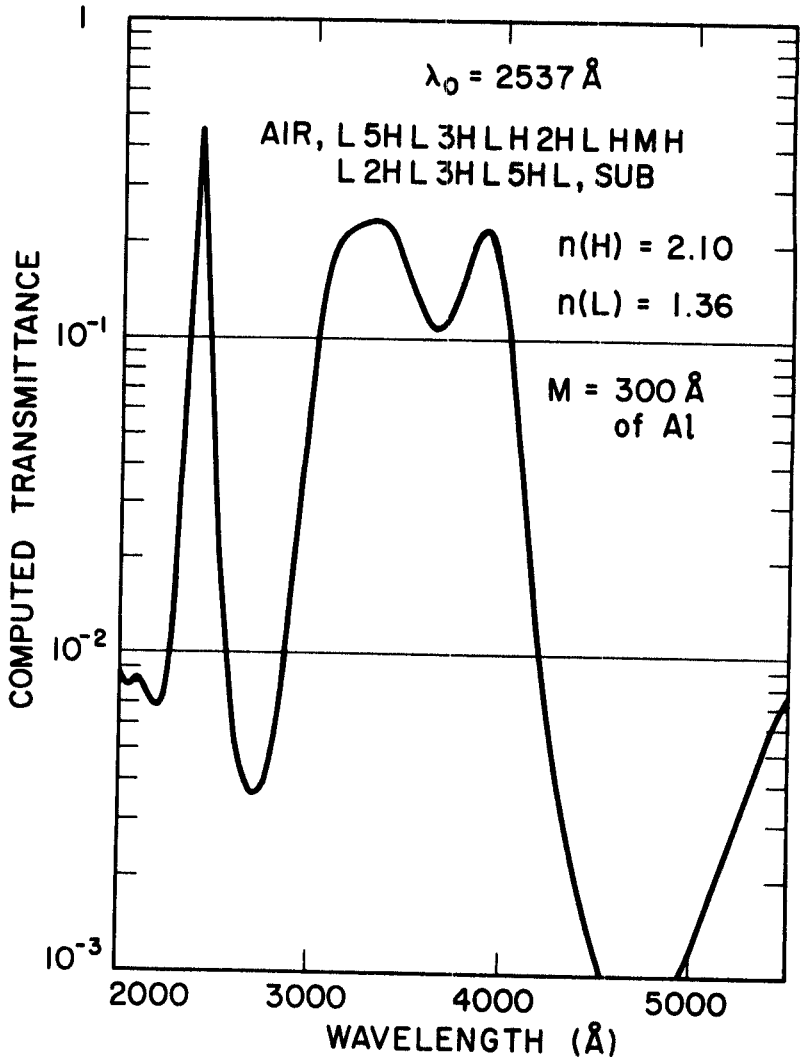

Figure 31 b. Computed Transmittance of a 1M Filter Using This Stack

Filters Containing Two Aluminum Layers

Three types of filter containing two aluminum layers will be considered. The first type is simply two 1M filters evaporated onto separate substrates. If the two 1M filters are evaporated onto the same substrate, we have the second type of filter. The third type has spectral characteristics very different from the first two, although it is obtained from the second by changing the thicknesses of only two of its layers.

The transmittance of the first type of filter in the region of the passband should be the square of the transmittance of a single 1M filter. However, the transmittance away from the passband should be greater than would be predicted in this manner; therefore the contrast is less than the square of the contrast of the single 1M filter. No computed transmittance curves are available for this type of filter, although a measured transmittance curve is shown in the following chapter.

The computed transmittance of the second type of filter is shown in Figure 32. The sharp transmittance peaks at 3000 Å and 3600 Å are about 5 Å wide and probably would not be seen in practice.

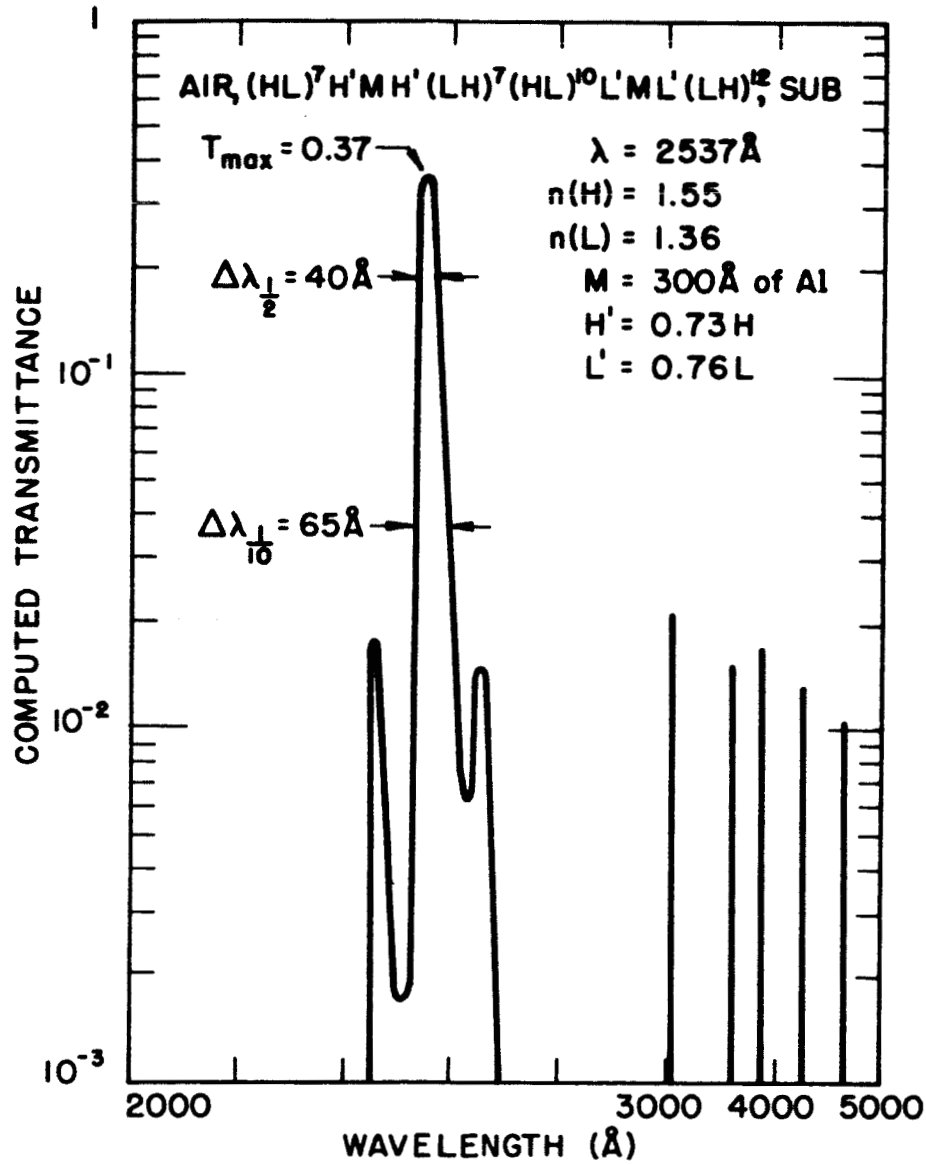

Figure 32. Computed Transmittance of Ganged 1M Filters

The third type is an antireflected form of a filter first described by Turner.[23] Before antireflection, this type of filter has very good rejection near the passband, which is narrower than obtained from the conventional Fabry-Perot with the same order number. However, further from the passband there are many sidebands which are in fact more highly transmitting than the passband. The transmittance of a Turner filter before and after modification is shown in Figure 33. Far from the passband the transmittance has been unaffected by the antireflection. The transmittance in the passband has been improved greatly. In fact it is now 0.34 as compared with a theoretical limit of 0.36 for two aluminum films 300 Å thick. The transmittance in the high rejection zones next to the passband has been only slightly affected, causing the contrast between the transmittance peak and the high rejection region to increase an order of magnitude.

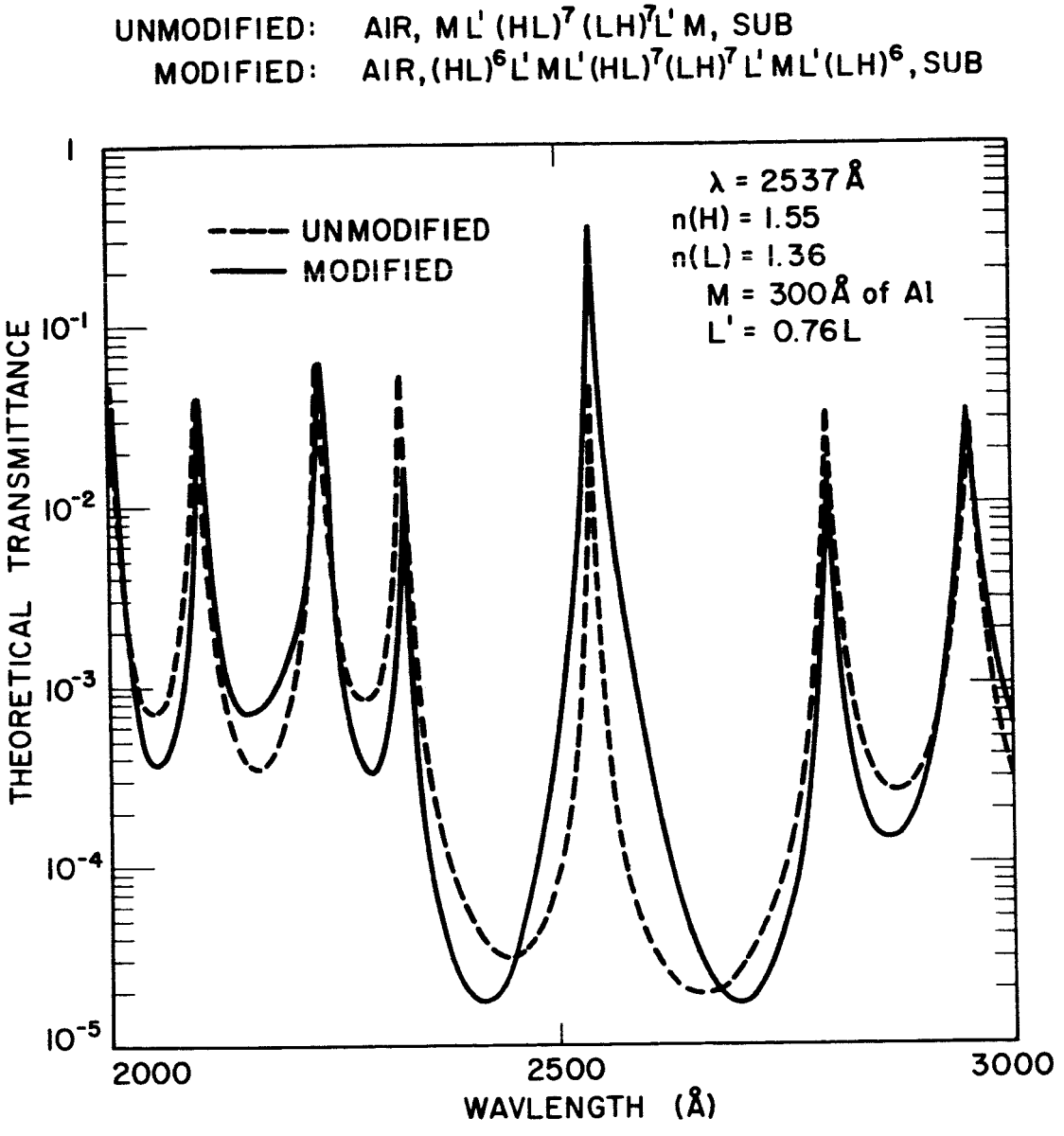

Figure 33. Theoretical Transmittance of Modified and Unmodified Turner Filters

III. EXPERIMENTAL

Ultraviolet interference filters consisting of a single aluminum layer sandwiched between two dielectric antireflecting stacks were produced by evaporation of thin films in vacuum. The transmittance properties of these experimental filters parallel closely the prediction of theory.

The equipment and procedures used to produce these filters are similar to those used for the production of conventional all-dielectric interference filters. Below is a brief description of apparatus and experimental methods used.

Apparatus

The equipment utilised in the production and analysis of the filters described later in this thesis can be divided into five categories. The first category includes an ultrasonic cleaner and a dust-free box used respectively to clean and store substrates. Next there is the vacuum chamber. An electron gun evaporation source with its power supply is in the third classification. The fourth category

is equipment which is required to stop the evaporation when the layers are of the desired thickness. It includes an optical monitoring system, the associated electronics, and a manually operated shutter. Last is the scanning spectrophotometer with which the transmittance of the completed filter is analysed.

Since the equipment in the first and last categories is of conventional design, it is not described in detail.

Vacuum Equipment

The vacuum chamber is a five-foot tall, thirty-inch diameter cylinder of stainless steel, evacuated by a ten-inch diameter diffusion pump with a rated speed of 1500 liters per second. A chevron baffle cooled by liquid nitrogen helps to prevent diffusion pump oil from migrating into the vacuum chamber and contaminating the films. A Rootes type blower is used in series with the forepump to decrease the pumpdown time.

The system is provided with a roughing line, blower bypass line, and valves before and after the diffusion pump. Pressures above 10^{-2} Torr. are measured on a thermocouple gauge in the foreline, while pressures below 10^{-3} Torr. are measured on an ion gauge sealed into the vacuum chamber wall.

Electron Gun Evaporation Source

The evaporation source is an electron beam gun as shown in Figure 34. The hairpin-shaped filament, at F in the diagram, is made of 0.04" diameter tungsten wire. Graphite electrode A, connected to one end of the filament, is kept at approximately 5,000 volts negative, while the tantalum electrode B and the crucible stage are grounded.

The strong electric field between electrodes A and B accelerates the electrons thermally emitted from the filament in the direction indicated in Figure 34. After leaving the vicinity of electrodes A and B, the 5 kV electrons are deflected by a magnetic field, produced by a coil wound about axis C in the diagram. The current in this coil is adjusted to deflect the electrons through 180^{o} so that they impinge on the material in the crucible. The barrel shape of the magnetic field due to the placement of the pole pieces D and D' in Figure 34, causes the electrons from the extremities of the filament to be deflected toward a central point on the crucible stage. The v-shaped beam about 1/4" wide heats the material in the crucible. If several crucibles are placed on the rotary crucible stage, each may be moved in turn into the electron beam.

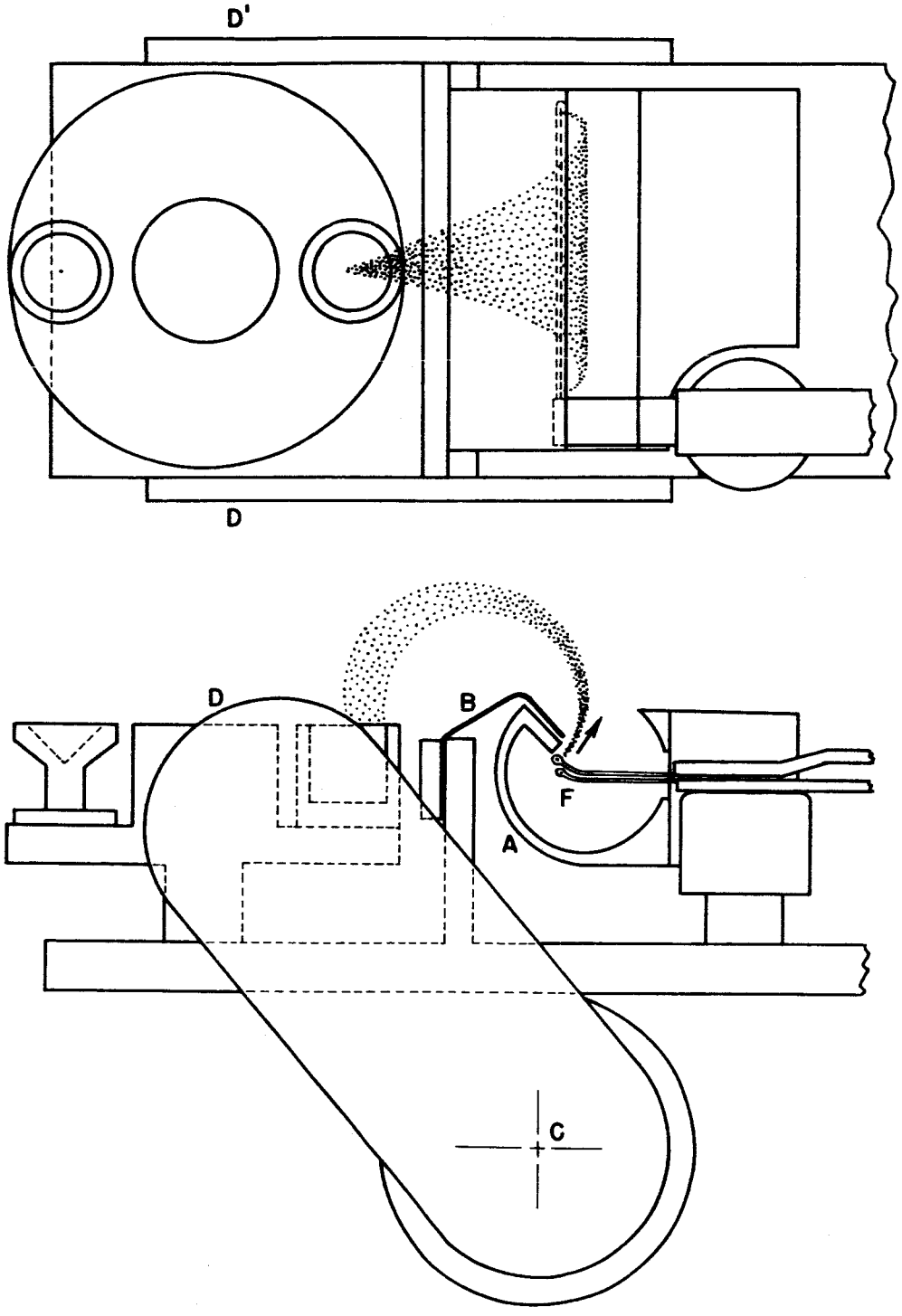

Figure 34. Electron Gun Evaporation Source

Crucibles which contain the aluminum are machined from HDA, a composite of boron nitride and titanium diboride, manufactured by the National Carbon Company. This material does not react with the molten aluminum. Graphite crucibles are used to hold dielectric evaporants, such as PbF_2, ThF_4, and cryolite.

The power required to evaporate aluminum depends on the shape and size of the crucible. A crucible with a large surface area radiates heat rapidly. The other major power loss is due to heat conduction to the base of the rotary crucible stage. Both the radiation and the conduction losses are minimized in a crucible shaped like a wineglass with a thin stem, as shown in Figure 34.

Monitoring System

The optical monitoring system is shown schematically in Figure 35. The lamps are low-pressure mercury vapor discharge lamps enclosed in #9823 glass. The envelope has a transmittance of 0.75 at 2537 Å and 0.85 at wavelengths longer than 3000 Å.[26] An EMI #6255-B photomultiplier is operated at 600 to 800 volts bias with a load resistance of 0.15 to 0.50 megohms. It has a quartz end window and an S13 surface. The discharge lamps and the

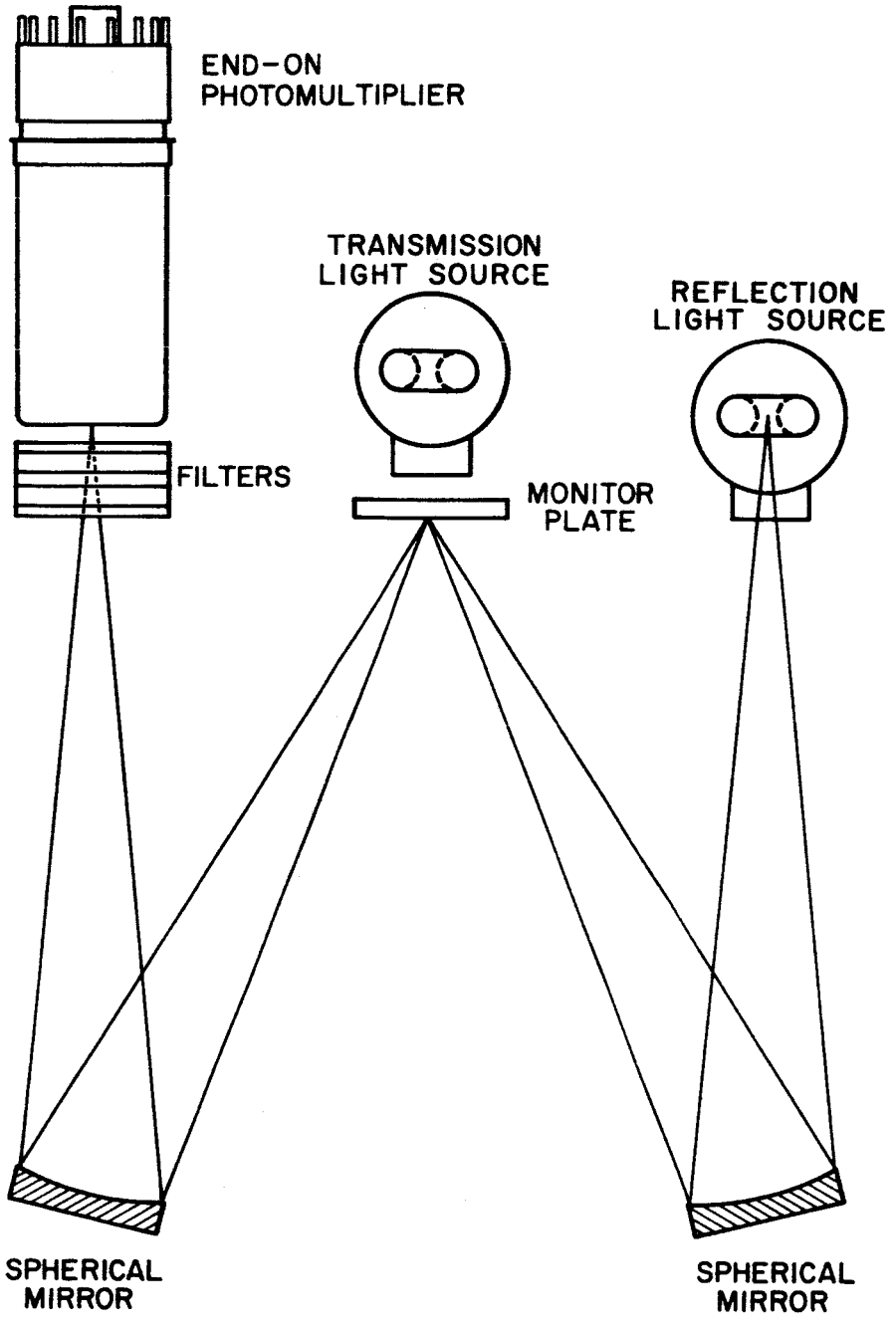

Figure 35. Geometry of the Optical Monitoring System

photomultiplier are mounted in water-cooled housings to minimize thermal drift of the monitoring signal. A concave aluminized mirror is mounted so that an image of the reflection monitoring lamp is formed on the monitor plate. The light reflected from the monitor plate is reimaged by a second aluminized mirror in the aperture of the filter holder. When used to monitor the transmittance of the monitor plate, the second mirror images the transmission source directly in the aperture of the filter holder.

The monitor plates are Suprasil I discs 1-3/16" in diameter and 1/16" thick and are finely ground on the back face to eliminate the back surface reflection. The monitor plate holder has a capacity of eight such monitor plates and is mounted 30" above the evaporation source on three adjustable points which facilitate its alignment and guarantee that it does not stray from alignment as new monitor plates are brought into the monitoring light beam. The surface of the monitor plate holder is covered with 45^{o} flutes so that any monitor beam striking it is not reflected toward the photomultiplier.

When the monitoring system was first used, a Schott glass UG-2 absorption filter eliminated the visible spectral lines of mercury as well as the lines below 3000 Å. The

effective wavelength of the monitoring system was therefore 3400 Å. Using this system, a conventional Fabry-Perot was made with two aluminum films and a magnesium fluoride spacer, which transmitted ten per cent at 2537 Å and less than one per cent at 3400 Å. It was evaporated onto a UG-5 substrate and thus transmitted less than a tenth of one per cent throughout the visible. This was then used in the filter holder, isolating the 2537 Å line while a better filter of the 1M type was produced.

The block diagram in Figure 36 represents the electronics associated with the monitoring system. The 410 cycle per second output of an audio frequency oscillator is amplified and serves as the driving voltage for the low-pressure mercury discharge lamps. Since the discharge frequency is twice that of the driving voltage, the light produced is modulated at double the frequency of the audio oscillator.

The signal from the photomultiplier is divided by the potentiometer, the use of which will be detailed in the subsection on monitoring technique. A cathode follower then provides an impedance match to reduce the capacitive loss of the signal in the coaxial cables. The tuned amplifier discriminates between the modulated signal and the

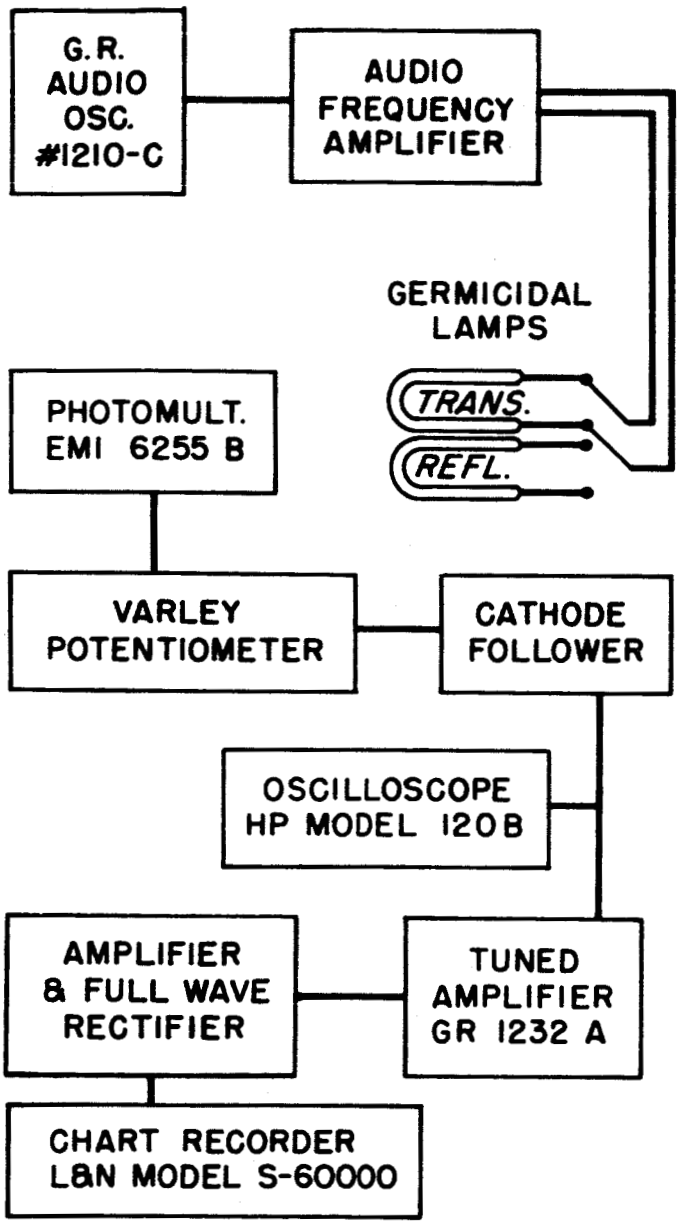

Figure 36. Electronics of the Monitoring System

d.c. background and other noise present in the signal from the cathode follower. The rectified output then drives the strip chart recorder.

Techniques

The durability and transmittance properties of interference filters depend on the techniques used in its production. For this reason, the method of cleaning substrates, monitoring film thicknesses, and evaporating aluminum are described.

Cleaning of Substrates

The surface to be the foundation of the multilayer interference filter must be clean and free of dust particles. Adsorbed water, oil, or foreign material of any sort causes nonuniform adhesion of the films to the substrate. Dust particles clinging to the surface of a substrate during evaporation produce pin holes in the completed filter. For these reasons, extreme care is taken in cleaning substrates and in keeping them dust free.

After previous films are removed by using a mild NaOH solution, the substrate is washed in a warm water solution of Alconox. The substrate is then rinsed thoroughly

in tap water two or three times. It is then placed while still wet in a shallow dish of distilled water. This dish is floated on the water surface in an ultrasonic generator. After ten or more minutes, the dish and contents are removed to a dust-free box. In order not to contaminate the substrate with organic compounds or dust particles, it is manipulated with a glass holder fashioned from a glass rod. Using this holder it is rinsed in distilled water and held at an angle for drying. A hand-operated rubber squeeze bulb is used to puff gently down the upper surface to aid uniform drying.

As the substrate is drying, light reflected from its surface is observed. If the receding film of water does not display an interference fringe system which uniformly retreats down the surface, then the substrate is recleaned.

The clean, dry substrate typically remains in the dust-free box for thirty minutes before being placed in the vacuum chamber. Substrates are not placed in the vacuum chamber more than five minutes before the pumpdown is started.

Vacuum Practices

In order to obtain an aluminum film with a high absorption constant, one should use rapid rates of evaporation in a high-vacuum environment.[27] It is thus necessary to obtain a high vacuum in the chamber and maintain it during the rapid evaporation of aluminum. Ion discharge cleaning is used to degas the chamber and clean the substrates. Premelting and outgassing the aluminum diminishes the pressure rise during the aluminum evaporation. The liquid nitrogen cooled chevron baffle is a cryogenic pump for water vapor as well as an oil trap. After the chamber is evacuated to a pressure of less than 20 microns, argon is admitted through a needle valve in the bottom of the chamber. When the pressure reaches 200 to 500 microns of argon as measured in the foreline, the needle valve is adjusted to maintain the argon pressure at 50 microns for the ion discharge cleaning. The power supply for the electron gun serves also as the source of the high negative discharge voltage, which is typically -3000 volts, producing a discharge current of 50 milliamperes. Pure aluminum wire, shielded from the substrates as advised by Holland[28] is used for the discharge cathode. After five

to ten minutes of ion discharge cleaning, the needle valve is closed, extinguishing the discharge when the pressure drops to 5 microns.

Within five minutes after opening the diffusion pump to the chamber, the pressure is less than 3×10^{-5} Torr. Before evaporation begins, the pressure is less than 2×10^{-5} Torr. and sometimes as low as 2×10^{-6} Torr. In order to minimize the pressure rise during the later evaporation of aluminum, it is premelted and outgassed before the filter is started.

Evaporation Procedure

The amount of power required to evaporate different dielectric materials is not entirely dependent on the material. Powdered substances require less power than the equivalent granulated materials. For example, cryolite in powdered form requires 600 watts of beam power, while in granulated form from Balzers it requires 850 watts to produce the same rate of evaporation. In general, powdered materials have these additional disadvantages: they require a larger crucible to hold a given quantity of material; they contain large amounts of gas; and the electron beam burrows into the powder causing the evaporant stream distribution

to be nonuniform. In order to reduce the latter effect, the beam is defocused slightly when powdered materials are used.

As shown in the Theory section, cf. Figure 4, a small decrease in the absorption coefficient of the metal layer results in a great decrease in the filter's contrast. In the evaporation of aluminum, a high k may be obtained only through a very rapid evaporation of high-purity aluminum in high vacuum.[27] The rates of evaporation used in making the filters described below were between thirty and one hundred angstroms per second. The total evaporation of the aluminum layer lasts from three to ten seconds. Aluminum of 99.99 per cent purity was obtained in the form of sheets 1/32 of an inch thick. The aluminum is not etched or treated in any way prior to use. The pressure during the evaporation is typically 1.5×10^{-5} Torr.

The rate of evaporation of the aluminum is not limited by the evaporation source or the monitoring system, but by the shuttering system. An operator of a manual shutter cannot with precision stop an evaporation lasting less than three seconds.

After the aluminum has been evaporated and shuttered, it is advisable to overcoat it with a protective dielectric

layer as soon as possible to prevent its oxidation. However, the shutter arrangement will not allow the evaporation of a dielectric without unshuttering the aluminum. Thus there is a thirty-second delay while the aluminum cools.

Monitoring Technique

The art of monitoring layer thicknesses is central to the production of interference filters. In making the 1M filter the two most critical layers are the layers preceding and the aluminum layer. ~~either side of the aluminum~~. These two layers are important because errors in their deposition cannot be remedied by adjusting thicknesses of succeeding layers.

Since the phase change upon reflection is more important than the reflectance of the matching stacks (cf. Figure 12 or Figure 17) in the filters being constructed, it is advisable to monitor the stack before the aluminum using a single monitor plate. If the last layer before the aluminum is of low index, then the evaporation should be halted when the reflectance has passed its minimum and is nearly to its maximum. Assuming that the reflectance versus thickness of this layer is represented by

$$R(d_{j+1}) = A + B\cos^2(2\pi\sigma n_{j+1} d_{j+1}) \tag{113}$$

$$= A + \frac{B}{2} + \frac{B}{2}\left[\cos(4\pi\sigma n_{j+1} d_{j+1})\right] \tag{114}$$

Substituting

$$n_{j+1} d_{j+1} = 1.76\left(\frac{\lambda_0}{4}\right) \tag{115}$$

$$R(d_{j+1}) = A + \frac{B}{2} + \frac{B}{2}\cos(1.76\pi) \tag{116}$$

$$= A + 0.87\,B \tag{117}$$

Since A is the minimum value of the reflectance and B is the difference between the original and the minimum reflectance, a rule of thumb is that the reflectance should be seven-eighths of the way from a minimum to the maximum. When using cryolite, an inhomogeneous film seems to be created, as was observed by Koppelmann.[29] This inhomogeneity

causes the maximum to be lower than the original value of the reflectance. For this reason, when using cryolite, the first maximum is passed and the evaporation stopped almost to the second maximum.

The aluminum layer is then monitored in transmission off the same or a different monitor plate. If a different plate is used, the previous monitor plate is also exposed to the evaporation and is then used in reflection to monitor the layers which follow the aluminum layer. When the same monitor plate is used as was used for the first dielectric stack, the transmittance ratio before and after the metal film should be computed. A typical value for 300 $\mathring{A}$ of aluminum and a monitoring wavelength of 2537 $\mathring{A}$ is a transmittance ratio of four to one. If a new monitor plate is used for the metal layer, the transmittance ratio is roughly the inverse of the transmittance at Y = 1.0, as shown in Figure 19. For the same parameters this ratio is forty to one.

Since the amplifiers are not linear over a range of forty to one, the potentiometer is used to increase the signal into the cathode follower by a known ratio without changing any of the parameters of the system. The transmittance light source is stabilized and the potentiometer

set at one-fortieth of its full-scale setting. The meter reading on the tuned amplifier is noted. Then, when the aluminum is evaporating rapidly, the shutter is opened and the potentiometer switched to full scale. The tuned amplifier meter initially reads above full scale. The aluminum film then attenuates the beam until the meter reading reaches the previously noted value, at which time the film is the proper thickness and the evaporation source is shuttered. In practice, although the meter needle is moving rapidly, the transmittance after completion of the aluminum layer is usually within ten per cent of the target value.

The first dielectric layer which is deposited on top of the aluminum causes the reflectance to decrease. If this is a low index layer, it is complete when the reflectance reaches a maximum. The succeeding quarter-wave stack is then evaporated, stopping high index layers at minima and low index layers at maxima. This stack is complete when the monitoring signal is less than two per cent. It might be noted that the second stack is easier to make than the one before the aluminum layer, because an error in thickness of any layer is partially compensated by the following layers.

Spectral Transmittance Measurement of the Filter

The spectral transmittance of the filter is measured within an hour after removal from the vacuum system. This measurement is accomplished on a Cary Model 14 scanning spectrophotometer, with the filter placed in the center of the sample holder, normal to the light beam, and with its coatings toward the light source. With the slit height used, the beam is f/8 indicating a maximum angle of incidence of 3.5^{o}. The wavelength scanning rate is usually ten angstroms per second, however a lower speed is used to determine the half-width and peak transmittance of a filter. In order to measure a transmittance below one per cent, a metal screen is inserted in the reference beam.

The measured transmittance is not corrected for the slight absorption in the substrate or for the reflection from the back surface of the substrate. The latter effect causes a decrease of the measured peak transmittance to 0.96 of its true value, while only slightly decreasing the background transmittance. Nor has any attempt been made to correct the transmittance curves for the slit widths of the spectrometer, which cause the band-width to be approximately 5 $\mathring{A}$. This finite bandpass would increase the measured bandpass of a 50 $\mathring{A}$ half-width filter by less than 2 $\mathring{A}$.

Observations

A few observations were made during the course of this work, which have not yet been thoroughly considered. During the initial heating of the aluminum prior to beginning the filter, it is noticed that a scum floats on the surface of the molten aluminum. Upon further heating, the scum migrates toward the edge of the crucible away from the fan-shaped electron beam and disappears. It is conjectured that this scum is aluminum oxide, and that it either evaporates or is dissolved in the molten aluminum.

While dielectric materials are being evaporated, the electron beam passing through the vapor stream excites some of the atoms. As might be expected, there is a yellow glow around the crucible when cryolite, Na_3AlF_6, is being evaporated. This yellow glow is presumably due to the sodium yellow resonance lines. Thorium fluoride produces a pale blue glow and lead fluoride gives a bright blue emission.

If the optical levels are being excited, then it is reasonable to expect that some of the vapor is being ionized. Although the average energy of the ions is expected to be three orders of magnitude lower than that of the electrons,

the ions' charge to mass ratio is also three orders of magnitude lower than that of the electrons. These ions should then be deflected by the magnetic field in an arc having about the same radius of curvature as the electrons' trajectory. However, the expected nonuniformity in vapor distribution has not been observed.

Results

The only possible test of the feasibility of a filter's design is the production of such a filter and comparison of its measured with its computed properties. In this section the feasibility is demonstrated of the aluminum 1M filter designed as an ultraviolet bandpass filter. Four filters are described, two of which follow closely their predicted spectral transmittance curves. An example is given of a filter which was poorly monitored, yielding lower peak transmittance and a wider passband than computed. In another case, the effect of using lead fluoride and a thicker aluminum film is shown. The result of using in series two 1M filters deposited on separate substrates is also illustrated.

First is shown a filter which was monitored using

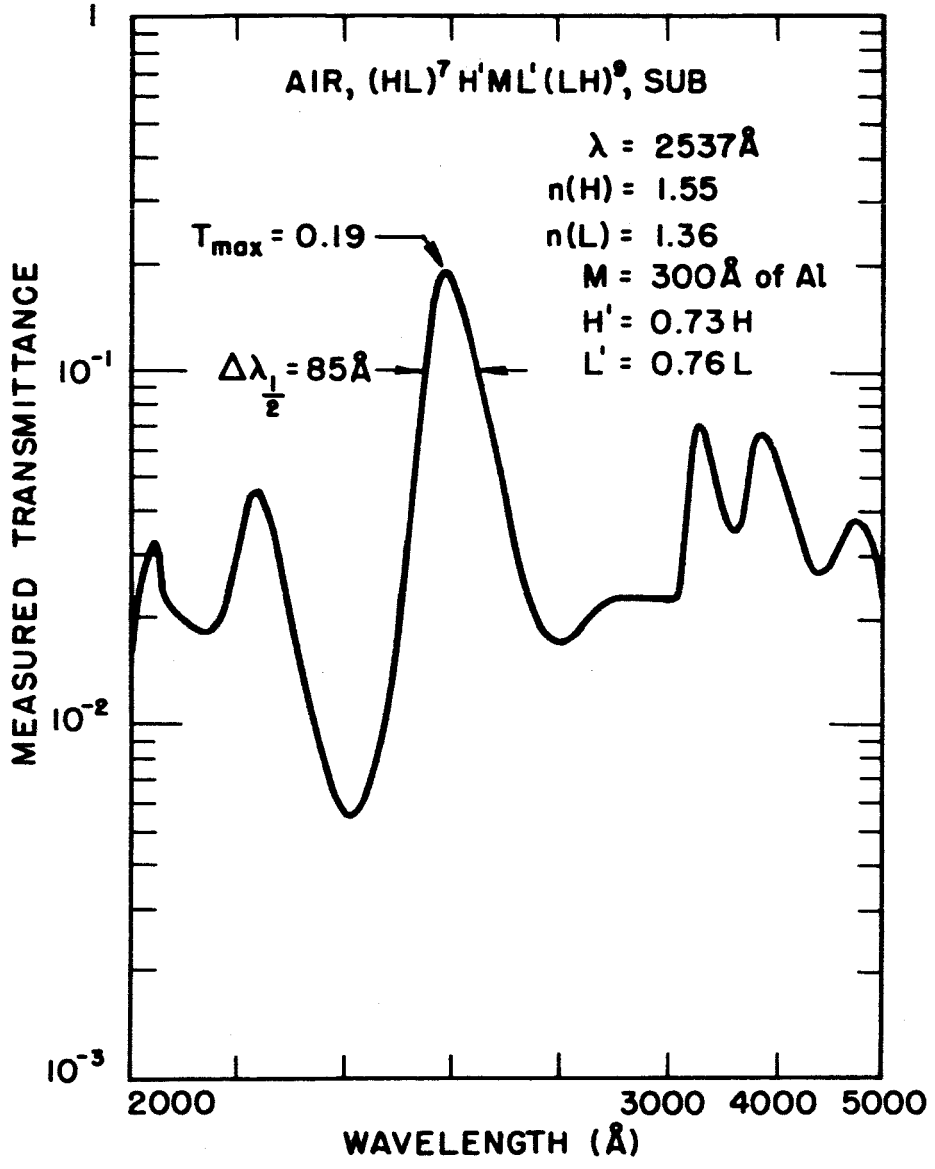

Figure 37. Measured Transmittance of a Poor 1M Filter Sample

two separate monitor plates. The first stack was monitored on one plate, while the 300 Å aluminum film and second matching stack were monitored on another monitor plate. The measured transmittance and design of this filter are shown in Figure 37. Its peak transmittance is much lower than the predicted 0.64 and its bandpass does not compare favorably with the computed value of 65 Å. Both the breadth of the peak and failure to reach T_{max} are thought to be due to antireflection stacks which are not tuned to the same wavelength.

The spectral transmittance shown in Figure 38 is a better example of what can be produced with a 1M filter design. This is essentially the same filter as shown in Figure 37, except that it was produced using only one monitor plate. The peak transmittance of 0.55 and passband of 65 Å compare well with the theoretical values of 0.64 and 65 Å; however, the contrast is only twelve compared with the predicted twenty. It is conjectured that this discrepancy is due to a ten per cent decrease in the absorption constant of the aluminum, due to the conditions in the chamber during the evaporation.

Note that the peak transmittance of the filter occurs at 2620 Å rather than at the 2537 Å monitoring system

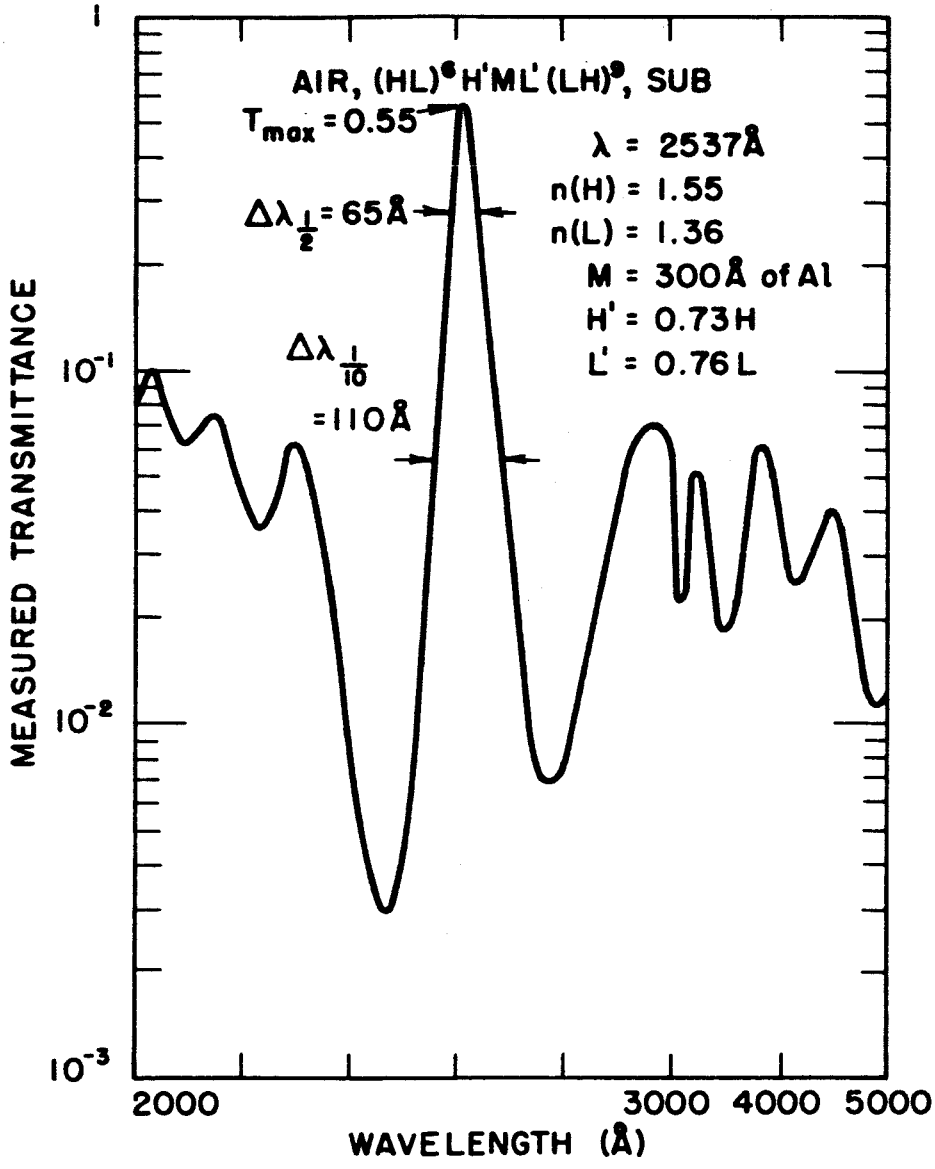

Figure 38. Measured Transmittance of an Experimental 1M Filter Using ThF_4 as the High Index Material

wavelength. Half of this shift is due to the angle shift introduced by a monitoring system which operates at an angle of incidence of 15°. The rest of the shift is due to inaccuracies in monitoring, which invariably yield thicker dielectric layers than desired, resulting in a shift of the peak toward longer wavelengths.

The filter shown in Figure 39 is made using PbF_2 as the high index material and an aluminum film 400 Å thick. The maximum transmittance and bandpass compare well with the values obtained from a computation in which the slight absorption and dispersion of the lead fluoride were taken into account. Note the absence of short wavelength side-peaks due to the onset of absorption at 2300 Å in the PbF_2. From Figure 22 we see that the maximum transmittance of a filter which contains a 400 Å layer of aluminum, and is tuned to 2537 Å, is 0.35. The difference between this figure and the 0.20 in the computed curve of Figure 39 is due to the absorption in the lead fluoride. For the wavelength and aluminum film thickness used, the finesse angle read from Figure 25 is 12.° or 0.21 radian. Combining this with the computed phase dispersion of the stack of Figures 20 and 38 which contains ThF_4 as the high index material, we obtain a bandpass of 29 Å, which is considerably lower than the 55 Å

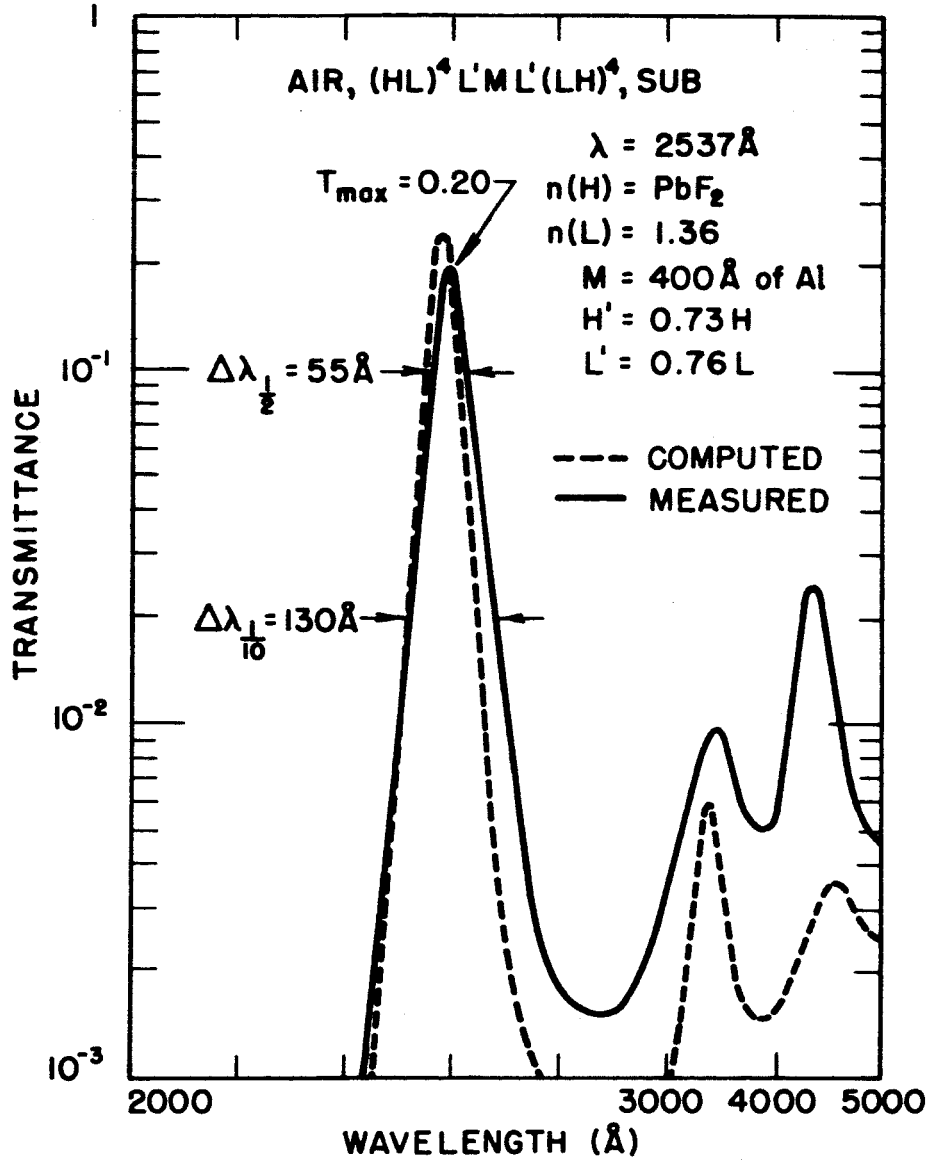

Figure 39. Transmittance of an Experimental 1M Filter Using PbF_2 as the High Index Material

bandwidth of Figure 39. If it were not for dispersion of the index of refraction of the lead fluoride, the bandpass would be about 60 Å, instead of the observed 55 Å. In summary, both the thicker aluminum film and the dispersion of the lead fluoride tend to narrow the transmittance peak, while the decreased number of films in the matching stacks tends to broaden the transmittance peak and the absorption in the lead fluoride decreases the peak transmittance and wipes out the short wavelength sidepeaks.

In Figure 40 is shown the spectral transmittance obtained when two 1M filters simultaneously deposited on separate substrates are viewed in series. Each of the 1M filters has a 300 Å film of aluminum and uses thorium fluoride as the high index material and cryolite as the low index material. There are no computed transmittance curves for this arrangement, although the spectral transmittance is expected to be close to that given in Figure 32, which has a peak transmittance of 0.36, a bandpass of 40 Å and a contrast over four hundred. The experimental results are much less spectacular, exhibiting a maximum transmittance of 0.10, a bandpass of 35 Å and a contrast of nearly one hundred. The decreased transmittance and bandpass are probably due to too thick an aluminum layer in the 1M filters.

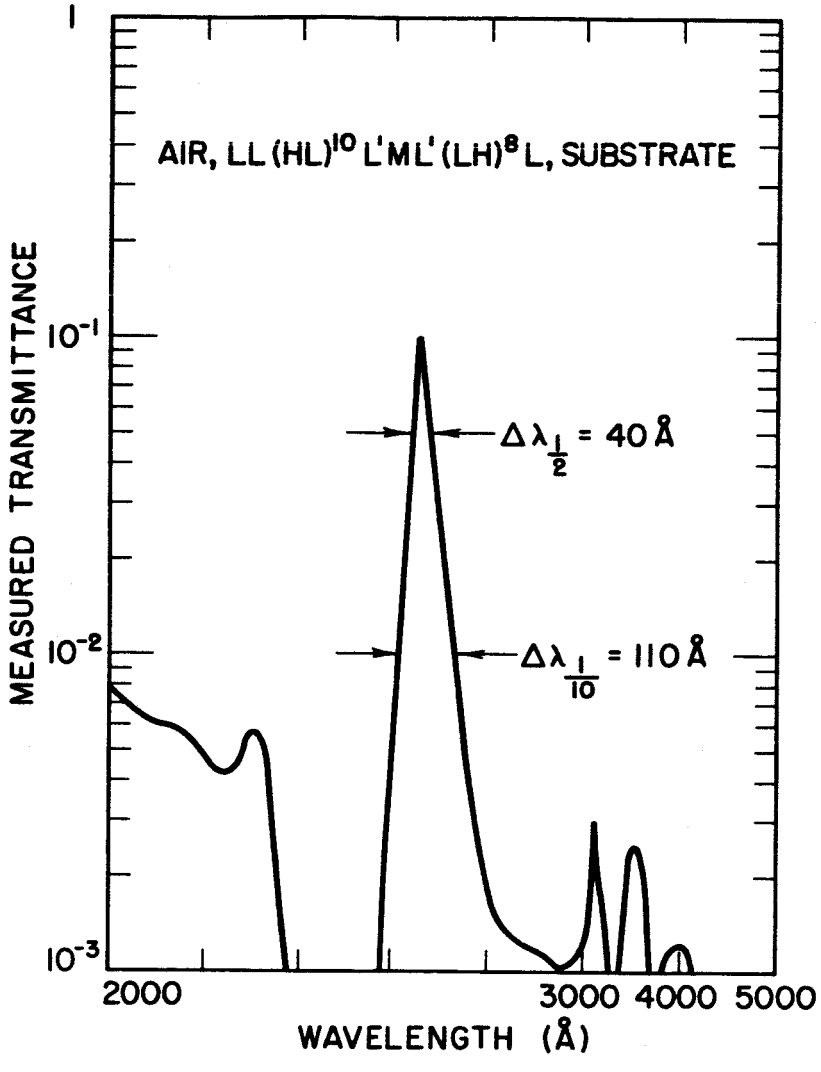

Figure 40. Measured Transmittance of Tandem 1M Filters Using ThF_4 as the High Index Material

IV. CONCLUSIONS

A systematic technique for the design of bandpass filters having only one metal layer was developed and its use illustrated in an example. Second, graphs were drawn of the maximum transmittance and contrast which can be attained with a 1M filter, as a function of the optical constants and thickness of the metal layer.

Third, filters containing aluminum were designed and constructed. Computed characteristic curves were drawn, from which the maximum transmittance, contrast, and bandpass can be determined, versus wavelength for several aluminum thicknesses.

In addition to the theoretical consideration of the 1M filters, two other types of filter which contain two metal layers were considered. The first is effectively two 1M filters evaporated onto the same substrate. Its bandpass is slightly less than that of the 1M filter, while its peak transmittance and contrast are the square of those of the 1M filter. Although it has many layers, it should not be too difficult to construct, provided one has crucibles large enough to hold the amount of material required to evaporate the seventy layers. The second type

is obtained by adding or subtracting a quarter wave from the two layers next to the internal aluminum interfaces. This "modified Turner design," as it is called, has the same number of layers as the first type, but would be much more difficult to make. Its bandpass is about one tenth that of the 1M filter, while its transmittance and contrast are nearly the same as those of the first type.

V. SUGGESTIONS FOR FUTURE WORK

Seven suggestions come to mind concerning the development of the theory of filters containing metal layers and the improvement of the apparatus and techniques used in producing the filters described above.

By designing an all-dielectric stack which lingers in the r plane near the transmittance peak, a broad band transmittance filter could be made. Similarly, one could make limited range high- or low-pass single metal layer filters.

Second, a narrow band transmittance filter could be made to transmit only one polarisation. The design would function in a manner similar to that of the MacNeille polariser.[30, 31] This design requires an incidence angle of about 45 degrees from a medium of index of refraction 1.50. Therefore, the filter would be evaporated on the face of a prism and another prism cemented onto it. It is not clear at this point that one could design or produce a broad band ultraviolet filter-polariser in this way, but it warrants investigation.

An automatic correction technique could be used to

improve the designs shown above. It may be that asymmetric admittance matching of the aluminum film would produce a filter with lower bandpass or reduced sidebands.

Fourth, interference filters containing two absorbing layers should be considered more thoroughly. The conventional Fabry-Perot filter as well as the Turner variation of it have been treated in the literature and have desirable characteristics. But it seems plausible that other designs will produce more desirable effects while using only two metal films in conjunction with many dielectric layers. Although the modified Turner filter described above may not be feasible in production, simpler forms with fewer periods in the internal high reflection stacks should be producible.

Since powdered materials provide so many disadvantages, it is suggested that they be fused prior to use. Vacuum fusion, vacuum distillation, or zone refining of the materials to be evaporated may also be worthy of the time and expense involved.

Sixth, if aluminum is to be evaporated in less than three seconds, automated electromechanical shuttering is necessary. Some attention might also be fruitfully given to an investigation of the effect of etching the aluminum prior to use and the value of getter pumping to obtain a

lower oxygen pressure during the aluminum evaporation.

Finally, all of the experimental work in this thesis was accomplished with a monitoring system wavelength of 2537 Å. The transmittance of the filters was thus fixed to the region near 2600 Å. If one is to eventually make filters for the vacuum ultraviolet region, he should have a variable wavelength monitoring system. This might involve the use of the continuum of a discharge lamp as the source of light and a vacuum ultraviolet monochrometer as a variable wavelength filter.

REFERENCES

1. C. B. Childs, Broad-band Ultraviolet Filters, J. Opt. Soc. Am. 51, 895 (1961).

2. E. B. Mayfield, Ultraviolet Radiometric Measurements of the Moon, Venus, and Selected Stars, J. Opt. Soc. Am. 54, 1386A (1964).

3. S. F. Pellicori, Transmittances of Some Optical Materials for Use Between 1900 and 3400 Å, Appl. Opt. 3, 361 (1964).

4. H. E. Bennett and W. R. McBride, Use of Filters for Suppressing Scattered Light in Spectrometers Used in the Ultraviolet, Appl. Opt. 3, 919 (1964).

5. C. M. Wolff and R. Pertel, Optical Transmittance Filter for Hg 1849 Å Radiation, J. Opt. Soc. Am. 54, 1168 (1964).

6. P. W. Baumeister and V. R. Costich, Optical Interference Filter for Hg 1849 Å, Appl. Opt. 4, 364 (1965).

7. G. Honcia and K. Krebs, Eine neue hochbrechende Subtanz für dielektrische Ultraviolett-Spiegel, Z. Physik 156, 117 (1959).

8. G. Honcia and K. Krebs, Hochbrechende Substanzen für dielektrische Spiegel systeme, Z Physik 165, 202 (1961).

9. W. Geffcken, Neuartige Interferenzlichtfilter, Angew. Chem. A60, 1 (1948).

10. D. J. Schroeder, Interference Transmission Filters for the Far Ultraviolet, J. Opt. Soc. Am. 52, 1380 (1962).

11. P. H. Berning and A. F. Turner, Induced Transmission in Absorbing Films Applied to Band Pass Filter Design, J. Opt. Soc. Am. 47, 230 (1957).

12. E. A. Lupashko and I. N. Sklyarevskii, Multilayer Dielectric Antireflection Coatings, Optics and Spectroscopy 12, 279 (1964).

13. S. D. Smith, Design of Multilayer Filters by Considering Two Effective Interfaces, J. Opt. Soc. Am. 48, 43 (1958).

14. F. Dow Smith, PhD dissertation, University of Rochester, Rochester, New York, 1951 (unpublished).

15. I. N. Shkliarevskii and A. A. Adveenko, Increasing the Transparency of Metallic Coatings, Optics and Spectroscopy 8, 439 (1959).

16. P. G. Kard, Theory of Increasing the Transparency of Metallic Coatings, Optics and Spectroscopy 9, 129 (1960).

17. P. G. Kard, Theory of Multilayer Asymmetric Reflectors, Optics and Spectroscopy 10, 193 (1961).

18. P. J. Leurgans, The Impedance Concept in Thin Film Optics, J. Opt. Soc. Am. 41, 714 (1951).

19. M. Born and E. Wolf, Principles of Optics (Macmillan, 1964) 2nd ed., p. 1 and p. 33.

20. F. Seitz, The Modern Theory of Solids (McGraw-Hill, 1940), p. 630.

21. W. Weinstein (W. Welford), Computations in Thin Film Optics, Vacuum 4, 3 (1954).

22. M. Born and E. Wolf, Principles of Optics (Macmillan, 1964) 2nd ed., p. 325.

23. Private communication from W. R. Hunter, U. S. Naval Research Laboratory, Washington, D. C.

24. A.Bigelmaier, Eine allgemeine Losung des Schicht-problems der Optik, Optica Acta 4, 3 (1957).

25. A. F. Turner, Some Current Developments in Multi-layer Optical Films, J. phys. radium 11, 457 (1950).

26. Private communication from J. Eby, Sylvania Light-ing Products, Salem, Massachusetts.

27. G. Hass and R. Tousey, Reflecting Coatings for the Extreme Ultraviolet, J. Opt. Soc. Am. 49, 593 (1959).

28. L. Holland, The Effects of a Glow Discharge on Glass and Organic Materials, Adv. in Vac. 2, 753 (1958).

29. G. Koppelmann, K. Krebs, and H. Leyendecker, Optische Untersuchungen des Aufbaus von Kryolith-Aufdampfschichten, Z. Physik, 163, 557 (1961).

30. S. M. MacNeille, U. S. Patent #2403731, July 9, 1946.

31. M. Banning, Practical Methods of Making and Using Multilayer Filters, J. Opt. Soc. Am. 37, 792 (1947).